5-2004

Application of Polymer Rheology in Melt Blowing Process and Online Rheological Sensor

Yizhong Wang
University of Tennessee - Knoxville

To the Graduate Council:

I am submitting herewith a dissertation written by Yizhong Wang entitled "Application of Polymer Rheology in Melt Blowing Process and Online Rheological Sensor." I have examined the final electronic copy of this dissertation for form and content and recommend that it be accepted in partial fulfillment of the requirements for the degree of Doctor of Philosophy, with a major in Chemical Engineering.

John R. Collier, Major Professor

We have read this dissertation and recommend its acceptance:

Billie J. Collier, Duane D. Bruns, Simioan Petrovan, Dong Zhang

Accepted for the Council:

Carolyn R. Hodges

Vice Provost and Dean of the Graduate School

(Original signatures are on file with official student records.)

To the Graduate Council:

I am submitting herewith a dissertation written by Yizhong Wang entitled "Application of polymer rheology in melt blowing process and online rheological sensor." I have examined the final electronic copy of this dissertation for form and content and recommend that it be accepted in partial fulfillment of the requirements for the degree of Doctor of Philosophy, with a major in Chemical Engineering.

John R. Collier
Major Professor

We have read this dissertation
and recommend its acceptance:

Billie J. Collier

Duane D. Bruns

Simioan Petrovan

Dong Zhang

Accepted for the Council:

Anne Mayhew
Vice Chancellor and
Dean of Graduate Studies

(Original signatures are on file with official student records)

APPLICATION OF POLYMER RHEOLOGY IN MELT BLOWING PROCESS AND ONLINE RHEOLOGICAL SENSOR

A Dissertation

Presented for the

Doctor of Philosophy

Degree

The University of Tennessee, Knoxville

Yizhong Wang

May 2004

DEDICATION

This dissertation is dedicated to my parents in law, Mr. Xiaofeng Rong and Ms. Yamin Gu, and my parents, Mr. Guanzheng Wang and Ms. Mie Zhou, and my wife, Dr. Haoming Rong, and the rest of my family.

ACKNOWLEDGEMENTS

My gratitude can never be expressed enough to the people I met here at the University of Tennessee, Knoxville, especially those in the Chemical Engineering department and Textile and Nonwovens Development Center (TANDEC).

I would like to express my deepest appreciation to my major professor Dr. John R. Collier for his guidance and encouragement during my study. I feel indebted to Dr. Simioan Petrovan, Dr. Duane Bruns, Dr. Billie Collier, and Dr. Dong Zhang for taking the time to serve on my committee and the helpful suggestions they made during this work.

I am very thankful to the following TANDEC faculty and engineers for their precious assistances and suggestions: Dr. David Garner, Dr. Allen Stahl, Mr. Van Brantley, Mr. Gary Wynn, and Mr. Stanley Gredig. I would like to give special thanks to Mr. Douglas Fielden, Mr. Mike Neal in Chemical Engineering Department for their great assistances on developing the online rheological sensor. The financial supports from Measure and Control Engineering Center (MCEC) and TANDEC at the University of Tennessee are most greatly appreciated.

Finally, I would like to thank my wife and rest of the family for their unselfish support, sacrifices and understanding.

ABSTRACT

Polymer rheology plays a significant role in many polymer-processing operations such as polymer extrusion, fiber spinning, and nonwovens processing. To develop real time, online process and quality control system in these operations, knowledge of polymer rheology and how the rheological properties can be determined is crucial.

In this work, rheological properties of two melt blowing grades polypropylene (PP) under different processing conditions were determined by various off line methods, which includes dynamic rheological properties, shear and elongational viscosities. The elongational viscosity was measured at different Hencky strain by using semi-hyperbolic dies developed in this research group. Good master curves were generated for the temperature and Hencky strain shifting, and simultaneous shifting with respect to both temperature and Hencky strain.

Carreau and Cross-rheological models were used to fit the rheological properties to generate different functions that were used to calculate the viscosity at different processing during typical melt blowing process conditions. The correlation between the melt blowing processing condition and the properties of final nonwoven products were achieved by introducing dimensionless numbers, such as air Reynolds number, polymer Reynolds number and Hencky strain.

A high resolution IR camera was used to capture thermographs during the melt blowing process. From these thermographs, a plateau or shoulder was evident in thermographs taken during fiber drawn down by high velocity air. This represented

the crystallization of polypropylene during the melt blowing process, assuming that fiber attenuation cease at the point of crystallization, which is a fundamental problem during the melt blowing process.

It was found that the polymer degraded to a small extent during the melt blowing process, the degree being dependent on the processing variables such as melt temperatures, airflow rate and throughput.

The rheological properties of PPs were used to determine the molecular weight and molecular weight distribution based on Mead's approach. The technique for measuring shear and elongational viscosities in the laboratory was used as the basis for an online rheological sensor to measure the shear and elongational viscosities simultaneously online in a twin-screw extruder by drawing a small amount of polymer melt from the main processing stream. A laptop with software based on Labview and instruments bridged by an OPC server for MODBUS communication protocol through RS485 serial interface were configured for the control and measurement.

TABLE OF CONTENTS

LIST OF TABLES

LIST OF FIGURES

NOMENCLATURE AND ABBREVIATIONS

Nomenclature

a_T	Temperature shift factor
A	Fiber cross section area
a_H	Hencky strain shift factor
$\underline{b}$	Internal body force
β	The polymer temperature divided by a reference polymer temperature
ξ	The air stagnation temperature in the die divided by a reference die stagnation temperature
φ	The die face air width divided by a reference die face air width
ψ	The mass flux ratio of air to polymer
Cf	Heat capacity of fiber
h	Heat transfer coefficient
N	Power-law exponent
$\underline{q}$	Energy flux
d	Diameter
R	Radius of the flow channel
t	Time
z	z direction (Ch. 2), axial flow direction (Ch. 3)
$F(M,t)$	Monodisperse relaxation function
$G(t)$	Relaxation modulus
G'	Storage modulus
G''	Loss modulus
G_N^0, G_N	Plateau modulus
$H(\lambda)$	Relaxation spectrum
$\hat{H}$	Enthalpy per mass unit

K_λ	Front factor
L	Centerline length of the die
Mp	Polymer flow rate
P	Pressure
R	Universal constant
R^2	Coefficient of determination
Re	Reynolds number
T	Temperature
T_0	Reference temperature
TR	Effective Trouton ratio
$W(M)$	Weight based MWD
α	Relaxation time exponent
$\dot{\gamma}$	Shear rate
ε_H , H	Hencky strain
ε_{H_0} , H_0	Reference Hencky strain
$\dot{\varepsilon}$	Elongational strain rate
$\dot{\varepsilon}_r$	Reduced elongational strain rate
η, η_s	Shear viscosity
η_0	Zero-shear-rate viscosity
η_e	Elongational viscosity
$(\eta_{eff})_r$	Reduced effective (uniaxial) elongational viscosity
η^*	Complex viscosity
η_r^*	Reduced complex viscosity
λ	Time constant
$\lambda(M)$	Characteristic relaxation time for the monodisperse system
$\underline{v}$	Velocity vector
υ_0	Initial velocity
υ_f	Fiber velocity

υ_r	Velocity component in r direction
υ_x	Velocity component in x direction
υ_y	Velocity component in y direction
υ_z	Velocity component in z direction
ρ	Density
ρ_f	Fiber density
$\underline{\underline{\tau}}$	Stress tensor
τ_{zz}	Axial normal component of the stress tensor
τ_{rr}	Transverse normal component of the stress tensor
Φ	Potential function
Ψ	Stream function
ω	Angular frequency
ω_r	Reduced angular frequency
ΔE	Activation energy of flow
ΔH	Enthalpy change
ΔG	Gibbs free energy
ΔP	Pressure drop
ΔS	Entropy change

Abbreviations

ACER	Advanced Capillary Extrusion Rheometer
ARES	Advanced Rheometric Expansion System
CD	Cross Direction
DCD	Die to Collector Distance
DSC	Differential Scanning Calorimeter
IR	Infrared Radiation
MD	Machine Direction
MFR	Melt Flow Rate

MW	Molecular weight
MWD	Molecular weight distribution
OLE	Object linking and embedding
OPC	OLE for Process Control
PC	Personal Computer
PLC	Programmable Logical Controller
PP	Polypropylene
RTU	Remote Terminal Unit
Scfm	Standard Cubic Feet per minute
TANDEC	Textile and Nonwoven Develop Center
USB	Universal Serial Bus
VI	Virtual Instrument

CHAPTER 1

INTRODUCTION

§1.1 RHEOLOGY: SHEAR, VISCOELASTICITY AND ELONGATION

Rheology is the science of deformation and flow of materials, which include solids, liquids, or gases, under the influence of stresses [1]. The subject of rheometry is extremely important to numerous engineering applications; rheometric techniques help to define the flow properties of materials from a practical view. For a broad perspective, rheology includes almost every aspect of the study of the deformation of materials under the influence of imposed stress. Commercial interest in synthetic polymer materials has given the greatest impetuous to the science of rheology. The rheology of a material defines whether or not the polymer can be processed, shaped, and formed into a desired article in an efficient and economical manner, while maintaining dimensional stability and high quality.

Rheometers are instruments designed to measure the rheological properties of materials. Most rheometers are built on the principle of a shear deformation; the quantity measured by the rheometers is a force, pressure drop or torque that is directly related to the shear stress. The simplest type of shear deformation is “simple shear”, which is the deformation generated when a material is placed between two parallel flat plates and one of the two plates is then translated, while the gap between

the plates is kept constant. If the gap is h and the linear displacement of the moving plate is Δx, then a measure of the deformation so generated is the "shear strain", γ, given by

$$\gamma = \Delta x / h \tag{1.1}$$

If the plate moves at a constant speed, v, then the "shear rate", $\dot{\gamma}$ is

$$\dot{\gamma} = v / h \tag{1.2}$$

The quantity measured is the shear stress, σ, defined, as the force required to move the plate, divided by the area of the plate wetted by the materials being deformed.

$$\sigma = F / A \tag{1.3}$$

Such an arrangement can be used to measure rheological properties by displacing the moving plate in some prescribed way and measuring the resulting shear stress. The rheological behavior can then be described by giving the relationship between the stress and the shear strain or the shear rate.

Materials consisting of a single liquid phase and containing only low molecular weight, mutually soluble components, are usual Newtonian fluids under normal conditions. For a Newtonian fluid, the shear stress is proportional to the shear rate. This can be expressed quantitatively by the following equation:

$$\sigma = \mu \dot{\gamma} \tag{1.4}$$

where μ is the viscosity of the fluid. For a Newtonian fluid the viscosity depends on composition and temperature but not on the shear rate. Many materials processed

commercially are multiphase fluids, which include fermentation broths, mineral slurries, paints and foodstuffs. Another important category of materials is polymeric liquids, either polymer solutions or molten resins. All these materials can be non-Newtonian. The simplest manifestation of non-Newtonian behavior is that the viscosity varies with the shear rate in steady simple shear, thus the relationship between them can be written as following,

$$\sigma / \dot{\gamma} = \eta(\dot{\gamma}) \tag{1.5}$$

where η is the viscosity. The most common type of non-Newtonian behavior is that the viscosity decreases as the shear rate increases, and such a material is said to be " shear thinning". Some concentrated suspensions can exhibit the opposite type of behavior with η increasing with $\dot{\gamma}$, which is called "shear thickening". A simple empirical equation, the "power law" viscosity model for describing the dependence of viscosity on shear rate over a certain range of shear rates is shown below:

$$\eta = k \dot{\gamma}^{n-1} \tag{1.6}$$

where n is the power law index. When $n = 1$, Newtonian behavior is indicated, while $n < 1$ implies shear thinning behavior, and $n > 1$ implies shear thickening behavior.

Polymeric liquids exhibit a combination of elastic and viscous flow and are therefore said to be "viscoelastic". A consequence of this is that their rheological properties are time dependent. The viscoelastic properties of polymeric fluids, in particular the storage and loss moduli defined below, can be very useful for

determining the molecular weight distribution or as measure of the extent of dispersion of particular filler [1]. Polymer viscoelasticity is usually described in terms of response of the fluid to a sinusoidal shearing, where the shear strain is given by

$$\gamma(t) = \gamma_0 \sin(\omega t) \tag{1.7}$$

where ω is the frequency of the oscillatory strain and γ_0 is the strain amplitude. If the strain amplitude is sufficiently small, the shear stress is also sinusoidal and is given by

$$\sigma(t) = \sigma_0 \sin(\omega t + \delta) \tag{1.8}$$

where δ is the phase angle or mechanical loss angle, and σ_0 is the stress amplitude. σ_0 at a given frequency is proportional to γ_0, if the strain is sufficiently small. This type of behavior is called linear viscoelasticity. The linear viscoelasticity could be described using trigonometric identity as follows:

$$\sigma(t) = \gamma_0[G' \sin(\omega t) + G'' \cos(\omega t)] \tag{1.9}$$

where $G'(\omega)$ is the storage modulus and $G''(\omega)$ is the loss modulus, which are functions of frequency.

Elongational flow is the dominant mode of fluid flow when a rapid change of shape such as stretching is involved. The velocity field for this flow is given by $\upsilon_x = \dot{\varepsilon}x,\ \upsilon_y = -\dot{\varepsilon}y/2,$ and $\upsilon_z = -\dot{\varepsilon}z/2,$ where the positive quantity $\dot{\varepsilon}$ is called the elongational rate, and υ_x, υ_y, and υ_z are the velocity components in x, y, and z

directions, respectively. Then the elongational viscosity is defined by the relation $\tau_{xx} - \tau_{zz} = \dot{\varepsilon}\eta_e$, which depends on $\dot{\varepsilon}$. When $\dot{\varepsilon}$ is negative, the flow is referred to as biaxial stretching. For Newtonian fluids it can be shown the $\eta_e = 3\eta,$ sometimes called the "Trouton viscosity" [2]. The "Trouton ratio" is defined as $T_R = \dfrac{\eta_e(\dot{\varepsilon})}{\eta(\dot{\gamma})}$. Viscoelastic liquids being noted for having high Trouton ratios. Typical examples of elongational flow are fiber spinning, film stretching, injection molding, and extrusion through converging profiles.

§1.2 THE MELT BLOWING PROCESS

The concept of melt blowing polymers was first introduced to the public through a Naval research laboratory project initiated by Wente in 1956 [3]. Since then, the melt blowing process and numerous melt blown products have been recognized, developed, and commercialized. In melt blowing a thermoplastic, fiber-forming polymer is extruded through a die containing several hundred or thousand small orifices. Convergent hot air streams (exiting from both sides of the die nosepiece) rapidly attenuate the extruded polymer stream to form extremely fine diameter fibers. The attenuated fibers are subsequently blown by high velocity air onto a collector screen, where a self-bonded nonwoven melt blown web is formed. The web produced is a nonwoven material composed of microfibers whose diameter is in the range of one to five microns. Although there are many different designs of melt blowing production lines, the basic melt blowing process consists of the

following operations: polymer melting, transport and filtration of polymer melt, polymer extrusion and filament forming by hot air blowing, and web formation on the surface of a wire screen collector drum or belt.

The melt blowing process is quite complex and involves many variables. The operating variables can be divided into two groups, viz. online variables and off-line variables. The online variables are those that can be adjusted according to requirements during production, such as polymer and air throughputs, die-to-collector distance, polymer/die and air temperatures, and quench environment. The off-line variables are those that can only be changed when the production line is not in operation, such as die hole size, air gap, die set-back, air angle, web collection type and polymer/air distribution. Most off-line variables are set at constant values for a certain product line.

Material variables in melt blowing include polymer molecular structure, molecular weight, molecular weight distribution, polymer additives, polymer degradation and polymer forms such as pellets or granules. Generally, all thermoplastics may be processed by the melt blowing process, but some common resins such as polypropylene (PP), polyethylene, poly(ethylene terephthalate), copolyester, and polyamide are most used. Polymers of low molecular weight and melt viscosity are manufactured specially for melt blowing. Low molecular weight polymers have high melt flow rate and they can be processed easily. Melt flow rate, (amount of material discharged through a standard die in a prescribed time, temperature and load), is often used instead of the molecular weight in industry, and

it can be measured easily in laboratory. Typical melt flow rates for melt blowing grade polypropylene are 12 to 1500. Currently, PP is widely used for melt blown nonwovens because of its low cost, ease of processing, good mechanical properties, and good chemical resistance.

A special die is used in the melt blowing process. The polymer melt passes through the spinning orifices leading into the edge of nosepiece of the die. Orifices typical have diameters of 0.2-0.4 millimeters and are spaced at 1-4 per millimeter apart on the nose tip edge. The air manifolds supply the high velocity hot air through slots to the two sides of the nosepiece on opposite sides of the extruded fiber. As soon as the molten polymer is extruded from the die holes, high velocity hot air streams attenuate the polymer streams to form microfibers. A large amount of surrounding air is entrained in the air stream causing the fiber to cool and solidify as the air stream containing the fibers moves toward the collector screen. Simultaneously the fibers are partially drawn and entangled. The solidified or partially solidified fibers are randomly deposited onto the collecting screen to form the web. The fibers in the web are held together by a combination of entanglement and self-bonding providing sufficient cohesion of the melt blown web in many applications. Additional calender bonding may be required in some special cases.

Microfibers with an average fiber diameter of 1-5 microns, offer high a surface area and small pores in the web structure, which gives the nonwoven fabric good thermo-insulating properties and filtration efficiency. Melt blown nonwovens may vary in basis weight from 8 to 350g/m^2 depending on the intended application. Melt

blown products cover a wide range of applications including: protective apparels, thermal insulators, filtration materials, baby diapers, battery barriers, industrial wipes, and respirators. [3]

§1.3 MOTIVATION FOR THE PRESENTED WORK

Measurement of rheological properties of polymeric materials is very important for many reasons. Knowledge of their values will be helpful to formulate the polymer system that would best provide a particular set of physical properties desired for the final products. Knowledge of these properties also helps one to choose the appropriate processing equipment because the rheological properties are intimately related to the processing conditions.

Rheological properties can be measured by rheometers that are typically classified as off-line, online and in-line types according to how they are installed. Off-line rheometry involves the use of specialized testing equipment to measure polymer melt rheology at a site remote from the processing operation, such as a polymer characterization facility, which has become a standard for academic and industry research due to the accurate and repeatable results. However, this off-line polymer melt characterization may add a further temperature history or strain to the material and a significant time delay involved in performing the test, which results in slower feedback of information to the processing operation. Online and in-line rheometers are tools that have the potential to characterize the flow behavior of polymer melts and solutions during processing, thereby reducing time delays

involved in performing the test. Also the information provided might be more indicative of the processing behavior of the polymer and the properties of the product since it is derived from a melt that has an identical or similar processing history to that of final product. The roles of online and in-line rheometry is expanding in academic and industrial research. Rheological data can be used to determine the properties of a polymer under processing; also those data can be readily used for process monitoring, quality control, and automatic process control or process optimization. An objective of the present work is development of an online rheometer to determine the rheological properties of polymer melt during melt blowing.

In this research, rheological properties of two melt blowing grades of PP from ExxonMobil chemicals were measured. The rheological properties of these polymers were applied in a fundamental investigation of the melt blowing process. Other tools such as a high resolution infrared camera and differential scanning calorimeter (DSC) were used to explore processing/structure/property relationships in the melt blowing process. An online rheological sensor was being developed to measure shear viscosity and elongational viscosity simultaneously. The online measurement and control system was based on the National Instruments Labview platform. A laptop with a RS485 serial interface was dedicated to the online rheological measurements. The online sensor was installed on a twin-screw extruder for the demonstration and will be used for the online measurements on a 6-inch melt blowing line in the near future.

CHAPTER 2

LITERATURE REVIEW

§2.1 RHEOLOGICAL MEASUREMENTS

Rheological properties are determined by molecular structure. As a result differences in molecular structure can often be identified using rheological measurements. Structure differences that can be identified with polymer melts are: molecular weight, molecular weight distribution, long chain branching, cross linking, and the dispersion of fillers and these variables affect the processing of polymers and the properties of final products. Thus molecular structure determines rheological properties and rheological properties determine processing behavior. In the polymer processing industry, more and more stringent control on properties relevant to the precision and geometric stability of products is required. Much research has emphasized quality control. The molecular orientation of a polymer extrudate is dependent on the viscosity of the melt under processing and the mechanical properties of the extrudate are influenced by the molecular orientation. Polymer rheology plays a very important role in quality control and testing [4-9].

A rheometer must have a number of important requirements in its design to be used as a process sensor. There are several practical issues dealing with the instrument's installation, use and maintenance and theoretical issues that affect the instrument's reliability. There are also important performance issues that affect an

instrument's usefulness in real-time applications. A sensor must be robust, requiring little maintenance and must operate at the process pressures with negligible leakage. The sensor output signal should be directly related to a well-defined rheological property. A sensor must produce a reliable signal, be reasonably free of noise and the sensor must react with a minimum of delay.

§2.1.1 Measuring the shear viscosity

2.1.1.1 Capillary rheometer

Capillary rheometers are the most popular of all rheometers, because of their simplicity in construction and use. The basic element of a viscosity measurement is the measurement of the pressure drop for a given flow rate. Alternatively, one can fix the pressure drop and measure the flow rate.

For fully developed flow in a tube, i.e. far from the entrance, the pressure gradient and the velocity profile do not change with distance, z, along the tube. By carrying out a force balance on a length, Δz, of tube, it can be shown that the shear stress at the wall, σ_w, is related to the pressure p_1, p_2, at the upstream and downstream ends, of this length, and to the radius R of the tube [68].

$$\sigma_w = \frac{(p_1 - p_2)R}{2\Delta z} \tag{2.1}$$

This schematic of a rheometer is shown in Figure 2.1.

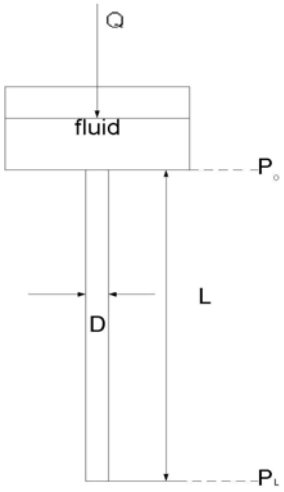

Figure 2.1. Sketch of Capillary Rheometer Geometry.

However, the more common procedure is to measure only the driving pressure p_d, in the reservoir feeding the tube rather than measure pressure at the two points in fully developed flow region. Then if the pressure at the exit of the tube, i.e. at $z = L$, is atmospheric, and this is assumed to be small compared to p_d, an apparent wall shear stress can be calculated

$$\sigma_A = \frac{p_d R}{2L} \tag{2.2}$$

For a Newtonian fluid, the velocity profile is parabolic, and the shear rate at the wall can be given by

$$\dot{\gamma}_w = \frac{4Q}{\pi R^3} \tag{2.3}$$

Thus, if Q is fixed and p_d is measured, the viscosity can be calculated from

$$\eta = \frac{\sigma_w}{\dot{\gamma}_w} = \frac{\pi R^4 p_d}{8LQ} \tag{2.4}$$

If the fluid is non-Newtonian, i.e. if the viscosity depends on the shear rate, there is a technique that can be used to determine the true wall shear rate in such a case, but it requires the differentiation of pressure data for a number of flow rates. In this case it is convenient to define an apparent wall shear rate as follows:

$$\dot{\gamma}_A \equiv \frac{4Q}{\pi R^3} \tag{2.5}$$

For the power law fluid, the true wall shear rate is given by:

$$\dot{\gamma}_w = \frac{3n+1}{4n}\dot{\gamma}_A \tag{2.6}$$

The value of n can be significantly different from 1 for many materials, so the difference between $\dot{\gamma}_A$ and $\dot{\gamma}_w$ can be large. Most capillary viscometers give as an output signal an "apparent viscosity" calculated as follow:

$$\eta_A = \frac{\sigma_A}{\dot{\gamma}_A} = \frac{\pi p_d R^4}{8LQ} \tag{2.7}$$

2.1.1.2 Slit rheometer

A slit is a rectangular flow channel with a rather large ratio of width to height. The flow can be considered to be two dimensional, which makes the equations needed to be calculated rheological properties no more complicated than those for capillary flow. The equations presented here are valid for a slit with a large aspect ratio, i.e. w/h, where w is the width and h the height. An aspect ratio of 10 is usually adequate for reasonable accuracy of the equations. For fully developed flow,

i.e. away from the entrance, the magnitude of the wall shear stress is related to the pressure drop as follows:

$$\sigma_w = \frac{(p_1 - p_2)h}{2L} \tag{2.7}$$

If the total driving pressure is measured rather than two pressures in the fully developed flow region, the pressure gradient corresponding to fully developed flow can only be determined if the entrance pressure drop is known. The situation is exactly analogous to that for a capillary rheometer. This flow geometry is illustrated in Figure 2.2.

For a Newtonian fluid, the magnitude of shear rate at the wall is

$$\dot{\gamma}_w = \frac{6Q}{h^2 w} \tag{2.8}$$

Thus, for a Newtonian fluid, the viscosity is

$$\eta = \frac{\sigma_w}{\dot{\gamma}_w} = \frac{(p_1 - p_2)h^3 w}{12QL} \tag{2.9}$$

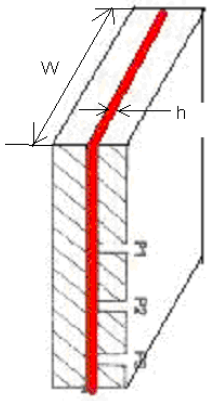

Figure 2.2. Sketch of Slit Rheometer Geometry.

2.1.1.3 Parallel disk rheometer

This flow geometry is illustrated in Figure 2.3. The shear rate varies linearly with r and is given by

$$\dot{\gamma} = \Omega r / h \tag{2.10}$$

where h is the gap between the disks, and Ω is the rotational velocity. For a Newtonian fluid, the viscosity is related to the torque as follow:

$$\eta = 2Mh/(\pi\Omega R^4) \tag{2.11}$$

where R is the radius of the disk and M is the measured torque.

Cone-and plate geometry is of special interest because the shear rate is approximately constant between the fixtures and given by

$$\dot{\gamma} = \Omega / \theta \tag{2.12}$$

Where θ is the cone angle, usually less than 5°, and Ω is the angular velocity. For the ideal geometry shown in Figure 2.4, the apex of the cone just touches the plate without transmitting torque to it.

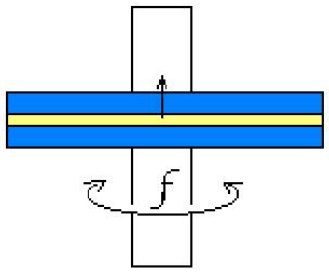

Figure 2.3. Sketch of Parallel Disk Rheometer Geometry.

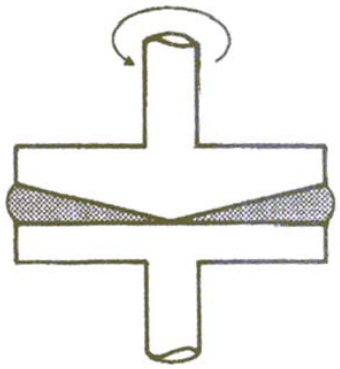

Figure 2.4. Sketch of Cone and Plate Geometry.

The shear stress is therefore also approximately uniform and is given by

$$\sigma = \frac{3M}{2\pi R^3} \tag{2.13}$$

Where M is the torque to turn the cone and R is the radius of the plate.

Thus, the viscosity is

$$\eta = \frac{3M\theta}{2\pi\Omega R^3} \tag{2.13}$$

Because of the uniformity of the shear rate, it is valid for non-Newtonian fluids.

§2.1.2 Measuring the elongational viscosity

It is generally agreed that it is far more difficult to measure elongational viscosity than shear viscosity, especially for polymer melts and solutions. The problem is not only producing a uniaxial elongational flow, but also maintaining the flow for a sufficient time for the stress or the strain rate to reach a steady state, thus enabling the steady elongational viscosity to be determined. There are several

different methods to measure the elongational viscosity of polymer melts and solutions, which can be mainly classified as homogeneous stretching methods, constant stress devices, contraction flow devices, and spinning techniques.

2.1.2.1 Homogeneous stretching method to measure elongational viscosity

The basic concept of the homogeneous stretching method is that a polymer sample is held between a stationary block and a movable block and the relationship between the stress and strain, corresponding to the elongational viscosity is determined. The work of Meissner [10-15] was pioneering in this method. A schematic diagram of the Meissner's apparatus is shown in Figure 2.5.

When the velocity of the movable block increases exponentially with time, a constant elongational strain rate in the sample can be obtained. In preparation a test specimen is melted and brought to test temperature in a bath of silicon oil. The molten specimen floating on this bath is clamped in two pairs of gears, which have a constant separation distance and rotate at an exponentially increasing speed to deform the specimen at constant elongational strain rate. The stress is measured by the deflection of a spring associated with one pair of rollers. Meissner's method has some disadvantages. In principle, control of the elongational strain rate can be accomplished with the most recent electronic-control techniques, but the accelerating motion of the clamp places a severe constraint on the strain rates that can be attained, given the requirement that the motion must be sustained for a sufficient time for the stress to reach a steady state value.

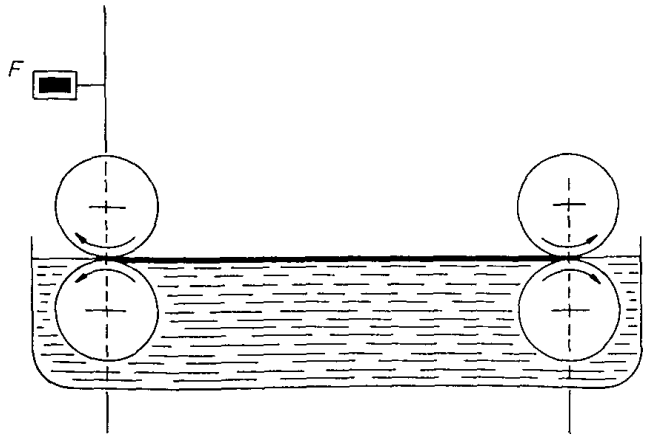

Figure 2.5. Schematic Plot of the Homogeneous Stretching Method.

Also this method is restricted to high-viscosity materials because the sample has to be held in a horizontal position in an oil bath, and the combination of force measurement and drawing will cause some experimental difficulties.

2.1.2.2 Constant stress devices

Cogswell [16] first introduced the technique of a constant stress device to measure elongational viscosity of polymer melts. In this method, the specimen is stretched at a constant stress, which is set by adjusting the applied force as the sample elongates. Cogswell achieved this using a cam to apply a programmed load, along with a convenient means of measuring the length of the sample as a function of time. Münstedt [17] further developed this method later. He designed an apparatus that can be operated at constant stretching rate, as well as at constant stress. In the Münstedt apparatus, the sample is vertically suspended in an oil bath, which is

heated by oil flowing through the hollow walls of the glass vessel. One end of the sample is fixed to a load cell located in the oil bath and its other end is fixed to a thin metal tape, which can be rolled up by a disk. The disk is mounted to the shaft of an extremely rapid DC motor. A displacement transducer serves as an indicator of the sample position. Its signals recorded as a function of time give a direct measurement of the elongation of the sample. Figure 2.6 shows the schematic drawing of this apparatus.

For experiments at constant stretching rate, the elongational strain rate is given as

$$\dot{\varepsilon}_0 = \frac{d\varepsilon}{dt} = \frac{d \ln l / l_0}{dt}, \tag{2.14}$$

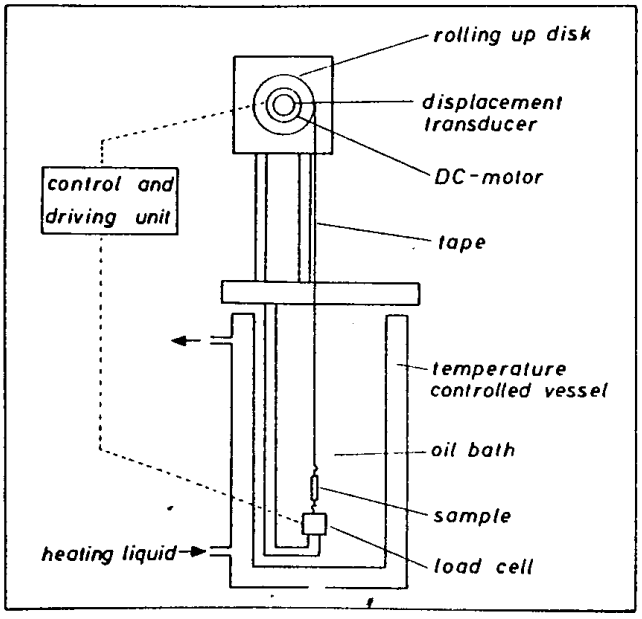

Figure 2.6. Schematic of the Constant Stress Extensional Rheometer [17].

The sample length *l(t)* at any time *t* has to be regulated according to

$$l(t) = \dot{\varepsilon}_0 \int_o^t l dt + l_0, \tag{2.15}$$

where l_0 is the initial length of the sample. Equation (2.15) is fed to a stretching rate controller, which calculates and performs the stretching rate (an exponentially increasing take up speed). The measured and the calculated position values are fed to a position control unit, which regulates the driving motor in such a way that the deviation between these two quantities is very small. The actual stress σ is calculated according to

$$\sigma = \frac{Fl}{A_0 l_0}, \tag{2.16}$$

where A_0 is the initial cross section area of the sample and F, the measured force. In a 'constant stress' experiment ($\sigma = \sigma_0$), the sample has to be elongated according to

$$l(t) = \sigma_0 A_0 l_0 / F, \tag{2.17}$$

The steady state elongational viscosity is given as

$$\eta_{es} = \sigma_0 / \dot{\varepsilon}_0 \tag{2.18}$$

Using the unique extensional rheometer, the elongational rheology of polyethylene, LLDPE , polypropylene, and polystyrene has been studied [18-23].

The homogeneous stretching method and the constant stress method are direct methods for the measurement of polymer melt elongational viscosity. But these two approaches have their limitations. A polymer melt that is a viscoelastic material takes time to reach dynamic equilibrium. When subjected to constant rate of

strain it takes a longer time and a larger deformation to complete the equilibrium than when the controlling feature is constant stress. Another big problem with the Meissner type device is the sagging of the melt under its own weight, so its application is limited to polymeric melts with high viscosities. Also, the sample has to be extremely homogeneous, as any small defect or weakness in the sample can cause a neck formation during stretching and thus significantly affect the test results. Using the constant stress approach, elongational flow measurements on crystalline polymers are carried out just below their melting points when they are readily deformable, but most of applications need the elongational viscosity at a high temperature in the molten state. The elongational viscosity of completely molten polymers, which can be quite different from that of partially crystalline materials, cannot be measured in this fashion due to the experimental limitations of this method.

2.1.2.3 Converging flow and elongational flow

Cogswell[18] proposed an indirect method for measurement of elongational viscosity of polymer melts using converging flows in order to overcome the difficulties and the limitations of the direct measurement methods. Cogswell proposed that such a flow field could be interpreted as an elongational deformation superposed onto a simple shear flow when the fluid flows from a reservoir into a die where the streamlines converge. According to Cogswell, the shearing component and the elongational component can be treated separately and added to give the total

flow, so the elongational viscosity can be measured by using capillary rheometry to study the simple shear component in isolation [16]. Numerous research projects on polymer rheology have been done in this research group and the elongational viscosity of polymer melts or solutions have been characterized by using a semi-hyperbolic die [24-26]. The method for the characterization of elongational viscosity initially involved the co-extrusion of a PP core with a polyethylene skin, where the skin with a much lower viscosity acted as a lubricating layer to dissipate shearing effects at the wall. Using hyperbolic dies, measurements showed that the core was essentially in purely elongational flow at constant strain rate. It was found that orientation-developing effects of the melt are so substantial that shearing gradients near the wall become comparatively insignificant later. This discovery was justified by developing stream functions expressing the hyperbolic flow convergence and potential functions describing the pressure profiles as the driving force theoretically. Figure 2.7 shows the semi-hyperbolic die and ACER.

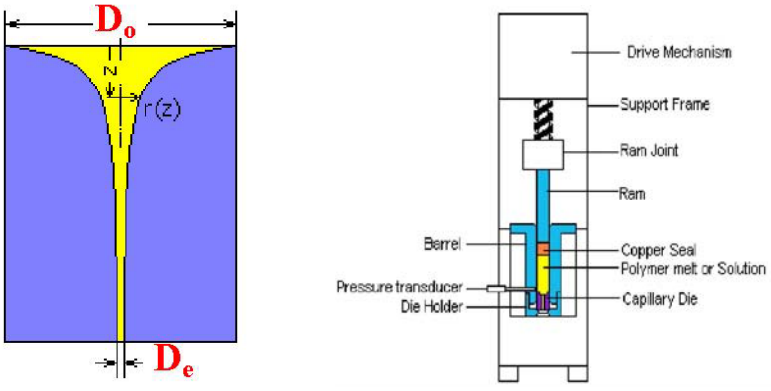

Figure 2.7. Schematic Diagram of the Semi-hyperbolic Die and ACER.

The Advanced Capillary Extrusion Rheometer (ACER) is a state-of-the-art capillary rheometer manufactured by Rheometric Scientific Inc and bought by Thermo Electron Corp. as shown in Figure 2.7 schematically. The ACER melts and extrudes samples through a capillary die and calculates an apparent viscosity for polymer or polymeric solutions. The extrusion of the melt or solution is accomplished by a ram, whose movement can be controlled at constant velocity through a precisely bored cylindrical barrel of certain diameter. From the barrel serving as a reservoir the melt enters the die with known length and diameter. Pressure transducers located just above the entrance of the die measures the melt pressure and transform the pressure into an electronic signal. The communication between the transducer and the computer has been set up by a special designed interface. The pressure values are displayed against the time continuously and updated on the computer screen, so a measurement at a set strain rate can be completed when the pressure has reached a steady state by checking the slope of pressure. The instrument has been running a fully automatic control at a constant strain rate operation. The elongation viscosity can be measured by setting the strain rates and the barrel and die dimension using the following equations when a semi-hyperbolic die is substituted for the capillary die [24-26].

$$\dot{\varepsilon} = \left(v_0 / L\right)\left(\exp \varepsilon_H - 1\right) \tag{2.19}$$

$$\eta_{eff} \equiv \frac{\Delta P}{\dot{\varepsilon}\varepsilon_H} \tag{2.20}$$

§2.1.3 Online rheometers

Online methods eliminate the flow interruption and contamination problem by performing tests on a side stream, which could be produced by a gear pump drawing the polymer melt from the main stream. The side stream also allows better temperature control and permits control of shear rate or frequency independent of the process. There are several approaches for online measurements by using different flow geometries, such as capillary, slit, rotary and oscillatory plates etc [27-30].

2.1.3.1 Online capillary rheometer

Figure 2.8 shows two typical online capillary rheometers, which contain two very important parts, gear pump and capillary die. The rheometer can be mounted on a single or twin-screw extruder between the screw and processing die. The gear pump draws the polymer melt from the main stream and controls the flow rate through the capillary die; a pressure transducer is used to record the pressure change during different flow rates. The rheological property can be calculated by adapting the method used by the off-line capillary rheometer.

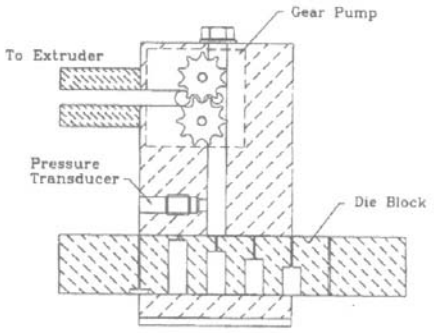

Figure 2.8. Schematic Diagram of Capillary Online Rheometer [30,32].

2.1.3.2 Online slit rheometer

Two slit rheometer methods are currently being studied. Figure 2.9 illustrates the rheometer system which uses three flush mounted pressure transducer along the slit [33]. The gear pump again gives the flow rate, which operates on a side stream and does not interrupt the process. The slit geometry is advantageous because the transducer can be readily mounted flush. Figure 2.9 is illustrating a slit rheometer, which uses pressure measurement at two points along the slit to determine the viscosity and a recessed transducer to determine normal stress difference. Due to curvature of the streamlines into the hole, normal stresses cause the reading on the recessed transducer to be lower than the opposite flush mounted one. However the sensitivity to normal stress difference is a bit low, the technique has required a delicate capacitive transducer and balancing methods to measure the pressure differences accurately. It has been more successful with polymer solution than melts.

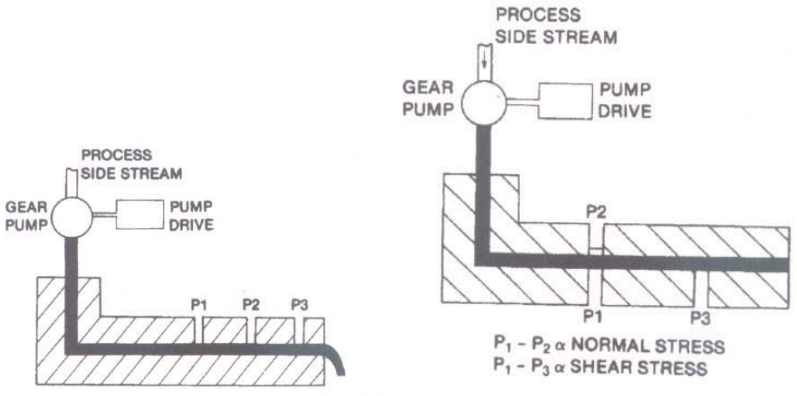

Figure 2.9 Schematic Diagram of Online Slit Rheometer [33].

2.1.3.3 Online oscillatory rheometer

The oscillatory (or dynamic) method is an approach used extensively in the field of rheology as an off-line technique for the study of the viscoelastic properties of polymers. Figure 2.10 shows how an online oscillatory rheometer works [33]. The main advantage of the oscillatory method is that it yields the linear viscoelastic spectrum directly. Measurements can be made from 0.01 to 500 radians/s, independent of process rates. The flow of the sample through the test chamber makes it self-cleaning, which minimizes maintenance. The technique allows measurements to be made with a given sample flowing continuously; the flow is controlled by the gear pump. The disadvantage of this method is that a separate motor is required for the characterization.

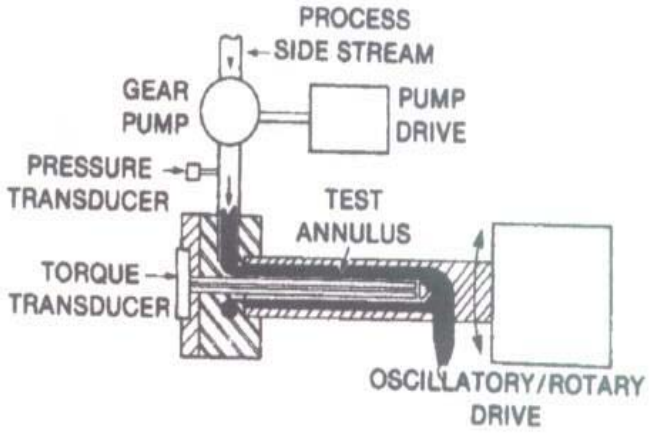

Figure 2.10 Schematic Diagram of Online Oscillatory Rheometer [33].

§2.2 MELT BLOWING PROCESS AND PROCESS MODELING

§2.2.1 Experimental study on melt blowing process

The melt blowing process is an ingenious method used in the production of nonwoven materials capable of producing microfibers in the one to five micron ranges. It is widely accepted that melt blowing is a complicated process involving many factors that contribute to the final fiber and web properties. Crystallinity, tensile strength, hydro head, filtration efficiency and average diameter are several of web characteristics, which can be incorporated into experimental investigation. The web properties have been shown to be strong functions of the fiber diameter. Polymer type, polymer grade, polymer melt temperature, polymer throughput, airflow rate, air temperature and die-to-collector distance are among the most important parameters for a specified product line.

Malkan [35] conducted a thorough study on the effects of molecular weight of PP, polymer throughput, airflow rates on the melt blown web properties. He found that the overall average fiber diameter increased with the polymer throughput regardless the average molecular weight, if airflow rate was not proportionally increased. He reported the polymer throughput had a significant effect on physical and morphological properties.

Straeffer and Goswami [36] found that an increase in air velocity or decrease in polymer throughput resulted in small diameter fibers. A very interesting discovery was that the fiber diameter distribution became narrow when the air jet velocities

were high. There did not exist a peak in the fiber diameter distribution at the lowest air jet velocity according to their experiments.

Khan [37] conducted extensive investigations of the effects of die geometry and process variables, including polymer throughput, nose tip setback, die orifice diameter and the orifice L/D ratio, air velocity and momentum on fiber diameter and quality of melt blown PP nonwovens. He found that the orifice diameter, orifice L/D ratio, PP resin MFR, air gap and polymer throughput all had a significant effect on the average fiber diameter. Khan found that the average fiber diameter decreased as the polymer throughput increased under the condition of constant mass ratio of polymer and hot air. His explanation was that the momentum acting on the fiber increased with an increase in the overall air velocity, also the filament quenching was reduced due to the increased polymer throughput, thus, the hot filaments was attenuated further to produce finer fiber. Within the measurement range (DCD from 8 to 25 inches), the DCD did not appear to affect the average fiber diameter.

Wadsworth et al [34,38] studied the effects of processing temperature, airflow rate, and die-to-collector distance on the web structure and filtration properties. They found that an increase in melt temperature or airflow rate improved the filtration efficiency due to a decrease in the fiber diameter. They did not find any significant change in fiber diameter with the collection distance.

Shambaugh et al [39] investigated the effect of polymer throughput, polymer temperature, airflow rate and air temperature on fiber diameter, crystallinity and strength using a circular die with an annular air jet surrounding the die. They found

that a small air nozzle diameter produced small fiber diameter when a constant flow rate of air and polymer are maintained. At a constant flux of air and polymer, high polymer throughput resulted in large fiber diameter. They applied over 4000 individual fiber diameters measurements to fit a power-law equation, which is useful in exploring the behavior of melt blowing processing, such as operation variables on the fiber diameter and to predict the suitable airflow rate to a specified fiber diameter. The equation is as follows,

$$d_f[\frac{d_{1,0}}{d_1}]^{1.25}[\frac{d_2}{d_{2,0}}]^{0.63}[\frac{M_{p,0}}{M_p}]^{0.47} = 38.1\psi^{-0.563} \tag{2.20}$$

where, d_f, average fiber diameter, μm

d_1, d_2, capillary and annulus inside diameter, mm

$d_{1,0}$, $d_{2,0}$, capillary and annulus references, mm

M_p, polymer mass flow rate, $g/\min$

$M_{p,0}$, polymer mass flow rate reference, $g/\min$

ψ, the mass flux ratio of air to polymer.

Milligan et al [40, 41] conducted experiments and fundamental research on melt blowing based on a single hole die. An empirical relationship for the melt blowing process was developed based on a large data set obtained under different processing conditions, which expresses the fiber diameter as a function of dimensionless independent variables. Several dimensionless parameters were defined to better describe the MB process, such as diameter ratio, δ, defined as the final

average fiber diameter divided by the die orifice diameter; momentum flux ratio, ψ, defined as the air momentum per unit of air exit area divided by the polymer momentum per unit of polymer exit area; mass flux ratio, Γ, defined as the air mass flow rate per unit of exit area divided by the polymer mass flow rate per unit of polymer exit area; polymer throughput ratio, β, defined as the mass flow rate of polymer divided by a reference mass flow rate of polymer, 0.8g/min/hole; polymer temperature ratio, θ, defined as the polymer temperature divided by a reference polymer temperature, $500^{o}F$; air temperature ratio, ξ, defined as the air stagnation temperature in the die divided by a reference die stagnation temperature, $375^{o}F$; and die face width ratio, φ, defined as the die face air width divided by a reference die face air width, $2.67mm$. Using these variables with the diameter ratio as the dependent variable statistical software, SAS, was used to perform regression analyses and statistical analyses of the experimental data expresses in the terms of dimensionless parameters. A modeling equation developed from a data set of 270 processing conditions was given as,

$$\delta = 0.0047 + 0.0149\Gamma^{-1.49}\beta^{-0.65}\varphi^{-1.12}\theta^{-3.47}\xi^{-0.92} \tag{2.21}$$

The applicability of empirical correlations to a multi hole die was examined, by keeping the exponents of the dimensionless parameters, but changing the two constants in the equations. This model was used to analyze the data obtained on the 6 inch pilot MB line at the University of Tennessee. The actual data showed agreement

with the model predictions. They recommended the following general equation to describe the common melt blowing process.

$$\delta = C_1 + C_2 \Gamma^{-1.49} \beta^{-0.65} \varphi^{-1.12} \theta^{-3.47} \xi^{-0.92} \tag{2.22}$$

where C_1 and C_2 would be determined for the particular melt blowing line and polymer in question by evaluating the constants at two different airflow rate. The model provided a pretty good tool to determine the fiber diameter for melt blowing processes and it is the variation of fiber diameter with the processing variables, such as throughput, polymer temperature, air temperature, and air flow rate, which is needed for process control.

Bresee [42-44] et al conducted some experimental investigations of melt blowing processing using high-speed digital imaging techniques. They reported that fiber attenuation occurred extremely rapidly close to the die where the mean fiber diameter was reduced to about 15% its original size after fiber traveled only about 7mm from the die. This indicates that fibers are very easily deformable and large elongational forces exist very close to the die. The fiber attenuation continued to occur all the way to the collector where drag forces are expected to be relative small.

§2.2.2 Theoretical modeling study on melt blowing process

Most of experimental studies are deficient in a thorough understanding of the physics involved in the melt blowing processing. A thorough understanding of the melt blowing process would help industry in many ways. For example, the process could be optimized, and properties of the products could be improved. Analytical

modeling can help us to understand the processing, but modeling the melt blowing process is lacking of publications compared to the modeling of ordinary melt spinning technology. The reason that melt blowing has not received much attention is the hidden complexities associated with the boundary conditions and appropriate modeling of the aerodynamic drag, heat transfer and viscoelastic properties of the polymer.

Shambaugh et al [45-48] did some fundamental investigations to help understand the melt blowing process and conducted a study on the macroscopic view of the melt blowing process. He performed a dimensional analysis, which yield various dimensionless groups, such as polymer and air Reynolds number, and Prandtl number.[49]

Uyttendaele and Shambaugh [50, 51] developed a model for steady polymeric melt blowing with a single-hole, concentric die by following earlier studies of conventional melt spinning. The momentum and mass conservation equations were assumed over the fiber cross-section. These average equations were assumed accurate at the locations beyond the die swell. Continuity, momentum and energy equations were applied for the fiber spinline only and the surrounding air temperature and velocity were taken as the boundary conditions to solve the equations. These equations are summarized as follows.

The application of the continuity equation to the spinline gives,

$$A_z \upsilon_{fz} = Q = const. \tag{2.23}$$

where, A_z, fiber cross section area; υ_{fz}, axial fiber velocity; Q, volumetric polymer flow rate. Implicit in this equation is the constancy of the polymer density. This assumption is not inaccurate because the polymer density changes only about 10% between the molten state at the spinneret temperatures and the solidification point.

The differential form of the momentum equation is given as,

$$\frac{d}{dz}[\pi \frac{d_z^2}{4}(\tau_{zz} - \tau_{xx})] = j\pi d_z C_f \rho_a \frac{\upsilon_{rel}^2}{2} + \rho_f Q \frac{d}{dz}\upsilon_{fz} - \frac{\pi d_z^2}{4}\rho_f g \qquad (2.24)$$

where, z is the axial position; τ_{zz} and τ_{xx} are components of the extra stress in the spinning and transverse directions respectively; C_f is air drag coefficient; ρ_a, ρ_f are densities of air and fiber respectively; d_z is fiber diameter; υ_{rel} is the velocity difference between the fiber and air; and g is the gravitational acceleration. The j factor accounts for the fact that, near the spinneret, the air exerts a positive force on the fiber and $j = 1$; but further down the threadline the force exerted by the air is negative and $j = -1$. The drag coefficient was correlated by Matsui with the relation [51],

$$C_f = \beta(\mathrm{Re}_{rel})^{-n} \qquad (2.24)$$

for melt blowing, the Re_{rel} is defined as

$$\mathrm{Re}_{rel} = \frac{d_z \upsilon_{rel}}{\nu_{az}} \qquad (2.26)$$

The equation of energy is given as

$$\rho_f C_{pf} \upsilon_{fz} \frac{d}{dz} T_{fz} = -\frac{4h_z}{d_z}(T_{fz} - T_{az}) \tag{2.27}$$

where ν_{az} is the air viscosity; h_z is the convective heat transfer coefficient; T_{fz} is the fiber temperature; T_{az} is the air temperature; and C_{pf} is the heat capacity of fiber.

The Newtonian fluid model and the Phan-Tien and Tanner rheological model were applied to describe the relationship between stress tensor and velocity gradient, so these equations can describe the mechanical and thermal history of a viscoelastic fluid in the melt blowing process. In the modeling of the melt blowing process, the dependence of the viscosity on the temperature is of primary importance, while the predictions of fiber diameter profiles from the both Newtonian and Phan-Tien-Tanner models did not show significant difference between the models. The model provided excellent predictions of fiber profile in the region of high fiber attenuation, which is very close to the die tip. However, the prediction of final fiber diameters are 10% ~ 20% higher than the actual measurements [51].

Haynes [52] also did an extensive experimental investigation on the production of microfiber using a single hole melt blowing process. An analytical model that was similar to existing melt spinning models was developed. This model had the ability to predict relative changes in fiber diameter for variations in air jet velocity, polymer throughput, and processing temperature. The model predicted general trends for varying processing conditions but predicted a larger fiber diameter consistently, which agreed well with the results from Shambaugh. Their general modeling principle was from the fluid mechanical and aerodynamics.

The modeling of the melt blowing process can be thought to be successful, however there are some problem with solving the equations, in other words, how to determine the boundary conditions, such as, where is the fiber-frozen point, and what is the crystallization onset temperature. Also the modeling of the melt blowing process cannot predict the properties of final nonwoven products.

CHAPTER 3

THEORETICAL BACKGROUND FOR DATA ACQUISITION

Experimentally observed phenomena must be translated into mathematical expressions to be applicable in practice. Besides the intrinsic mathematical interest of the problems it presents, there are two primary reasons for the development of a theory. The first is to generalize the experimentally observed flow behavior in terms of material parameters that may be determined by independent experiments. The second is to formulate the flow problem in a way for which it is possible to predict the unobserved flow. In order to accomplish these objectives, it is necessary to understand the fundamental concepts of fluid dynamics, heat transfer, and mass transfer. The basic equations describing flow are the equations of continuity (mass balance), motion (momentum balance), and energy (energy balance), as following [24], Mass balance:

$$\frac{D\rho}{Dt} = -\rho[\nabla \cdot \boldsymbol{v}] \tag{3.1}$$

Momentum balance:

$$\rho \frac{D}{Dt}\boldsymbol{v} = -(\nabla P) + \left[\nabla \cdot \boldsymbol{\tau}\right] + \rho \boldsymbol{b} \tag{3.2}$$

Energy balance:

$$\rho \frac{D\hat{H}}{Dt} = -\left(\nabla \cdot q\right) + \left(\tau : \nabla v\right) + \frac{DP}{Dt} \tag{3.3}$$

Where τ, a second-order tensor, denotes the stress, first-order tensor v and q denote velocity and energy flux respectively, and b denotes the body force term [25]. Also the theoretical analysis of the flow in different geometries is the foundation of the design of an online rheological sensor.

§3.1 ANALYSIS OF FLOW IN THE CAPILLARY DIE

The capillary die rheometer is one of the simplest and most widely used instruments for rheological characterization. Figure 2.1 shows the flow in a capillary for rheometers, in which a fluid is forced at the steady rate from a large reservoir into a small diameter capillary tube of length L.

Assume steady, isothermal flow of an incompressible fluid and $L/R >> 1$. Applying the equation of motion in cylindrical coordinates, (r,θ,z), the equation of motion can be written as following,

$$\rho(\frac{\partial v_r}{\partial t} + v_r \frac{\partial v_r}{\partial r} + \frac{v_\theta}{r}\frac{\partial v_r}{\partial \theta} + v_z \frac{\partial v_r}{\partial z} - \frac{v_\theta^2}{r}) = -\frac{\partial p}{\partial r} - [\frac{1}{r}\frac{\partial}{\partial r}(r\tau_{rr}) + \frac{1}{r}\frac{\partial}{\partial \theta}\tau_{\theta r} + \frac{\partial}{\partial z}\tau_{zr} - \frac{\tau_{\theta\theta}}{r}] + \rho g_r \tag{3.4}$$

$$\rho(\frac{\partial v_\theta}{\partial t} + v_r \frac{\partial v_\theta}{\partial r} + \frac{v_\theta}{r}\frac{\partial v_\theta}{\partial \theta} + v_z \frac{\partial v_\theta}{\partial z} + \frac{v_r v_\theta}{r}) = -\frac{1}{r}\frac{\partial p}{\partial r} - [\frac{1}{r^2}\frac{\partial}{\partial r}(r^2\tau_{r\theta}) + \frac{1}{r}\frac{\partial}{\partial \theta}\tau_{\theta\theta} + \frac{\partial}{\partial z}\tau_{z\theta} - \frac{\tau_{r\theta} - \tau_{\theta r}}{r}] + \rho g_\theta \tag{3.5}$$

$$\rho(\frac{\partial v_z}{\partial t} + v_r \frac{\partial v_z}{\partial r} + \frac{v_\theta}{r}\frac{\partial v_z}{\partial \theta} + v_z \frac{\partial v_z}{\partial z}) = -\frac{\partial p}{\partial z} - [\frac{1}{r}\frac{\partial}{\partial r}(r\tau_{rz}) + \frac{1}{r}\frac{\partial}{\partial \theta}\tau_{\theta z} + \frac{\partial}{\partial r}\tau_{zz}] + \rho g_z \tag{3.6}$$

If the entrance and exit losses in the capillary tube are ignored, then we postulate

1 $v_\theta = 0; v_r = 0$, and $v_z = f(r)$

2 the flow region is laminar

3 the density is constant

4 the fluid is Newtonian

5 there is no slip at the wall

6 the flow behaves as continuum

By inserting Newton's law of viscosity,

$$\tau_{zr} = \tau_{rz} = -\mu[\frac{\partial v_r}{\partial z} + \frac{\partial v_z}{\partial r}] \tag{3.7}$$

The $z-$equation of motion reduces to

$$\mu \frac{1}{r}\frac{d}{dr}(r\frac{dv_z}{dr}) = c_0 = \frac{dp}{dz} \tag{3.8}$$

The p equation can be integrated at once. The v_z equation can be integrated by merely peeling off one operation after another on the left side. This gives

$$p = c_0 z + c_1 \tag{3.9}$$

$$v_z = \frac{c_0}{4\mu} r^2 + c_2 \ln r + c_3 \tag{3.10}$$

The four constants of integration can be found from the boundary conditions:

B.C.1 at $z = 0, p = p_0$

B.C.2 at $z = L, p = p_L$

B.C.3 at $r = R, v_z = 0$

B.C.4 at $r = 0, v_z = \textit{finite}$

The resulting solutions are:

$$p = p_0 - (p_0 - p_L)(z/L) \tag{3.11}$$

$$v_z = \frac{(p_0 - p_L)}{4\mu L}[R^2 - r^2] = \frac{\Delta p}{4\mu L}(R^2 - r^2) \tag{3.12}$$

Once the velocity profile has been established, various derived quantities can be obtained:

The volumetric flow rate Q is obtained by integrating the velocity on the cross section of the capillary.

$$Q = \int_0^R 2\pi r v_z dr = \frac{\Delta p \pi R^4}{8\mu L} \tag{3.13}$$

The shear rate can be obtained by derivation of the velocity equation:

$$\dot{\gamma} = \frac{dv_z}{dr} = \frac{\Delta p r}{2\mu L} \tag{3.14}$$

So the shear rate at the wall of capillary becomes:

$$\dot{\gamma} = (\frac{dv_z}{dr})_{r=R} = (\frac{\Delta p r}{2\mu L})_{r=R} = \frac{4Q}{\pi R^3} \tag{3.15}$$

The shear stress at the wall of capillary becomes:

$$(\tau_{zr} = \tau_{rz})_{r=R} = -\mu[\frac{\partial v_r}{\partial z} + \frac{\partial v_z}{\partial r}]_{r=R} = -\frac{\Delta p}{2L} R \tag{3.16}$$

The viscosity is as following:

$$\mu = \frac{\Delta p \pi R^4}{8QL} \tag{3.17}$$

Finally these variables can be used to determine the shear stress, shear rate and viscosity and then to plot the flow curves, which are the basic information for the chemical engineering with flow process and property characterization.

For incompressible Newtonian fluids the expression for the stress tensor is given by,

$$\boldsymbol{\tau} = -\mu(\nabla \boldsymbol{v} + (\nabla \boldsymbol{v})^{+}) \equiv -\mu \boldsymbol{\gamma} \tag{3.18}$$

The generalized Newtonian fluid model can describe the non-Newtonian viscosity by simply replacing the constant viscosity μ by the non-Newtonian viscosity η, a function of the shear rate, which in general can be written as the magnitude of the rate of strain tensor. The generalized Newtonian fluid model is:

$$\boldsymbol{\tau} = -\eta(\nabla \boldsymbol{v} + (\nabla \boldsymbol{v})^{+}) \equiv -\eta \boldsymbol{\gamma} \quad \text{, with } \eta = \eta(\dot{\gamma}) \tag{3.19}$$

The simplest empiricism for $\eta(\dot{\gamma})$ is the two-parameter power law expression:

$$\eta = m\dot{\gamma}^{n-1} \tag{3.20}$$

in which m and n are constants characterizing the fluid. This simple relation describes the non-Newtonian viscosity curve over the linear portion of the log-log plot of the viscosity versus shear rate for many materials.

The expression of shear stress distribution for any fluid in developing steady flow in a capillary may be obtained as follow:

$$\tau_{rz} = -m\dot{\gamma}^{n-1}\frac{dv_z}{dr} \tag{3.21}$$

since v_z is postulated to be a function of r alone, and $\dot{\gamma} = \sqrt{\frac{1}{2}(\gamma : \gamma)} = \sqrt{(\frac{dv_z}{dr})^2}$,

since $\frac{dv_z}{dr}$ is negative in tube flow, so that

$$\tau_{rz} = -m(-\frac{dv_z}{dr})^{n-1}\frac{dv_z}{dr} = m(-\frac{dv_z}{dr})^n \tag{3.22}$$

By solving the equation of motion in the capillary when the no-slip boundary condition at $r = R$ is used, the velocity distribution can be obtained,

$$v_z = (\frac{\Delta pR}{2mL})^{1/n}\frac{R}{1/n+1}[1-(\frac{r}{R})^{1/n+1}] \tag{3.23}$$

When this is integrated over the cross section of the circular tube the volumetrical flow rate can be obtained.

$$Q = \frac{\pi R^3}{1/n+3}(\frac{\Delta pR}{2mL})^{1/n} \tag{3.24}$$

§3.2 ANALYSIS OF FLOW IN THE SEMI-HYPERBOLIC DIE

Elongational flow is the dominant mode of fluid flow when a rapid change of shape such as stretching is involved in the operation. Electrodischarge machined semi-hyperbolic dies were designed to generate a constant elongational strain rate throughout the core; to accomplish this, the flow channel decreases as $R^2 z = C$, where z is the axial flow direction, R is the radius of the flow channel, and C is a constant. This concept was implemented on an Advanced Capillary Extrusion Rheometer (ACER), by replacing the capillary die with a semi-hyperbolic die to

determine the uniaxial elongational viscosity of polymer. A sketch of a semi-hyperbolic die is shown in Figure 2.6.

The basic equations describing the flow are the equations of continuity, motion and energy. Solution of these equations for flow in two or three dimensions is more difficult to obtain. The basic procedure is similar to that shown in section 3.1: one solves simultaneously the equations of continuity and motion along with the appropriate initial and boundary conditions, to obtain pressure and velocity profiles. However, having both velocity and pressure as dependent variables in equation of motion presents more difficulty in multidimensional flow than in capillary flow. It is therefore frequently convenient to eliminate the pressure by taking the curl of the equation of motion, after making use of the vector identity $[\boldsymbol{v}\cdot\nabla\boldsymbol{v}\ ]=\frac{1}{2}\nabla(\boldsymbol{v}\cdot\boldsymbol{v}\ )-[\boldsymbol{v}\times[\nabla\times\boldsymbol{v}\ ]]$. For fluids of constant viscosity and density, the operation gives,

$$\frac{\partial}{\partial t}[\nabla\times\boldsymbol{v}\ ]-[\nabla\times[\boldsymbol{v}\ \times[\nabla\times\boldsymbol{v}\ ]]]=\nu\nabla^2[\nabla\times\boldsymbol{v}\ ] \tag{3.25}$$

This is the equation of change for the vorticity $\nabla\times\boldsymbol{v}$ [44]. For viscous flow problems one can then solve the vorticity equation together with the equation of continuity and relative initial and boundary conditions to give the velocity distribution. For axisymmetric flows the vorticity equation can be reformulated by introducing the stream function ψ. The stream function itself is not without interest. Surfaces of constant ψ contain the streamlines, which in steady-state flow are the

paths of fluid elements, the volumetric rate of flow between the surfaces $\psi = \psi_1$ and $\psi = \psi_2$ is proportional to $\psi_2 - \psi_1$. The vorticity equation may be simplified by omitting the term containing the kinematic viscosity. If, in addition, the flow is steady and two dimensional, then the vorticity $\nabla \times \boldsymbol{\nu}$ is constant along a streamline. The flow will be such that $\nabla \times \boldsymbol{\nu}$ will be zero throughout the entire flow field; that is, the flow will be irrotational. It is very convenient to introduce a velocity potential Φ to solve the problem of flow.

When the melt flows through the semi-hyperbolic channel it assumes the shape of the die surface; i.e., layers of the melt may be viewed as stream lines experiencing the same conditions. These streamlines can be described by the stream function, ψ, forming a two dimensional surface. The stream function is defined to satisfy the continuity equation, and in shear free flows the potential function Φ can also be defined to solve the flow problem [24-26]. In the cylindrical coordinates for the flow in a semi-hyperbolic converging die the stream function is given as:

$$\psi = -\frac{\dot{\varepsilon}}{2} r^2 z \tag{3.26}$$

and the potential function is given as:

$$\Phi = \dot{\varepsilon}\left(\frac{r^2}{4} - \frac{z^2}{2}\right) \tag{3.27}$$

with the pressure *P* as linear to $\rho\dot{\varepsilon}\Phi$, where $\dot{\varepsilon}$ is the elongational strain rate. The velocity components in cylindrical coordinates are:

$$v_z = -\frac{1}{r}\frac{\partial \psi}{\partial r} = -\frac{\partial \Phi}{\partial z} = \dot{\varepsilon} z \tag{3.28}$$

$$v_r = \frac{1}{r}\frac{\partial \psi}{\partial z} = -\frac{\partial \Phi}{\partial r} = -\frac{\dot{\varepsilon}}{2} r \tag{3.29}$$

As mentioned earlier, the semi-hyperbolic shape is one that provides a constant strain rate and assuming the stress is a unique function of the strain rate then the stress is constant also. The flow is therefore at constant acceleration as shown by the velocity gradient equations.

The Hencky strain was defined as [24,25],

$$\varepsilon_H = \ln\left(\frac{r_0^2}{r_e^2}\right) \tag{3.30}$$

The energy balance can be integrated from the entrance to exit, and the stress component in cylindrical coordinates is

$$\tau_{zz} = \frac{2}{3}\frac{\Delta P}{\varepsilon_H} + \frac{2}{3}\frac{\rho \Delta \hat{H}}{\varepsilon_H} = \frac{2}{3}\frac{\Delta P}{\varepsilon_H} + \frac{2}{3}\frac{\Delta H}{\varepsilon_H} \tag{3.31}$$

The elongational viscosity, η_e, in cylindrical coordinates is defined and results in this geometry as follows:

$$\eta_e = \frac{\tau_{zz} - \tau_{rr}}{\dot{\varepsilon}} = \frac{3}{2}\frac{\tau_{zz}}{\dot{\varepsilon}} \tag{3.32}$$

Therefore, the elongational viscosity is

$$\eta_e = \frac{\Delta P}{\dot{\varepsilon}\varepsilon_H} + \frac{\rho \Delta \hat{H}}{\dot{\varepsilon}\varepsilon_H} = \frac{\Delta P}{\dot{\varepsilon}\varepsilon_H} + \frac{\Delta H}{\dot{\varepsilon}\varepsilon_H} \tag{3.33}$$

The enthalpy term represents either a real or apparent phase change that may be induced by the imposed orientation on the polymer melt or solution. Therefore, an effective elongational viscosity is defined which is related to η_e as follows [25]:

$$\eta_{eff} \equiv \frac{\Delta P}{\dot{\varepsilon}\varepsilon_H} \tag{3.34}$$

and

$$\eta_e = \eta_{eff} + \frac{\Delta H}{\dot{\varepsilon}\varepsilon_H} \tag{3.35}$$

This definition of effective elongational viscosity assumes that any enthalpy change is included in this. The elongational strain rate is defined as [24,25]

$$\dot{\varepsilon} = \left(\nu_0 / L\right)\left(\exp \varepsilon_H - 1\right) \tag{3.36}$$

where ε_H is the Hencky strain as defined previously, L is the centerline length of the die, and ν_0 is the initial velocity.

The enthalpy change associated with the flow-induced transformation to what can be considered a metastable crystalline form can be estimated as follows. The effective Trouton ratio is η_{eff} / η_s. Making the assumption that the non-Newtonian character of the melt in excess of that caused by the shear viscosity η_s at equal value of shear rate is due to the resistance towards orientation, the actual Trouton ratio would be η_e / η_s. Hence, the elongational viscosity can be expressed in terms of a measured shear viscosity and combined with the above given expression for η_e to give:

$$\Delta H = -\dot{\varepsilon}\varepsilon_h\left(\eta_{eff} - \eta_s\right) \tag{3.37}$$

The entropy change, ΔS, is an indicator as to what extent orientation develops. It can be determined using $\Delta G = \Delta H - T\Delta S$, where ΔG is the Gibbs free energy and T is the absolute temperature. Assuming that due to orientation development the flow reaches a quasi or transient steady state equilibrium, then $\Delta G = 0$ and $\Delta S = \Delta H/T$.

Recently, this attractive technique for measuring the elongational viscosity has been generalized and evaluated using numerical simulations by Collier et al [86]. The analysis of the flow equations has been generalized to use less restrictive assumptions than reported in previous studies. Numerical simulations showed that the term involving the enthalpy could be neglected and that provides a very good approximation to the true elongational viscosity of the material. This was done by using finite element techniques to calculate the flow of a LDPE melt in the semi-hyperbolic die. Excellent agreement was found between the results of the simulations and the elongational viscosity computed by integrating the constitutive equation for the LDPE melt in elongational flow. Moreover, experimental data taken from a different LDPE in the semi-hyperbolic die showed the same trend as that seen in the simulation data. The simulations of a Newtonian fluid also showed that the elongational viscosity satisfied the Trouton ratio. Strictly speaking, the shape of the die produces elongational flow only when the fluid fully slips along the wall, thus eliminating all shear effects. It was also shown that the semi-hyperbolic dies could be used to obtain transient elongational viscosity data at constant strain or constant

strain rate. Thus, they provide an attractive alternative for measuring elongational viscosity of polymeric fluids. Compared to many other elongational rheometers proposed by Meissner et al [12-15], experiments in the semi-hyperbolic die are relatively easy and inexpensive to perform. The apparatus itself can be constructed simply by replacing the die in a capillary rheometer with a semi-hyperbolic die and placing a pressure transducer on the wall at the die entry.

CHAPTER 4

MATERIALS AND INSTRUMENTS

§4.1 MATERIALS

Given necessary processing equipment nearly all thermoplastics could be processed by the melt blowing process, but some general resins such as polypropylene, polyethylene, poly (ethylene terephthalate), copolyester, and polyamide are most preferred in practice. Polymers of low molecular weights and melt viscosities are manufactured for melt blowing, with the typical melt flow rate being 12 to 1500 for polypropylene [38]. Currently, PP shares about 90% of the melt blown nonwovens market because of its low cost, ease of processing, good mechanical properties, and chemical inertness. For this study two ExxonMobil Escorene® polypropylene samples were selected: PP3546G and PP3505G. PP3546G is specifically designed for melt blown nonwoven applications. It contains peroxide to control the polymer rheology during processing. PP3505G is a general fiber grade granular resin for melt blown nonwoven processes. Table 4.1 lists properties of two polymers.

Table 4.1 Properties of PP3546G and PP3505G.

Resin properties	ASTM Method	Typical values of PP3546G	Typical values of PP3505G
MFR ($230^{o}C$/2.16kg)	D1238	1200g/10min	400g/10min
Density	D792	$0.90g/cm^3$	$0.90g/cm^3$
Typical particle size	ExxonMobil Method	>80% (25-35 mesh) 0% (<200 mesh)	>85% (25-35 mesh) 0% (<200 mesh)

§4.2 INSTRUMENTS AND DATA ACQUISITION

Shear and elongational viscosity measurements were accomplished using the Advanced Capillary Extrusion Rheometer (ACER) by Rheometric Scientific™. Measurements of complex viscosity, storage and loss moduli were done using the Advanced Rheometric Expansion System (ARES) by Rheometric Scientific™. Infrared images were captured by Phoenix IR camera.

§4.2.1 Advanced Capillary Extrusion Rheometer (ACER)

A schematic of the ACER is shown in Figure 4.1. Capillary dies were used to measure the shear viscosity under different processing conditions, such as temperature and shear rate. Three semi-hyperbolic convergent dies of Hencky stains 5, 6, and 7 were used to measure the elongational viscosity. Polymer sample were charged into the barrel and allowed to melt and attain the desired steady state temperature after waiting for 30 minutes. The computer connected with ACER recorded the pressures collected with time evolution at set rates via a pressure transducer located right above the entrance of the die. The experiments were then performed by sweeping a series of shear or elongational strain rates until a steady state of pressure is accomplished for each rate. From the knowledge of the measured steady state pressure, rate, and Hencky strain, the software gave the shear or elongational viscosity.

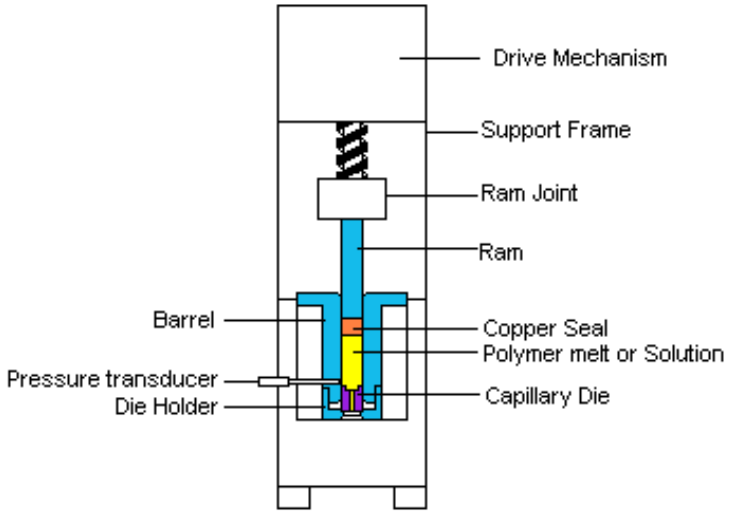

Figure 4.1 Schematic Diagram of the Advanced Capillary Extrusion Rheometer (ACER).

§4.2.2 Advanced Rheometric Expansion System (ARES)

Dynamic properties can be determined by applying two particular flows, oscillatory flow and relaxation flow. In the former experiment the system has imposed on it sinusoidal external conditions of known frequency and amplitude. The frequency, amplitude, and phase of the response of the fluid are measured. In the later experiment the system has applied to it relaxation external conditions, such as force, or strain, then undergoes a rapid change from one steady state to a second steady state. The response of the fluid as it approaches the new equilibrium state is measured.

Parallel plate geometry is used for all the experiments. The plates are enclosed in a forced air convection oven, which is used to control the temperature of the sample inserted between the plates. The lower plate of the rheometer is attached

to a motor whose motion mode can be controlled by the computer and the upper plate is attached to the torque and force transducers that are interfaced with the computer. The motor can rotate in both steady and oscillatory mode depending on different experiment setting. ARES has two transducers with different torque ranges, which can be switched from the lower range transducer to the higher range transducer automatically by the instrument during a test based on the torque measured by the computer. Circular disks of polypropylene samples were prepared by compression molding at ~180°C for the testing. A simplified schematic of the ARES with parallel plate geometry is shown in Figure 4.2.

§4.2.3 Phoenix IR camera

A Phoenix high speed IR camera was used to capture the infrared images and the die temperature and web temperatures were used as boundary conditions to convert the infrared data to temperature profiles.

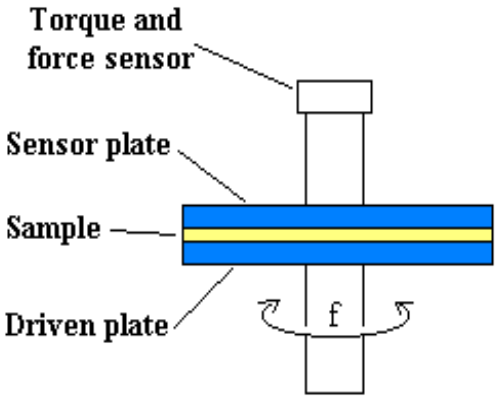

Figure 4.2 Simplified Schematic of the Advanced Rheometric Expansion System (ARES).

The IR camera has a 320 x 256 Pixels Focal Plane Array, and it has a temperature resolution 0.015^{o}C. The camera can be used as snapshot mode or high-speed video recording, which has a full frame at 128 Hz, 16 x 16 pixels at 50,000 Hz. The IR camera is connected to a computer and software named as Image-Pro^{R} Plus (Version 4.1) from Media Cybemetics, Inc is used to deal with the IR image and extract the IR intensity for the image, which is linear with the temperature. The IR camera is shown in the Figure 4.3. This IR camera has been used in other research areas, such as metal alloy materials [54-59], but it is the first introduction of the use of IR camera to fundamental understand the melt blowing processing [85].

Figure 4.3 Phoenix IR Camera.

§4.3 MELT BLOWING LINE, NONWOVEN CHARACTERIZATION AND EXPERIMENTS

The PP polymers were processed on a Reicofil® bicomponent melt blowing line built by Reifenhaüser, GmbH, operating in a monocomponent mode. The melt-blowing die has 601 holes, each with a 400-micron diameter. The length of the air/filament parallel flow region was determined by the interaction of a planar laser beam with the collection of 601 filaments as a function of distance from the die face [84]. The first melt blowing trial used PP3546G. The air temperature was held at 240°C, and the gear pump speed were 5, 10, and 15 rev/min respectively. The airflow rates used were 166, 258, and 430 standard cubic feet per minute (scfm). All the nonwoven fabrics were used to measure the properties to explore the processing/properties relationship. For the second trial running of melt blowing line, the polymer throughput was held constant at a pump rate of 5 rev/min/pump. A polymer throughput at 5 rev/min/pump was chosen for those runs because PP3505G has a relative high viscosity and would therefore have runnability issues at higher throughputs. The air temperature was held constant at 240°C. Polymer melt temperatures used were 220°C, 230°C, 240°C and the airflow rate was controlled at either 298 or 415 scfm. Six runs were performed for each of the two polymers, PP3546G and PP3505G. A special case was made on the PP3546G at a throughput of 25 rev/min/pump for purposes of comparison of the infrared thermographs. Nonwoven fabrics from all the runs were used to measure the rheological properties

that in turn were used to determine the degradation during the melt blowing processing. A schematic of the bi-component melt blown line is shown in Figure 4.4. The processing conditions chosen for different runs on the melt blowing line are shown in Table 4.2 and Table 4.3. The physical properties tests were air permeability, basis weight, tensile strength, hydrohead. Air permeability is the rate of airflow perpendicular through a known area under a prescribed air pressure. This test was performed according to ASTM Standard D737. Basis weight test gives the mass per unit area of the nonwoven fabric. This test was performed according to ASTM Standard D3776. The tensile strength testing was performed according to ASTM Standard D5035. Hydrohead test measures the resistance of nonwoven fabrics to the penetration of water under low hydrostatic pressure. This test was performed according to INDA Standard IST 80.6.

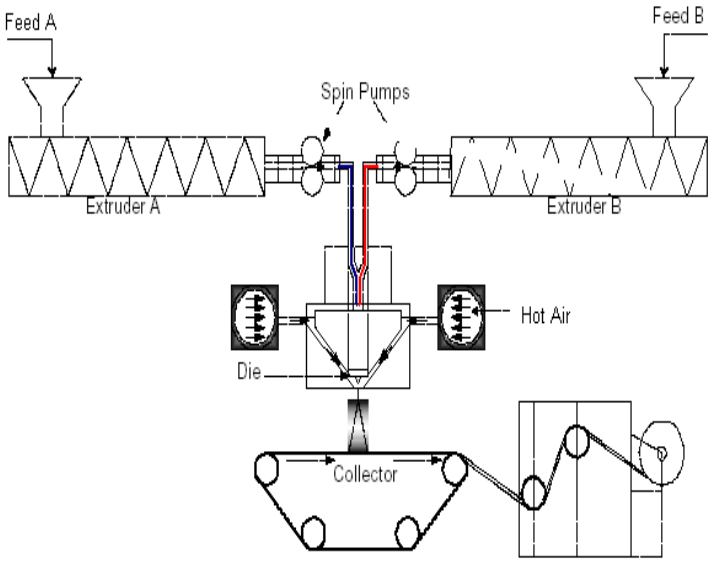

Figure 4.4 Schematic of the Melt Blowing Process.

Table 4.2 Trial 1Run Conditions.

Run #	Polymer	Throughput (rev/min/pump)	Melt Temp (^{o}C)	Air Temp (^{o}C)	Air flowRate (scfm)
1	PP3546	5	220	240	166
2	PP3546	10	220	240	166
3	PP3546	15	220	240	166
4	PP3546	5	230	240	166
5	PP3546	10	230	240	166
6	PP3546	15	230	240	166
7	PP3546	5	240	240	166
8	PP3546	10	240	240	166
9	PP3546	15	240	240	166
10	PP3546	5	220	240	258
11	PP3546	10	220	240	258
12	PP3546	15	220	240	258
13	PP3546	5	230	240	258
14	PP3546	10	230	240	258
15	PP3546	15	230	240	258
16	PP3546	5	240	240	258
17	PP3546	10	240	240	258
18	PP3546	15	240	240	258
19	PP3546	5	220	240	430
20	PP3546	10	220	240	430
21	PP3546	15	220	240	430
22	PP3546	5	230	240	430
23	PP3546	10	230	240	430
24	PP3546	15	230	240	430
25	PP3546	5	240	240	430
26	PP3546	10	240	240	430
27	PP3546	15	240	240	430

Table 4.3 Trial 2 Run Conditions.

Run #	Polymer	Throughput (rev/min/pump)	Melt Temp (^{o}C)	Air Temp (^{o}C)	Air flowRate (scfm)
1	PP3505	5	220	240	298
2	PP3505	5	220	240	415
3	PP3505	5	230	240	298
4	PP3505	5	230	240	415
5	PP3505	5	240	240	298
6	PP3505	5	240	240	415
7	PP3546	5	240	240	415
8	PP3546	5	240	240	298
9	PP3546	5	230	240	415
10	PP3546	5	230	240	298
11	PP3546	5	220	240	415
12	PP3546	5	220	240	298
13	PP3546	25	230	240	298

Thermal degradation results in scission of the polymeric chains, and consequently will lower the viscosity of the polymer melt. Thus measurement of rheological properties is a very convenient way to determine the extent of degradation. Also rheological property measurement is a relatively easy method to determine the molecular weight and molecular weight distribution. All rheological properties of the melt blown samples were measured on the ARES rheometer using parallel plate geometry. Melt blown samples were collected and compressed in a cold molding machine to remove the air then molded at $180^{o}C$ to prepare the specimens that were used to measure the rheological properties. The study of the thermal stability in the parallel plate rheometer was done at a shear rate of $1s^{-1}$ and in the dynamic operation mode at different temperatures. The thermal behavior of the analyzed polymers was also measured using a METELER TOLEDO STAR differential scanning calorimeter (DSC) instrument. DSC was carried out under nitrogen atmosphere and the heating rate was $10^{o}C$/min.

CHAPTER 5

RESULTS AND DISCUSSIONS

§5.1 RHEOLOICAL PROPERTIES OF POLYPROPYLENE

Temperature, pressure, stress, flow geometry and time are the most important factors that determine a polymer rheological properties, which include dynamic properties, shear viscosity and elongational viscosity. Even in the simplest flows, such as capillary extrusion, the temperature and stress may be complex due to the complex structure of the polymer and its viscoelastic character. In addition some rheological properties are time dependent. From the point view of polymer processing, rheological properties dictate applications and processing methods.

§5.1.1 Dynamic properties

Dynamic properties are determined by the polymer molecular characteristics; also they are strongly influenced by the experimental factors, such as temperature, frequency, stress and strain. There are many reasons for the determination of the linear viscoelastic response of materials, including being able to elucidate the molecular structure of materials, which sometime is useful in quality control of industrial products.

Linear viscoelastic properties, such as complex viscosity, storage and loss moduli, are presented in the form of graphs instead of transformation into the

relaxation function or the relaxation spectrum. PP3546G had a lower complex viscosity, as would be predicated from its higher melt flow rate. The complex viscosity changed very slightly with the increase of angular rates, and its rheological behavior liked the Newtonian fluid. PP3505G also had a low complex viscosity; its complex viscosity decreased as angular rates increased, which was typical non-Newtonian behavior. Complex viscosity changed very little at low angular rates; it was very similar to a Newtonian fluid. With increasing temperature the complex viscosity decreased significantly. Figure 5. 1 shows the complex viscosities of two PPs. Figure 5.2 and 5.3 give the storage and loss modulus respectively.

The relaxation time and normal force were very small because of the very low viscosity of these polymers. As the temperature increased, these two parameters of the polymer decreased sharply. An important phenomenon in polymer processing is the die swell. When a viscoelastic liquid is extruded from a die, it usually swells to a much great diameter than that of the hole. The die swell increases with the increase of the flow rate. During the melt blowing process, it is desired to control the die swell to be as small as possible in order to manufacture small diameter fibers. Very low normal forces and quick relaxation times of these polymers can help reduce the die swell during the melt blowing process. The initial diameter of extruded fiber for the die orifice on the melt blowing die was assumed to be the diameter of the die orifice described in §4.3. Figures 5.4-5.7 show the relaxation and normal force of these two polymers at different shear rates and temperatures.

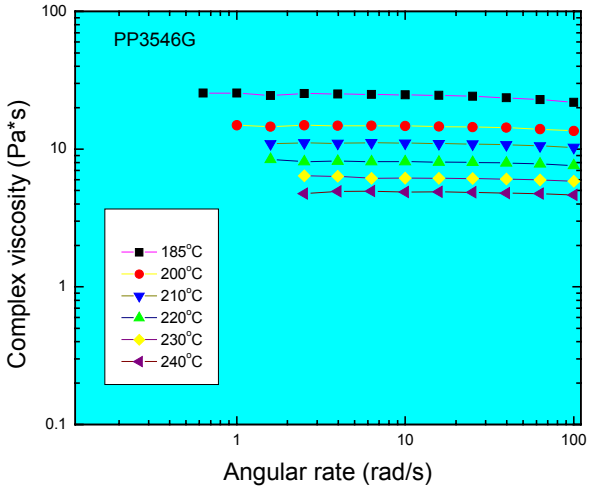

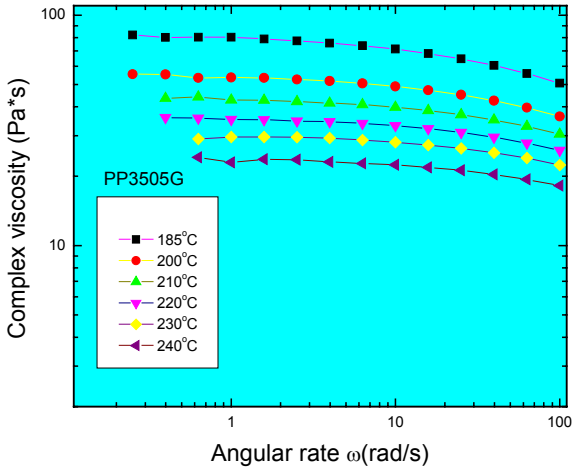

Figure 5.1 Complex Viscosity of PP.

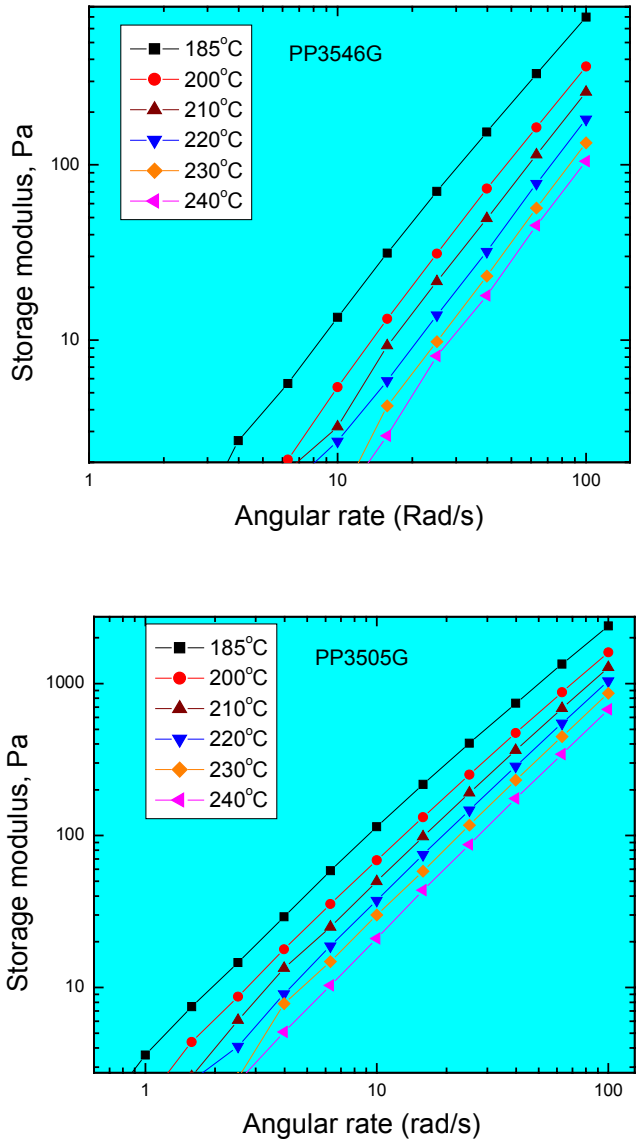

Figure 5.2 Storage Modulus of PP.

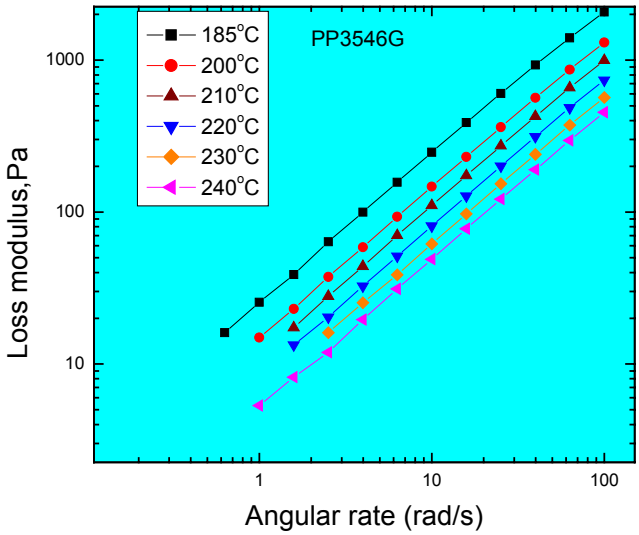

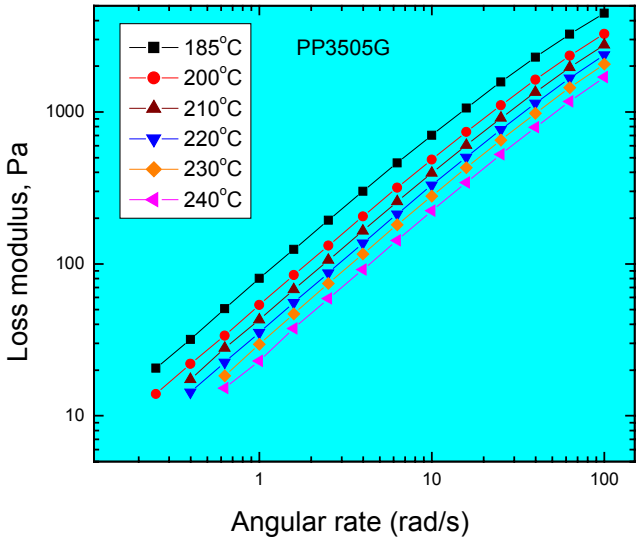

Figure 5.3 Loss Modulus of PP.

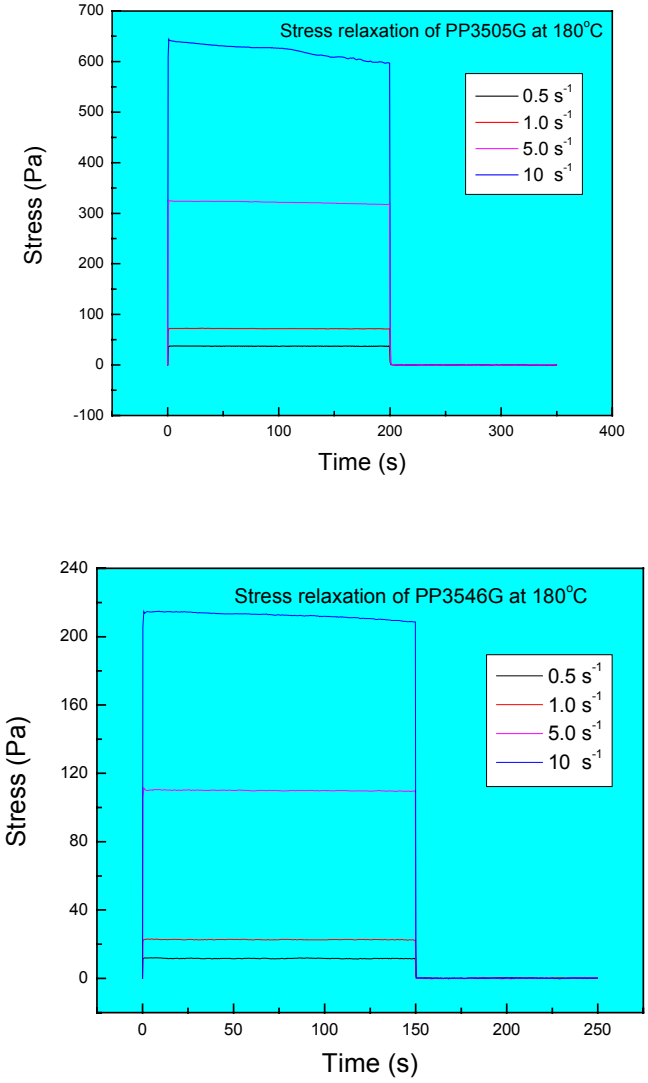

Figure 5.4 Stress Relaxation of PP at 180°C.

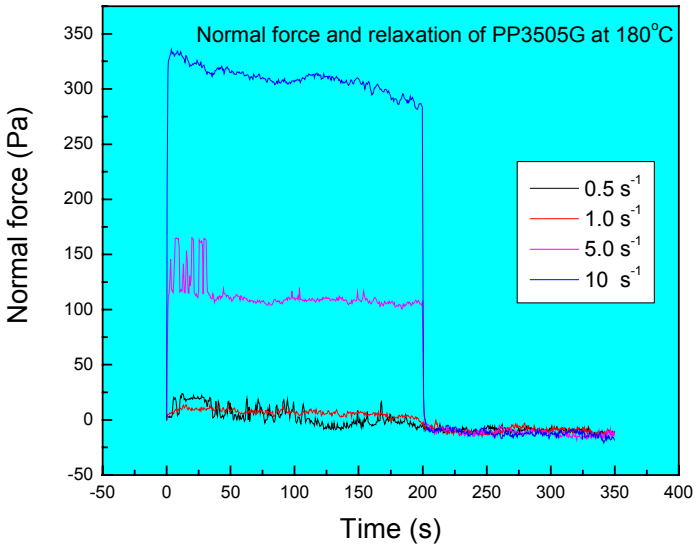

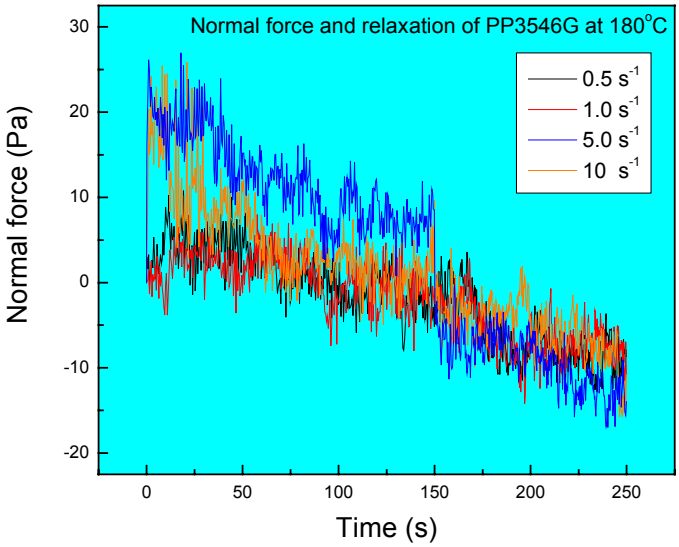

Figure 5.5 Normal Force and Relaxation of PP at 180°C.

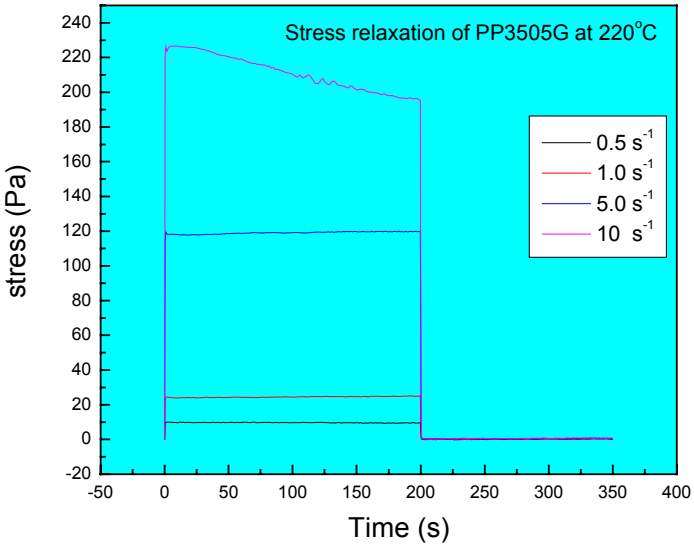

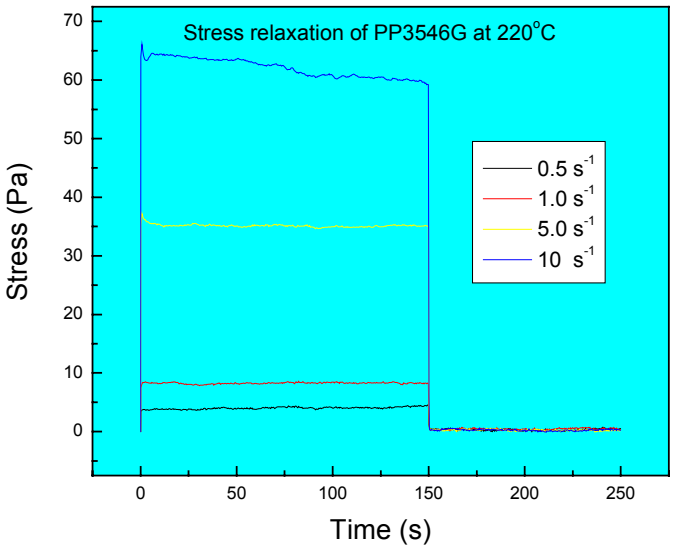

Figure 5.6 Stress Relaxation of PP at 220°C.

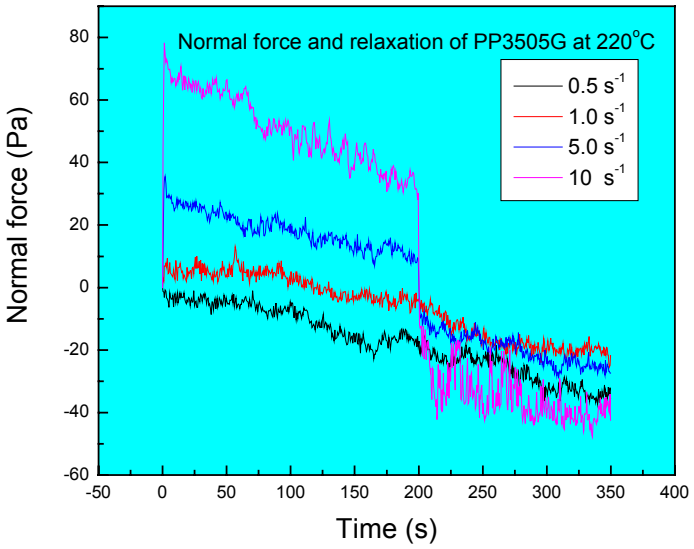

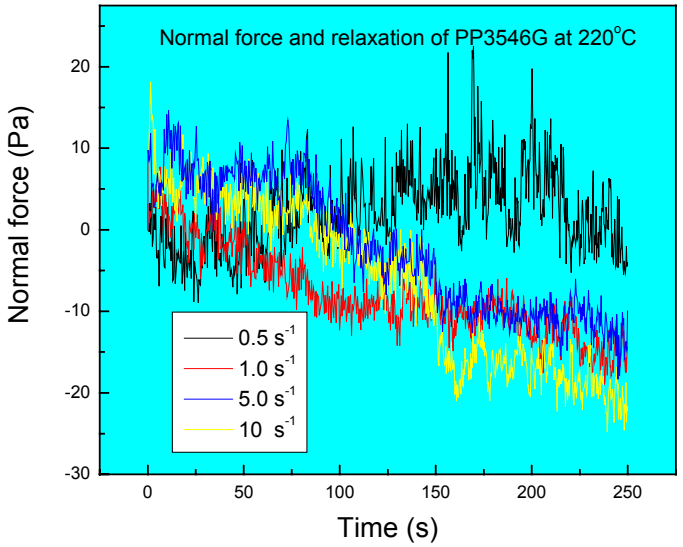

Figure 5.7 Normal Force and Relaxation of PP at 220°C.

§5.1.2 Shear viscosities

Shear viscosity is often regarded as a most important material function and any practical research requiring knowledge of material response would automatically resort to the viscosity as the first moment. The shear viscosity is an extremely important material variable during the melt blowing process. Low shear viscosity is demanded for the extrusion due to the small diameter of the spinneret and this viscosity dictates the flow rate in the spinneret. The viscosity of a real material can be significantly affected by such variables as shear rate, temperature, pressure and time of shearing.

Figure 5.8 gives the shear viscosities of two PPs, which are typical of responses for non-Newtonian fluids. Their shear viscosities are low compared with other PPs, which are used for other processing methods and application. With an increase in shear rate, the shear viscosity decreases very quickly, so the shear rate is a good way to control the viscosity, and it can be controlled with several points by changing the flow rate. However for some polymer processing applications the shear rate cannot be changed for a broad enough range to sufficiently control the shear viscosity. With a temperature increase, the shear viscosity decrease significantly, so the processing temperature can be a good method for controlling viscosity during processing, but higher temperatures will cause the polymer to degrade. For this reason the processing temperature of PP is usually controlled between 260 to 280^{o}C for these polymers.

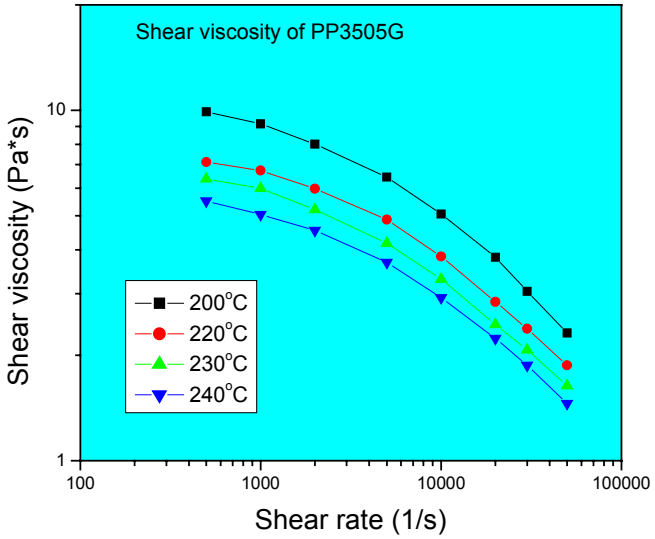

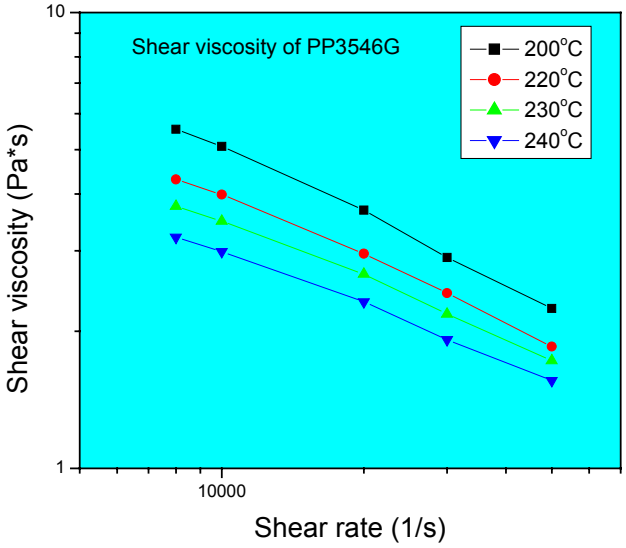

Figure 5.8 Shear Viscosity of PP .

§5.1.3 Elongational viscosities

In polymer processing, some operations involve a significant component of elongational flow, with the obvious conclusion that the measurement of elongational viscosity may sometimes be at least as important as the determination of shear viscosity. Any reasonably abrupt change in the geometry in polymer processing will generate an elongational component of flow. As a result, flows through an orifice often lead to flow characteristics, which cannot be predicted on the basis of the shear viscosity alone. The spinnability of a polymeric melt can be dependent on its elongational viscosity behavior. The elongational viscosity dictates the attenuation of fibers extruded from the die orifices during the melt blowing process. With an increase in elongational rate, the elongational viscosity decreased very quickly, so the elongational rate can be a good way to control the viscosity. For certain polymer processing applications however, the elongational rate is controlled by the flow rate and the flow geometry, so it cannot be changed over a large range to control the shear viscosity. Increasing the temperature significantly decreased the elongational viscosities, so the processing temperature can be a good method to control the viscosity during processing. Figures 5.9-5.11 show the elongational viscosities of these two PP samples with different Hencky strains respectively. Figure 5.12 gives the comparison of the elongational viscosity of these polymers measured at different Hencky strains. Such an increase in elongational viscosity with increasing strain is called ‘strain hardening’ – a phenomenon well documented in the literature [60-62].

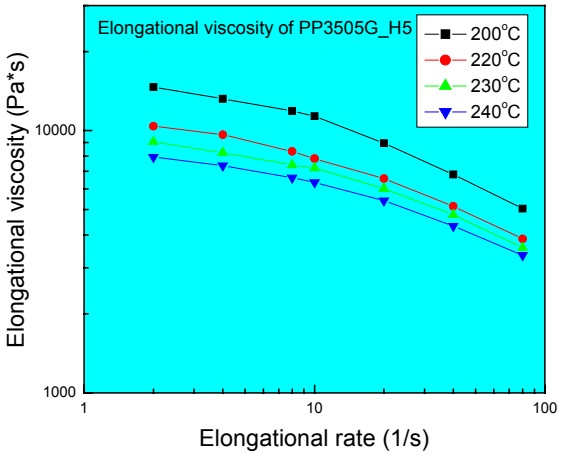

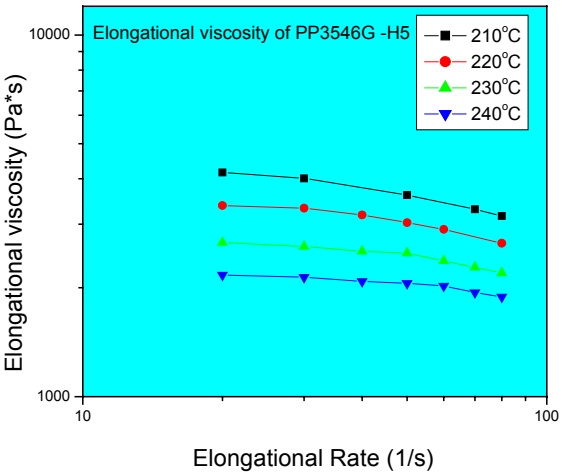

Figure 5.9 Elongational Viscosity of PP at Hencky 5.

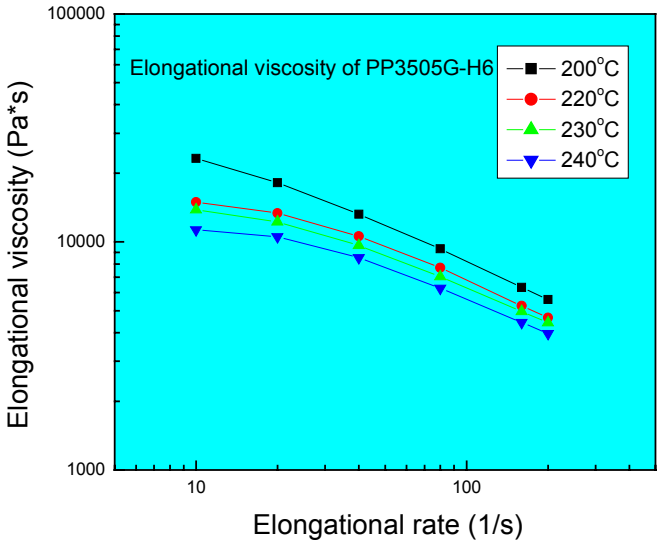

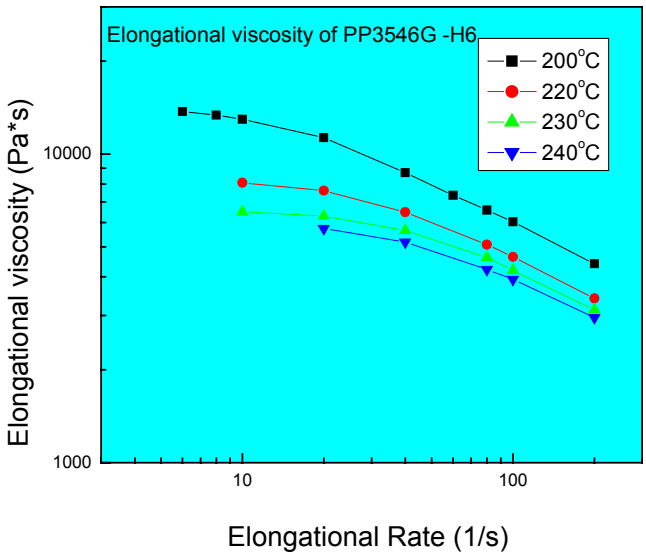

Figure 5.10 Elongational Viscosity of PP at Hencky 6.

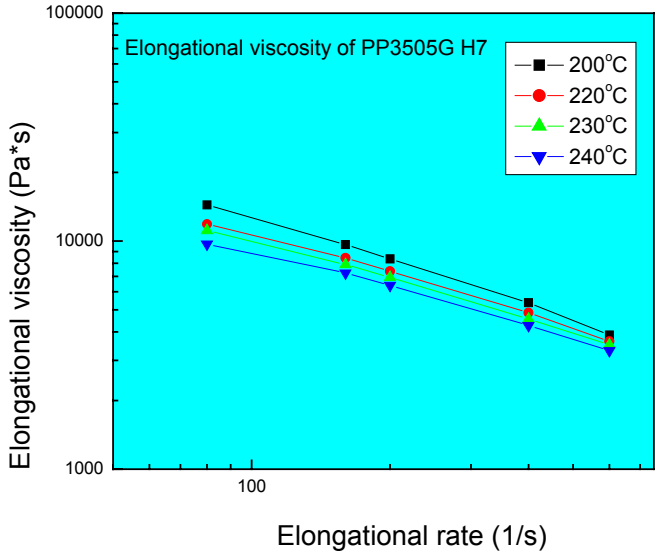

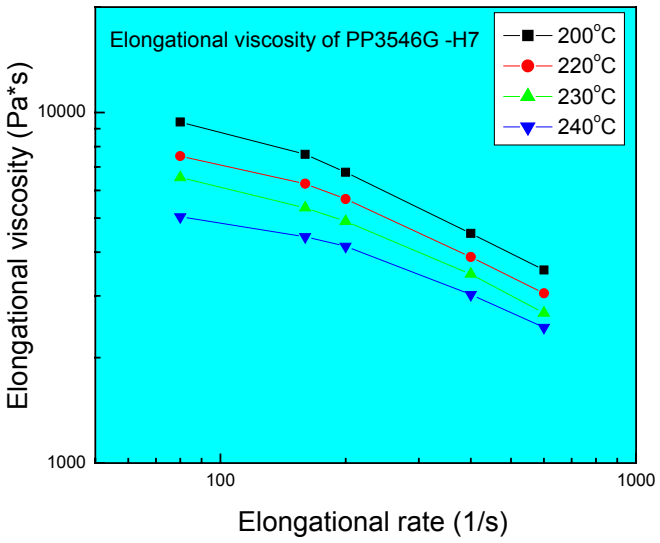

Figure 5.11 Elongational Viscosity of PP at Hencky 7.

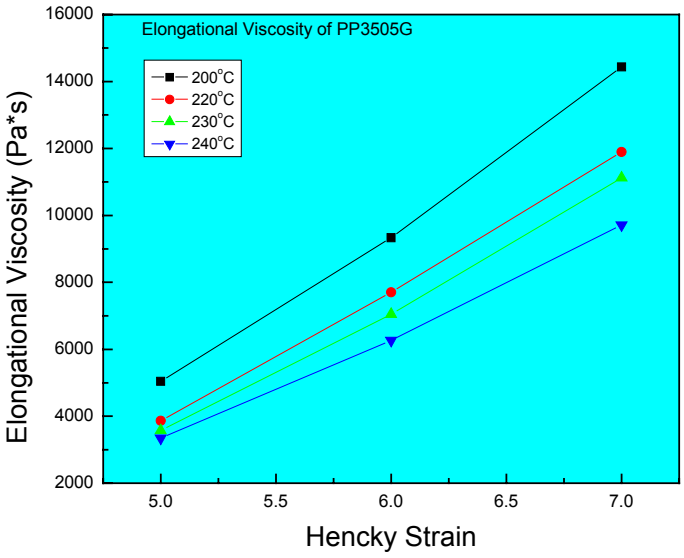

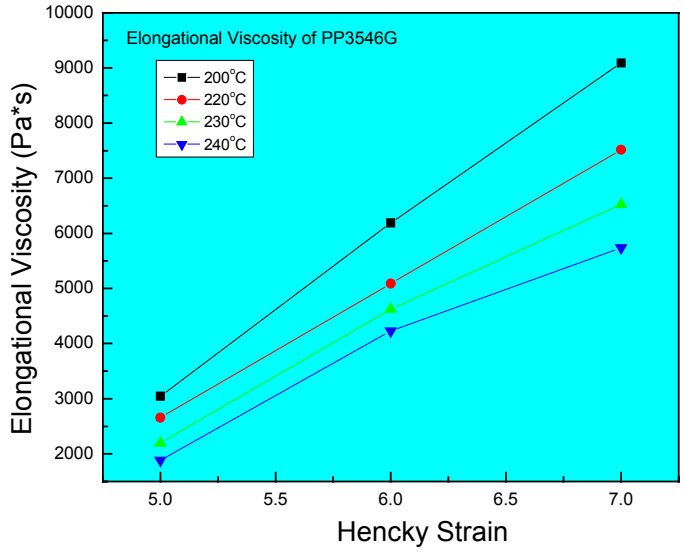

Figure 5.12 Comparison of Elongational Viscosity of PP at different Hencky Strain.

§5.1.4 Master curves

Shifting of the shear viscosity versus shear rate data obtained at different temperatures to a master curve at a reference temperature were done by using the reduced variables method and calculating a shift factor, a_T [53, 63-67]. The shear viscosity of a polymer melt becomes independent of the shear rate at very low shear rates, which indicates that the polymer melt is in a Newtonian fluid region, and the constant value of viscosity is called 'zero shear viscosity'. The shift factor, a_T, can be calculated by the ratio of viscosities in this region with respect to temperature [63]:

$$a_T = \frac{\lambda_j(T)}{\lambda_j(T_0)} = \frac{\eta_0(T)T_0\rho_0}{\eta_0(T_0)T\rho} \tag{5.1}$$

where T is the measurement temperature, T_0 is the reference temperature to which the data are being shifted, $\lambda_j(T)$ is the relaxation time of the j^{th} Rouse chain at T and $\lambda_j(T_0)$ is the relaxation time of the j^{th} Rouse chain at T_0, and ρ and ρ_0 are the polymer melt densities at T and T_0. It is further generally assumed that the density of polymer in the measuring temperature region, ρ, is equal to ρ_0, at T_0 so that

$$a_T = \frac{\eta_0(T)T_0}{\eta_0(T_0)T} \tag{5.2}$$

Zero-shear viscosities of polymer melts often cannot be measured directly due to the measurements at very low shear rates are not possible. The Carreau rheological model was used to predict the zero-shear viscosity of polymer melts from the experimental data [69]. The Carreau model is given as

$$\frac{\eta-\eta_\infty}{\eta_0-\eta_\infty}=\left[1+\left(\lambda\dot{\gamma}\right)^2\right]^{(n-1)/2} \tag{5.3}$$

where, η_∞ is the infinite shear rate viscosity, λ is a time constant that is related to the λ_j's in equation (5.1), and n is the power law exponent. Using this method a master curve is formed by plotting a reduced shear viscosity, η_r, vs. the reduced shear rate, $\dot{\gamma}_r$, which are typically calculated by the following equations:

$$\dot{\gamma}_r = a_T \cdot \dot{\gamma} \tag{5.4}$$

$$\eta_r = \eta(\dot{\gamma},T)\frac{\eta_0(T_0)}{\eta_0(T)} \tag{5.5}$$

This method can be also used to shift the complex viscosity data since the complex viscosity is a function of frequency in essentially the same way that the shear viscosity is a function of shear rate. The Carreau model was also used to construct a master curve that can be used to calculate the complex viscosity at other temperatures. The Arrhenius equation is often used to describe the temperature dependence of a_T [53], and is given as

$$a_T = \exp\left[\frac{E_a}{R}\left(\frac{1}{T}-\frac{1}{T_0}\right)\right], \tag{5.6}$$

where E_a is the activation energy of flow and R is the universal constant. Figure 5.13 gives the temperature shifting of complex viscosity. The shifting results are very good since most of the shifted points are on the same curve. Figure 5.14 gives the shifting results of shear viscosity and Figure 5.15 gives the shifting factor dependence on the temperature and activation energy.

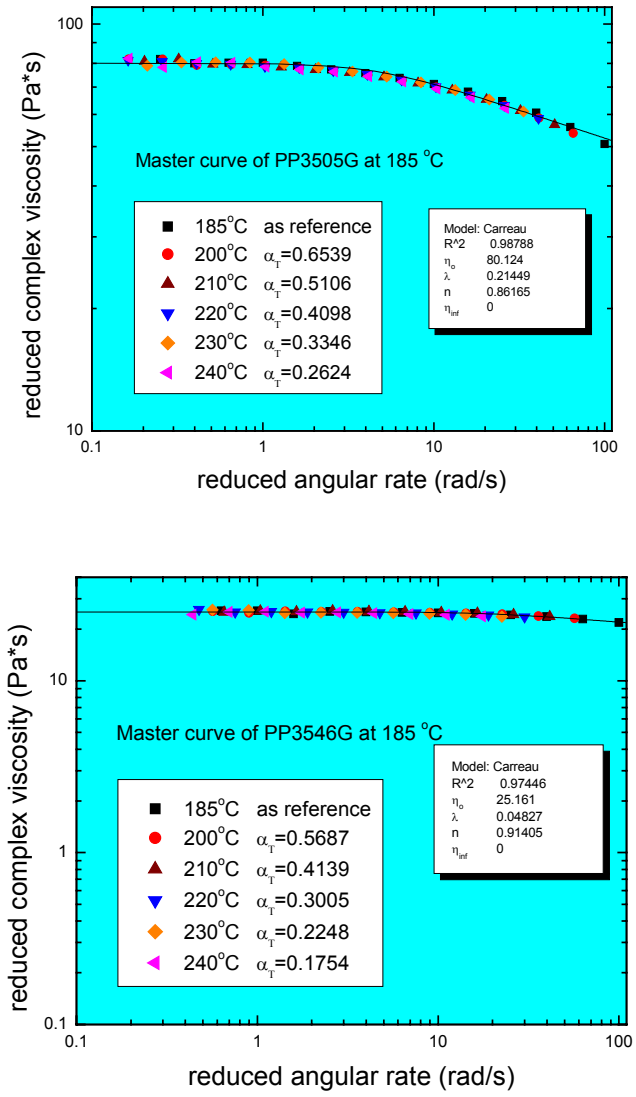

Figure 5.13 Temperature Shifting of Complex Viscosity of PP.

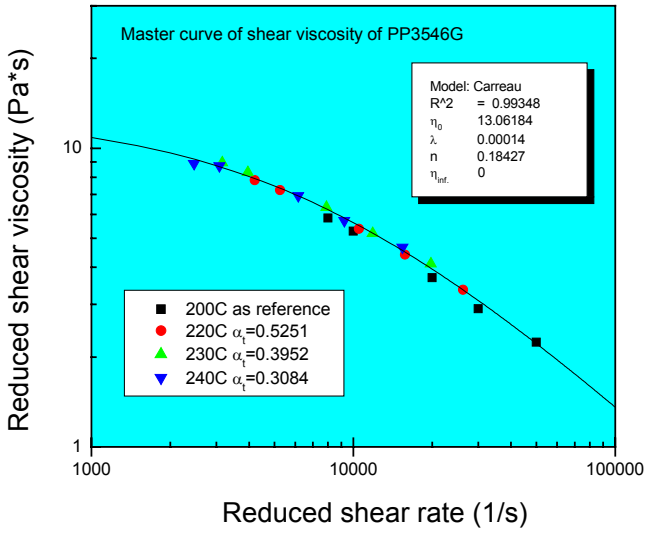

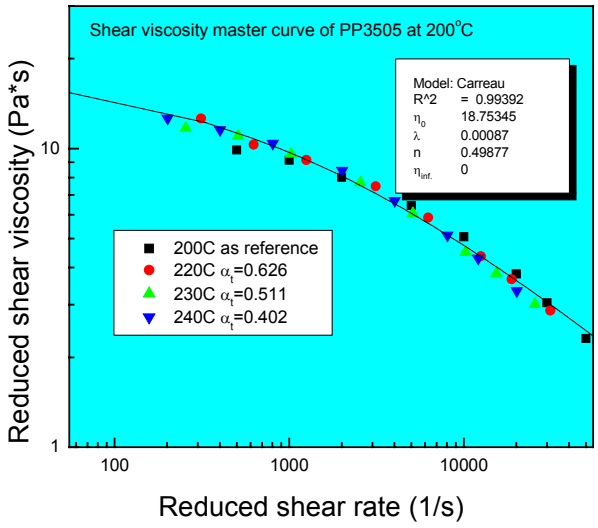

Figure 5.14 Temperature Shifting of Shear Viscosity of PP .

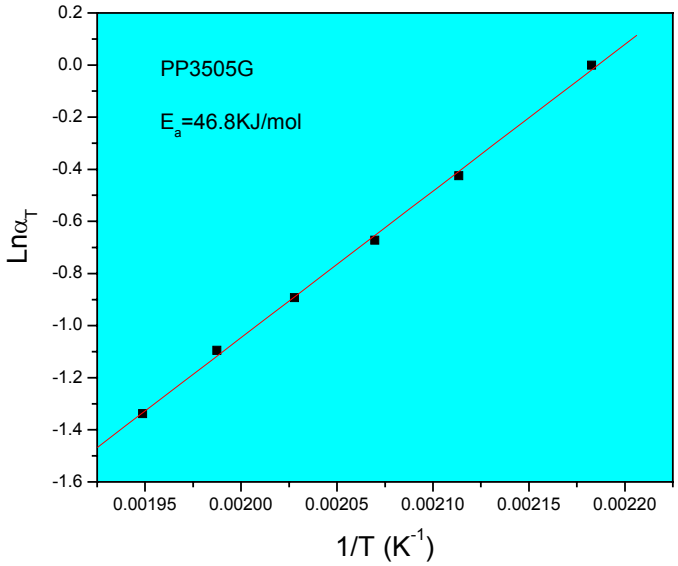

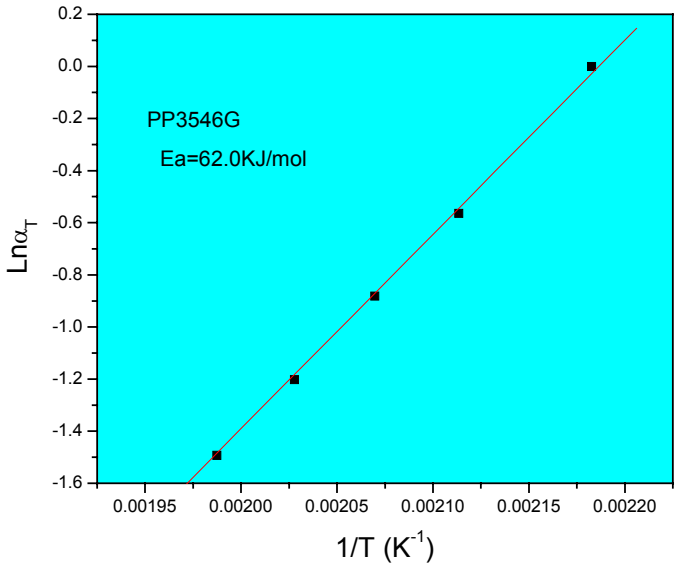

Figure 5.15 Temperature Dependence of Shifting Factor.

The temperature shift factor, a_T, is the ratio of relaxation times of the polymers at two temperatures. The relaxation time is a unique characteristic of the polymer at a given temperature and does not depend on the type of deformation. Hence, the dependence of relaxation times on temperature should be the same whether the polymer is in shear flow or elongational flow. Thus, the same temperature shift factor that is used to shift the shear viscosity can be used to shift the elongational viscosity [65, 67, 70].

The Carreau and Cross rheological models are often used to fit shear rheological properties [68,69]. From the experimental data, the data curves have the same shape with those models. So these models were used to fit the data. The Carreau model can fit the data very well at lower elongational or shear rates, while the Cross model shows better fit at higher elongational or shear rates [68]. The Cross rheological model is given as

$$\frac{\eta - \eta_\infty}{\eta_0 - \eta_\infty} = \frac{1}{\left(1 + K[\dot{\gamma}]^m\right)}, \tag{5.7}$$

where K and m have similar significance to that of λ and n in the Carreau model.

Figures 5.16-5.18 give the temperature shifting of elongational viscosity. The shifting results are good since most of the data points are on the same curve, and the model fitting results are also good. Rheological properties at other processing conditions, such as higher temperature, higher shear or elongational rate, can be obtained according to these models.

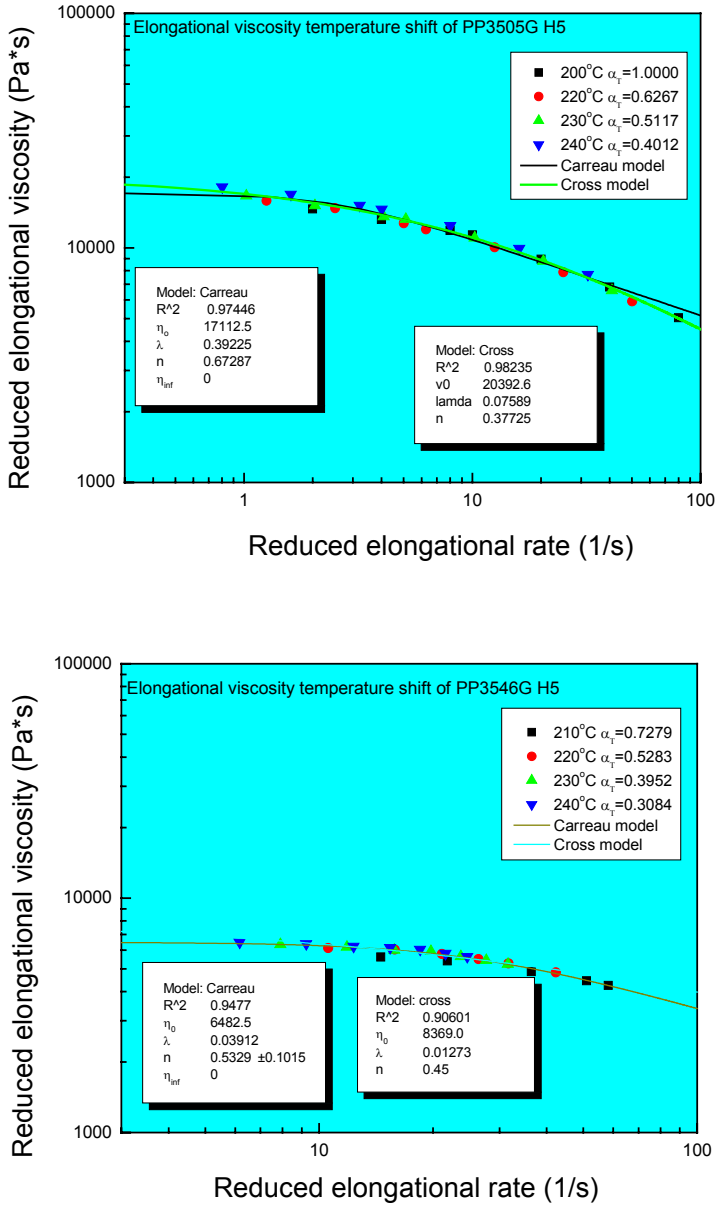

Figure 5.16 Temperature Shifting of Elongational Viscosity of PP at Hencky Strain 5.

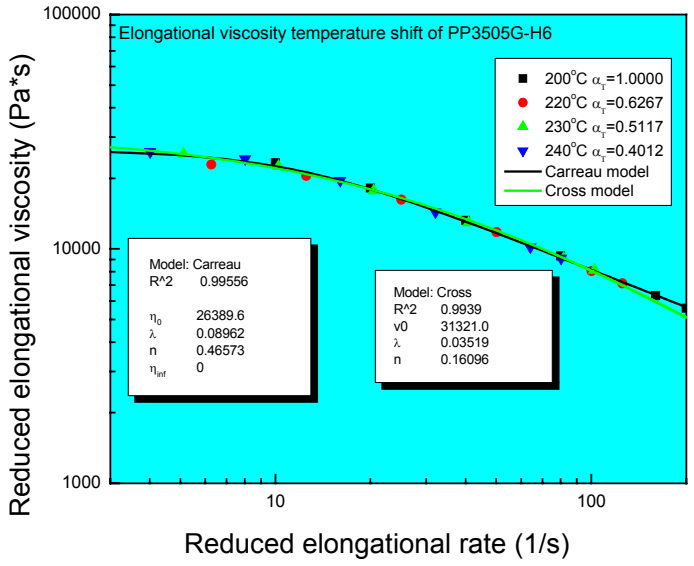

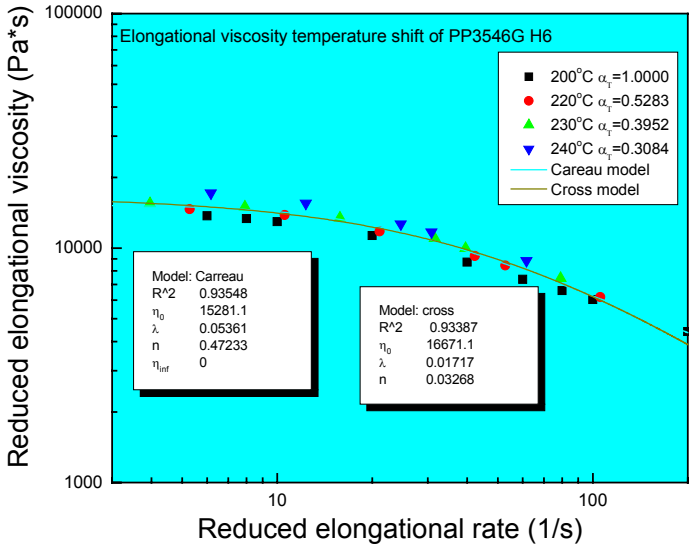

Figure 5.17 Temperature Shifting of Elongational Viscosity of PP at Hencky Strain 6.

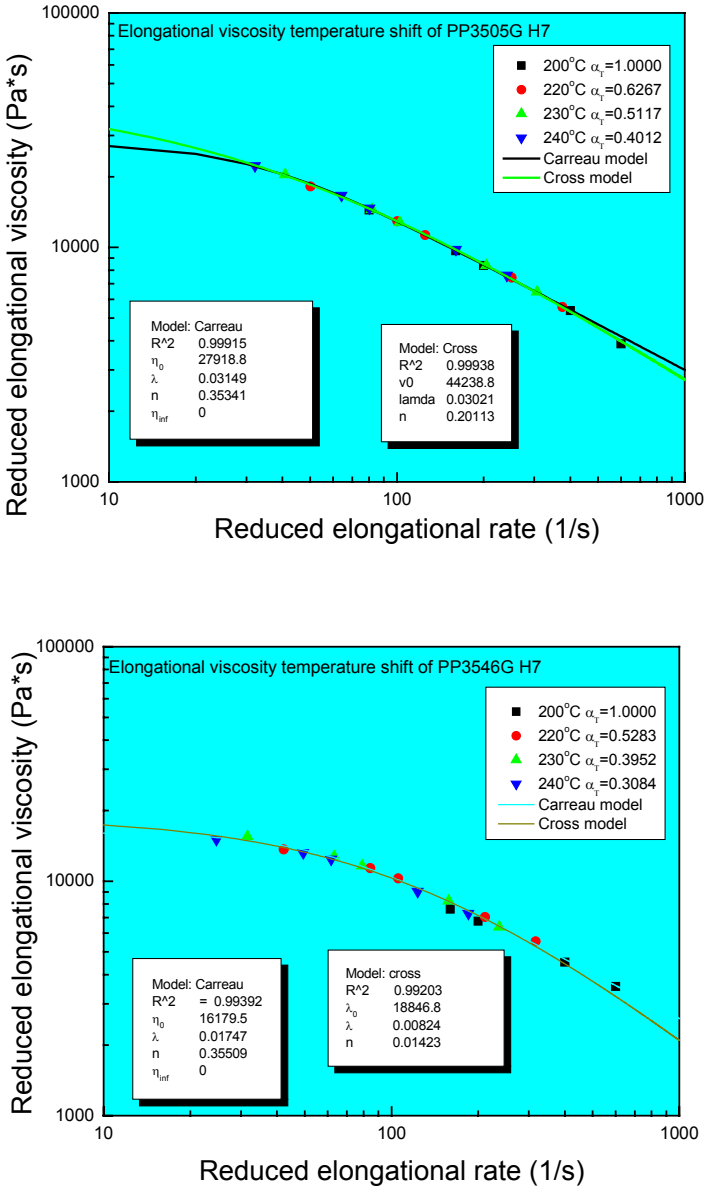

Figure 5.18 Temperature Shifting of Elongational Viscosity of PP at Hencky Strain 7.

The dependence of elongational viscosity on the Hencky strain is a result of the orientation developing in the polymeric fluid as it is being elongated in the semi-hyperbolic die. The shifting of elongational viscosity on Hencky strain has been successfully accomplished in this research group [64-67]. The enthalpy change associated with the flow-induced transformation that can be considered as a transformation to a metastable liquid crystalline form can be estimated as follows. The Trouton ratio, T_R, is η_e/η_s, where η_s is the shear viscosity measured at the same temperature and at an equivalent magnitude shear rate. If the assumption is made that the non-Newtonian character of the fluid in excess of that reflected in η_s is due to the resistance to orientation development, then the actual Trouton ratio would be $\eta_e/\eta_s = 3$, where η_e is the expected isotropic state elongational viscosity. By measuring η_s then $\eta_e = 3\eta_s$, the enthalpy per unit volume, ΔH, can be calculated from the resultant equation:

$$\Delta H = -\dot{\varepsilon}\varepsilon_h\left(\eta_e - 3\eta_s\right) \tag{5.8}$$

This implies that the term $[\eta_e - 3\eta_s]$ is a viscosity related measure of the orientation development due to this flow geometry and that the fluid does not remain in an isotropic state during flow; therefore, the term $[\eta_e - 3\eta_s]$ is the "orientational contribution" to the effective elongational viscosity, i.e. the "orientational viscosity". The concept of "orientational viscosity" is important in understanding the Hencky strain shifting of elongational viscosity data [70]. For a Newtonian viscous fluid $\eta_e = 3\eta_s$, that is $TR = 3$, and no "orientational contribution" to the elongational viscosity

occurs. For the polymer melts in this study TR is generally greater than 100 and therefore, the $\eta_e - 3\eta_s$ term can be assumed equal to η_e.

A definition of a Hencky strain shift factor, a_H, based upon an orientation ratio being equal to the relaxation ratio, could be obtained by assuming normalized strain rate states and an appropriately corrected equivalent shear viscosity state as follows based on the research in this group [65, 67, 70]. The term $\dot{\varepsilon}\varepsilon_H$ occurs in the derivation of the elongational viscosity, η_e, and reoccurs in the enthalpy and entropy derivations. This term is assumed in this derivation to be a normalized elongational strain rate, i.e. a strain rate corrected for the effects of orientation development in the polymer melt or solution. Therefore to be at equivalent normalized elongational strain rates:

$$\dot{\varepsilon}\varepsilon_H = \dot{\varepsilon}_0\varepsilon_{H_0} \tag{5.9}$$

and the shear viscosity at an equivalent shear strain rate (to the normalized elongational strain rate) is assumed to be adjusted also so that:

$$\eta_s\dot{\varepsilon}_H = \eta_{s_0}\dot{\varepsilon}_{H_0} \tag{5.10}$$

The shift factor, reduced elongational viscosity, and reduced elongational strain rate are defined by [76]

$$a_H = \frac{[TR-3]\varepsilon_{H_0}}{[TR-3]_0\varepsilon_H} \tag{5.11}$$

$$[\eta_e(\dot{\varepsilon},\varepsilon_H)]_r = \frac{\eta_e(\dot{\varepsilon},\varepsilon_H)}{[a_H\ ]^2} \tag{5.12}$$

$$\dot{\varepsilon}_r = a_H \dot{\varepsilon} \tag{5.13}$$

where a_H is a Hencky strain shift factor, *TR* is the Trouton ratio, η_e/η_s, η_e and η_s are the elongational viscosity and shear viscosity, respectively, ε_H is Hencky strain, and $\dot{\varepsilon}$ is the elongational strain rate. The subscript "0" indicates the value of the variable at the reference state. Figures 5.19-5.21 give the Hencky strain shifting of the elongational viscosity.

Using this approach, the elongational viscosity obtained at different temperatures can be generated into a single master curve according to the results of temperature shifting shown above using the temperature shift factor obtained from the shifting of the shear viscosity. Therefore, by combining the temperature and Hencky strain shifting operations, and using the appropriate shift factors, a generalized master curve could be obtained and the elongational strain rate range of the experimental geometry extended [70]. The reduced variables are defined by

$$[(\eta_e)_{r_{TH}}] = \frac{\eta_e}{(a_T)[(a_H)]^2} \tag{5.14}$$

$$(\dot{\varepsilon}_{r_{TH}}) = (a_T)(a_H)\dot{\varepsilon} \tag{5.15}$$

The shifting results are good since most of the data points are very close to the curve and rheological models were used to fit the data; all the parameters of the rheological models are listed in Figure 5.22. The rheological properties at other processing conditions can be calculated based on the shifting factors and these rheological models.

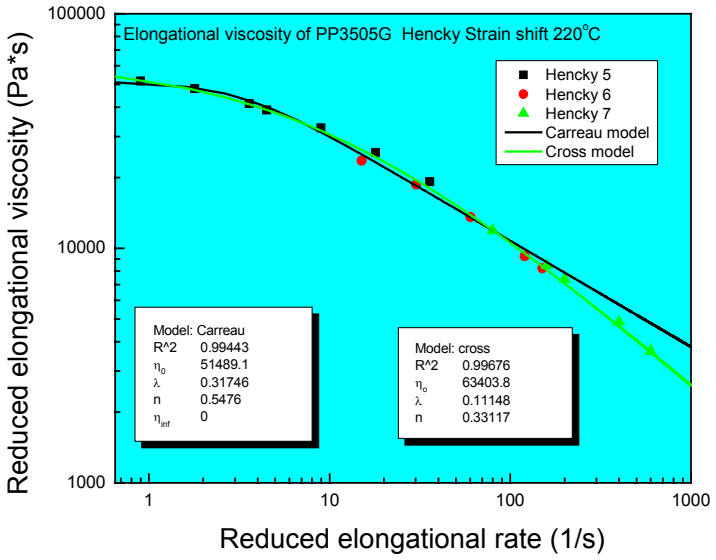

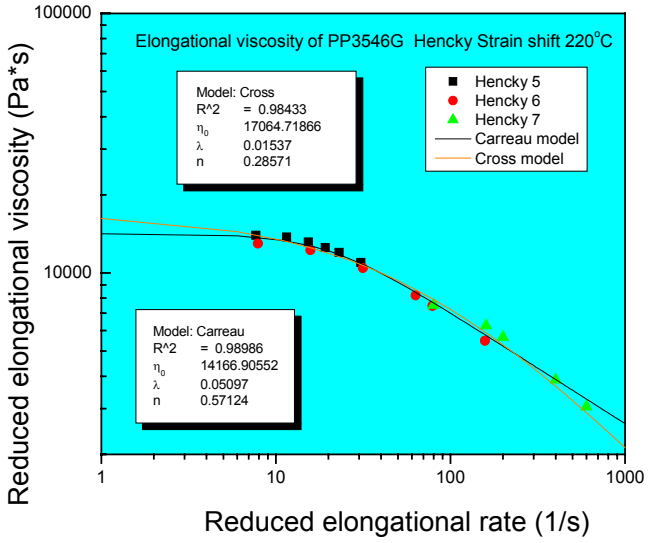

Figure 5.19 Hencky Strain Shifting of Elongational Viscosity of PP at 220°C.

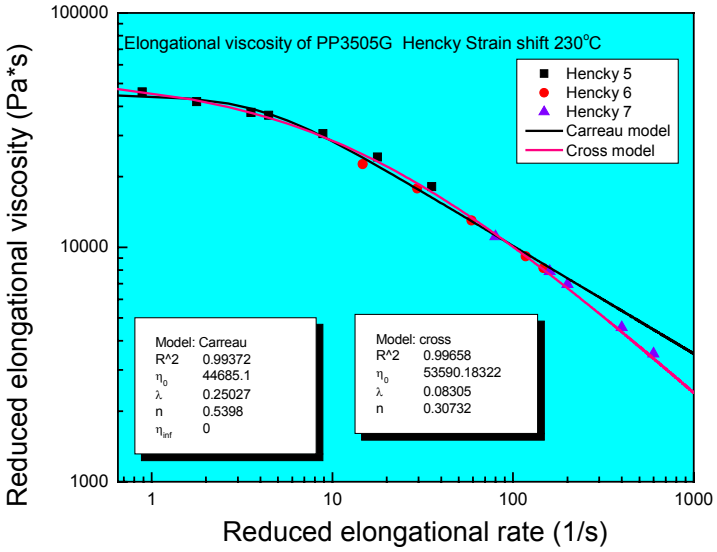

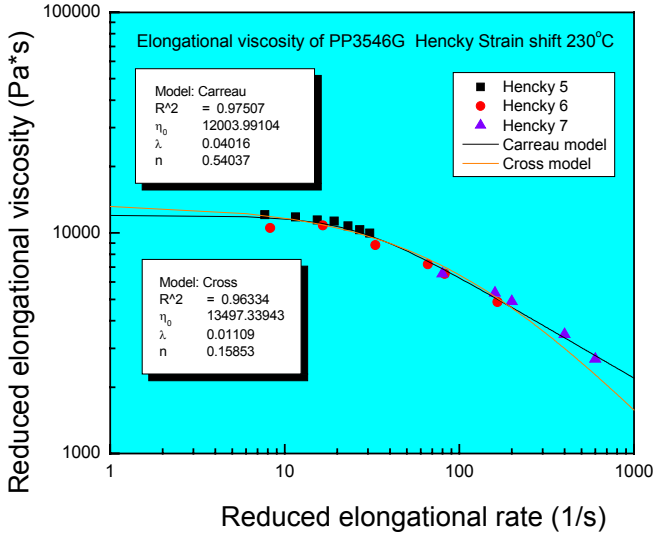

Figure 5.20 Hencky Strain Shifting of Elongational Viscosity of PP at 230°C.

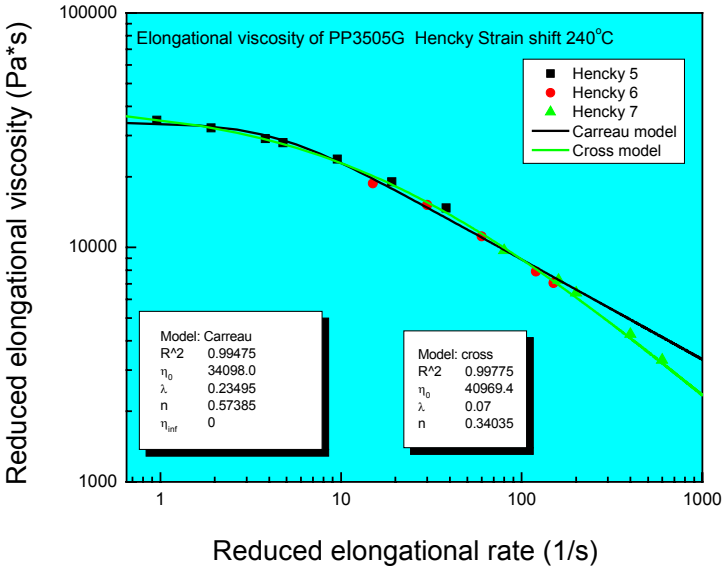

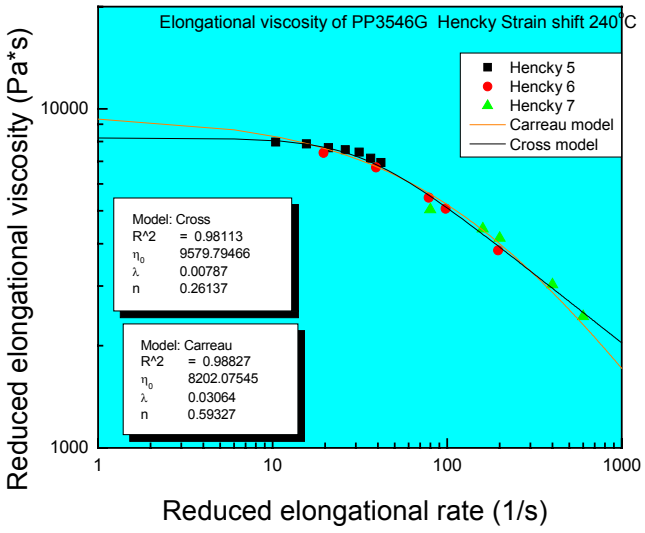

Figure 5.21 Hencky Strain Shifting of Elongational Viscosity of PP at 240°C.

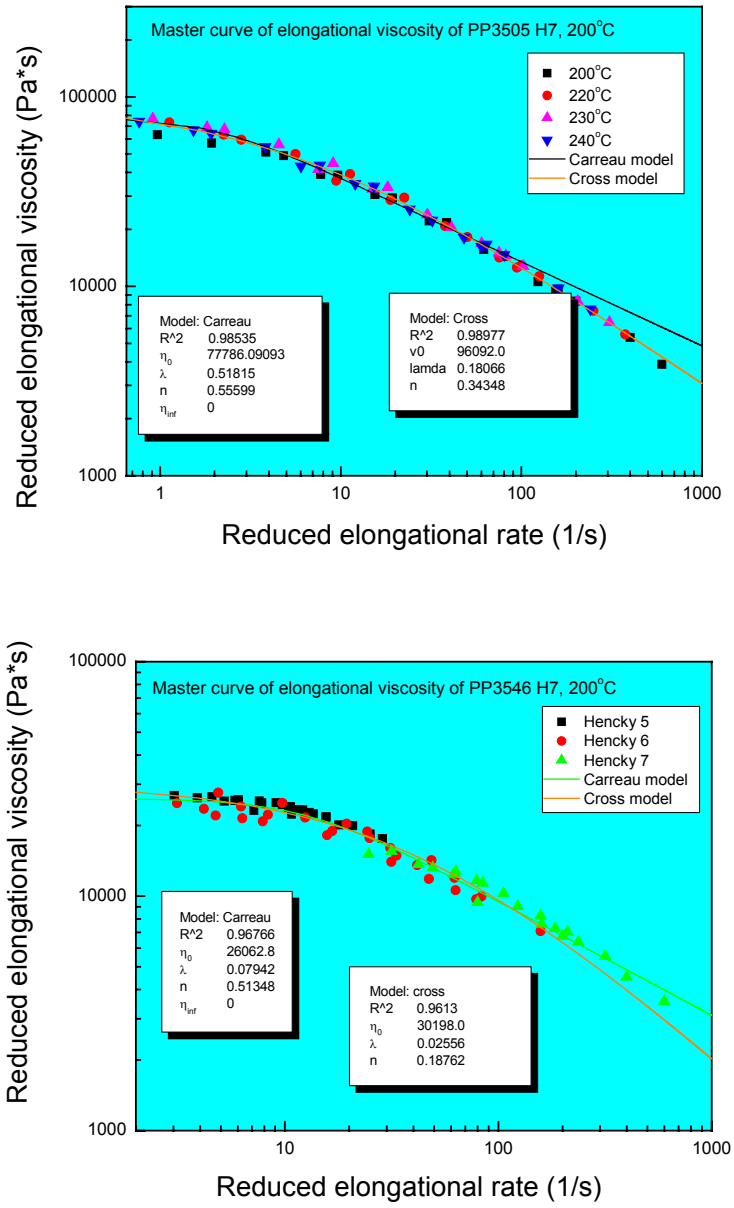

Figure 5.22 Master Curve of Elongational Viscosity of PP at Hencky 7 and 200°C.

§5.2 PROCESSING/PROPERTIES OF MELT BLOWN NONWONVEN MATERIALS

§5.2.1 Dimensionless numbers and their relationships during melt blowing

The hot air that flows through the air gap on the die manifold causes fiber attenuation and entanglement. The entanglement results from inducing chaotic flow of fibers at certain small region just below the die block, The fiber mass is deposited onto a collector belt with the aid of the hot air flow and suction applied beneath the collection belt. The flow behavior of the fibers between the die and the collector belt is critical to the final properties of the nonwoven material. Dimensionless analysis is a very useful tool in the fluid dynamics. Dimensionless numbers have been used to characterize systems and understand observed behaviors during fiber attenuation [84].

The Reynolds numbers for the cooling air was given by

$$N_{Re,\,air} = \frac{(L_c \rho_{air} v_{air})}{\mu_{air}} \tag{5.16}$$

where L_c is the critical length, ρ_{air} is the density, v_{air} is the air velocity at the die tip calculated from the air flow rate and the set parameters of die settings, and μ_{air} is the viscosity at the die tip temperature and humidity. The critical length, Lc, is assumed to be the length of fiber at the transition of the fibers from parallel to chaotic interaction. The Hencky strain is used to express the overall strain in the fiber and is defined as:

$$\varepsilon_h = 2\ln\frac{D_o}{D_f} \tag{5.17}$$

where D_o and D_f are the initial and final fiber diameters. The initial fiber diameter is assumed to be the diameter of the die holes; the die swell of the polymer extrusion is minor due to very low viscosity, small normal force and fast relaxation. The final diameter is an average of the fiber diameters measured by microscopy in the laboratory using samples of the fabric. For the polymer, the Reynolds number is calculated by

$$N_{Re,\,polymer} = \frac{(D_f \rho_f v_f)}{\eta} \tag{5.18}$$

where ρ_f , and η are the density, and viscosity of the polymer at the polymer melt temperature, respectively, and v_f is the final velocity of the fiber determined from the volumetric flow rate and average final fiber diameter of the fibers. Since the density of the polymer does not change much with the temperatures used in this experiment, the polymer density was assumed constant. In the region just below the die before the onset of chaotic behavior, which is in the range of 10 to 25 mm, the attenuated fibers can be modeled by assuming the semi-hyperbolic flow shape that is used to measure the elongational viscosity in the laboratory. This assumption implies an isothermal system and quasi-equilibrium attenuation, both of which are reasonable conditions over a short length just below the die block because the polymer melt temperature and air temperature are high at that range and may result in minimal

errors. So the elongational viscosity is used to calculate the Reynolds number. Figure 5.23 shows the correlation between these dimensionless numbers.

§5.2.2 Relationship between dimensionless numbers and properties of nonwoven materials

The laminar flow region only occurs over a short distance (10-20 mm) from the die plate during melt blowing. Below this point, the behavior of the fibers becomes chaotic, probably due to shedding of vortices in the air. Once the fibers reach the collector belt, it is this chaotic behavior that is responsible for the entangled web, which determines the structure of the melt blown fabric. In fact, these entanglements are related to many of the desirable properties of nonwoven fabrics. In an ideal structure, the fibers in the web have truly random orientation, and all the properties of fabric are isotropic.

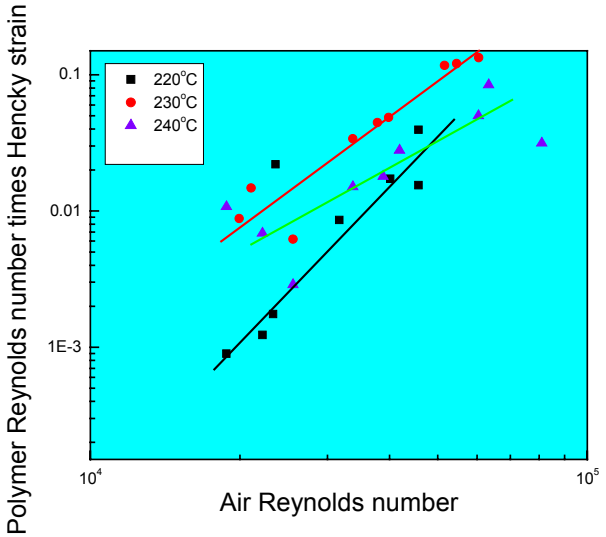

Figure 5.23 Relationship between Dimensionless Numbers.

Also, random orientation of fibers should result in a small pore size that produce improved barrier properties, such as air permeability and hydrohead. Knowing the correlation between the Reynolds number of air and the Reynolds number of the polymer is useful information for the production of nonwovens, because this will allow for the prediction of physical properties. Due to the blowing of high velocity hot air, the viscosity of the polymer changes with distance from the die plate to the collector during the processing. Since the laminar flow region is such a short length compared to the distance from the die to the collector (greater than 300mm), it is reasonable to assume that the viscosity is constant in that short region. Although the elongational viscosity is more representative of the system, the shear viscosity was used to calculate the polymer Reynolds number instead of elongational viscosity because it is easier to measure and is the value typically used in industry. Figures 5.24 and 5.25 show the correlation between the Reynolds number and the properties of nonwovens. With the an increase in airflow rate, the air Reynolds number increased, and the aerodynamic force acting on the fiber increase dramatically. The fiber diameters decreased due to the strong attenuation by the aerodynamic force. The small diameters led to small pore sizes and uniform distribution of the pore size. From these figure, it is obvious that there are critical points of Reynolds numbers, which are approximately 30,000 and 0.002 for the air and polymer Reynolds number respectively. The properties of the nonwoven webs changed sharply below these points, but only slightly above the critical points [84].

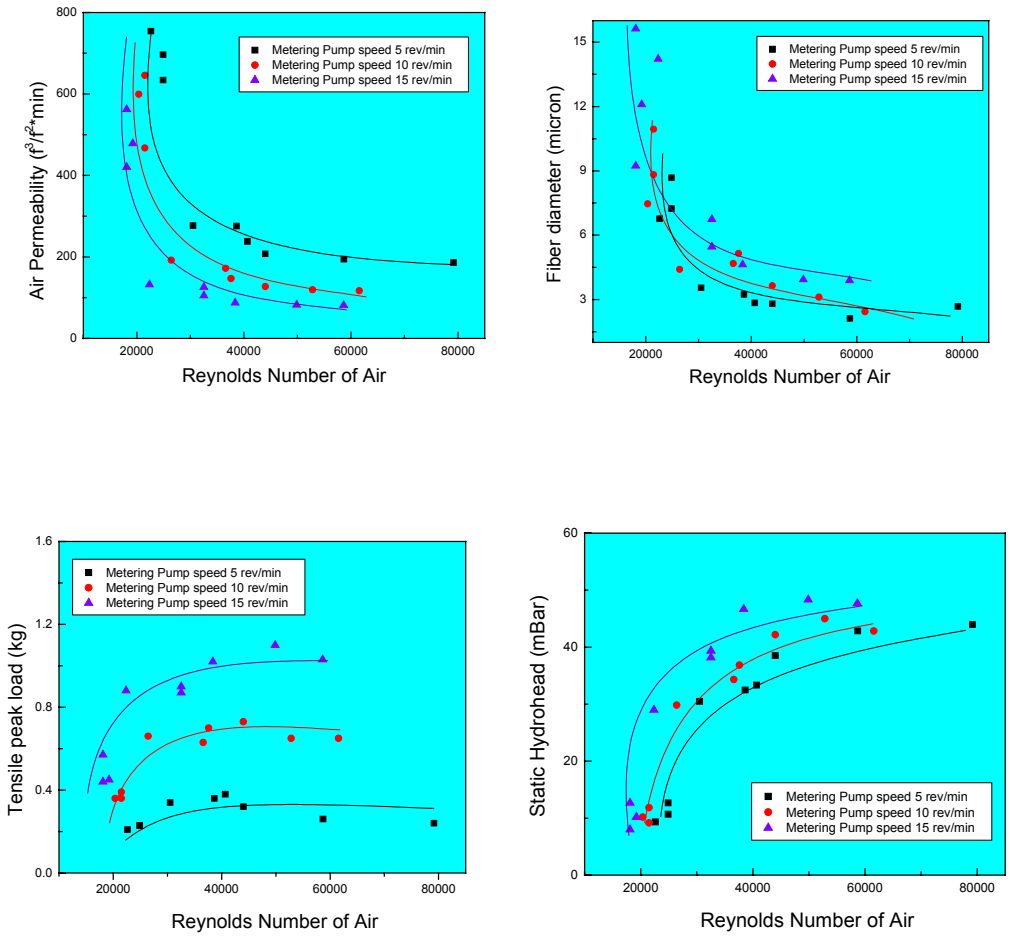

Figure 5.24 Relationship between Air Reynolds Numbers and the Properties of Nonwoven Materials.

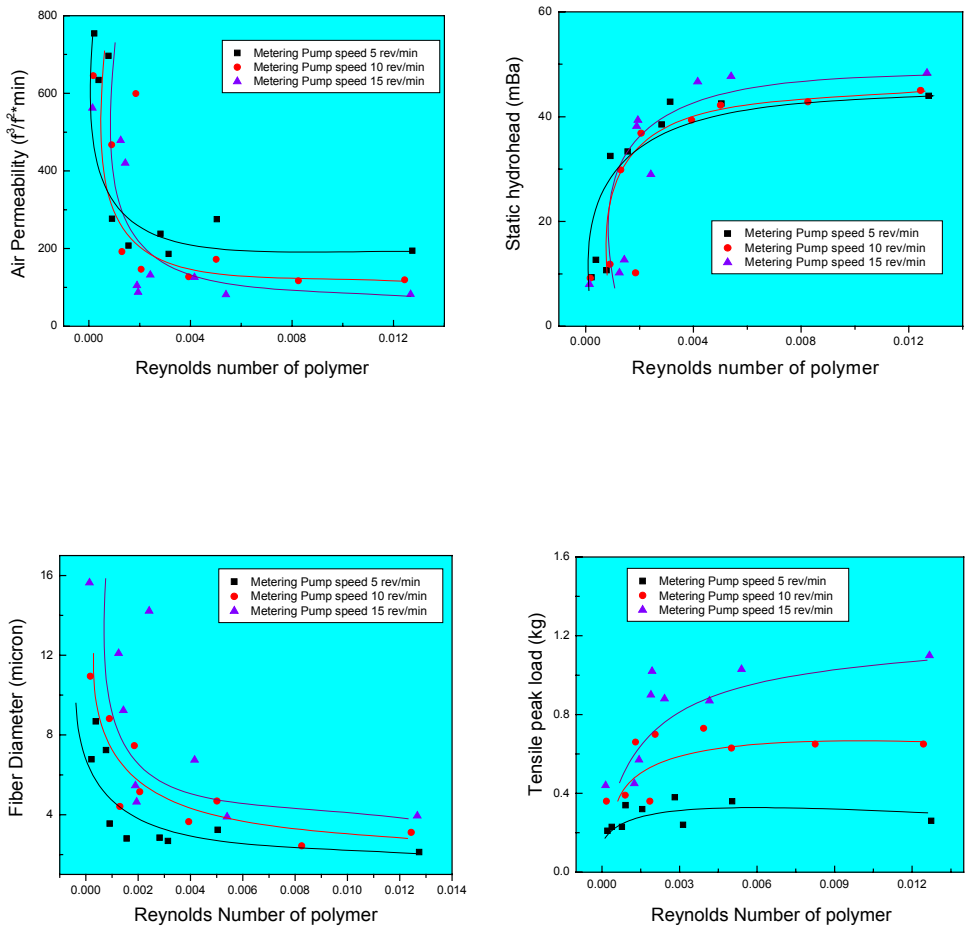

Figure 5.25 Relationship between Polymer Reynolds Numbers and the Properties of Nonwoven Materials.

§5.2.3 IR image analysis of melt blowing process

As the fibers are drawn down rapidly, the polymer chains inside each fiber become oriented in the direction of the fiber. This high degree of molecular orientation enhances crystallization, causing it to occur at temperatures well above the normal crystallization temperatures for bulk polymer of the same type. The significance of the temperature and location of crystallization to the final properties of a nonwoven material is not known; however, there is some reason to believe that it has some effect. When the fiber surface becomes rigid due to polymer crystallization, fiber attenuation will essentially end. These crystallized fibers may behave in the chaotic region more like stiff rods and transmit an additional draw down force back to the molten polymer closer to the die that is still above the crystallization point. Crystallization affects the lay down pattern of the fibers as they are deposited onto the collection belt and contact between the fibers prior to crystallization enhances nonwoven fiber adhesion. Under commercial processing conditions in melt blowing the crystallization rate of PP generally increases as orientation develops and also as the temperature decreases. The resulting exothermic character of the phase transformation during rapid deformation and unsteady state cooling can have a significant effect on the cooling curves.

High velocity hot air from the air gap in the die manifold drew in a large amount of ambient air, lowering the temperature of the air surrounding the attenuating filaments, and causing rapid unsteady state cooling of the filaments.

When crystallization occurs a competition between the heat removal by the cooler air and the heat generated by the crystallizing polymer occurs. If the heat generation rate is near that of the rate of heat removal then at least a shoulder occurs in the cooling curve, and if the two rates are nearly identical, a near isothermal region will result.

An infrared (IR) imaging technique demonstrated to be effective in determining temperature profiles in various systems and was applied to determine temperature profiles during the melt blowing process. Since the melt blowing die is a coat hanger die that is very common in the film extrusion industry, the temperature profile of the die is very important to control the uniformity of nonwovens especially for bicomponent fabrics, which can be controlled by the rheological properties of different polymers at certain temperatures. A different temperature distribution on the die block led to a different fiber distribution in the nonwovens.

Figure 5.26 showed the IR image of different runs in the melt blowing process. In these photos, different colors represented different IR intensities that could be measured by a linear tool in the software that was the accessory of the IR camera. Also the intensities were converted into temperature based upon the die block temperature and temperature of fabric on the belt measured by thermocouples. In these images, the orange color at the top of the image represented the die block that had the highest temperature, the color changed from warm to cold from the top to the bottom where the collector was located, indicating the fibers cool down from the die to the collector with the blowing of high velocity of air.

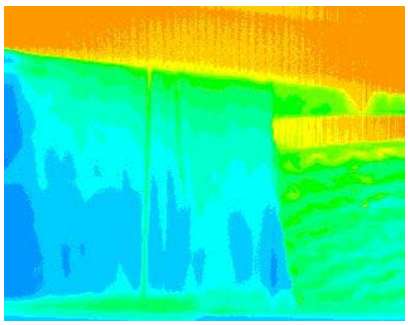

run8

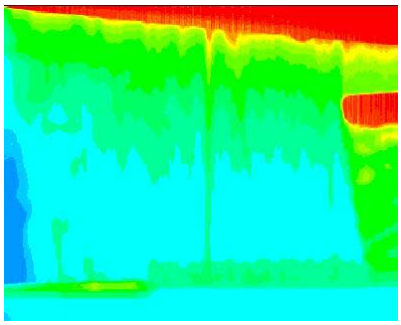

run9

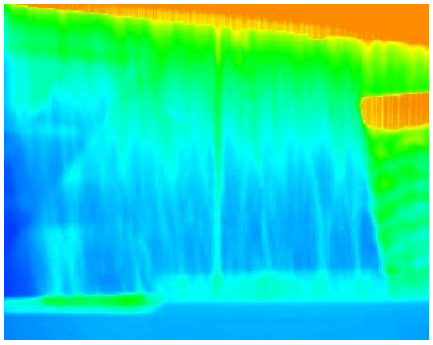

run10

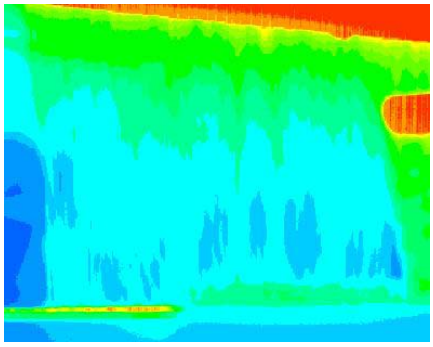

run11

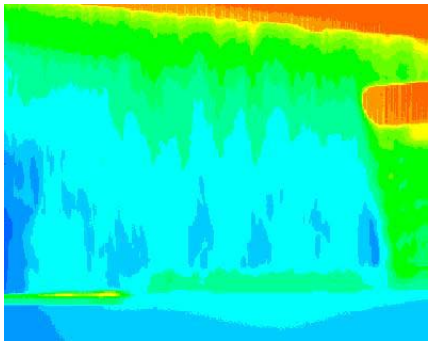

run12

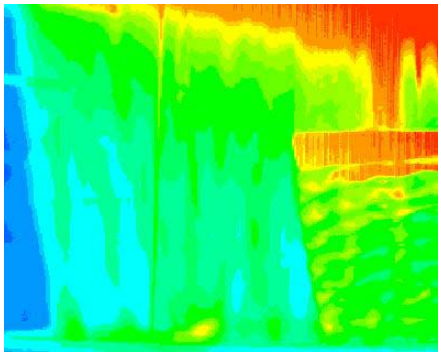

run13

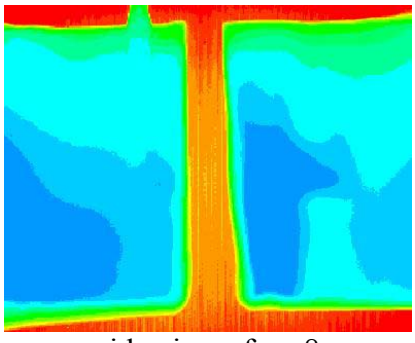

side view of run8

Figure 5.26 IR Image of Melt Blowing Process.

Figure 5.27 gives the intensity of the IR radiation that can be transformed into temperature. Figure 5.28 shows the temperature profile during the melt blowing process. A certain shoulder or isothermal region can be observed in the cooling curve on these plots that represent different processing conditions. From these figures, it appears that the temperature distribution is not uniform; the highest temperature was located at the center of the die and the temperature at the left side was lower than that at the right side. In the same run, the shoulder or isothermal region occurred at different locations due to different temperatures and cooling rates at different positions. There are several possible reasons for this, including the malfunctioning of the temperature controller for the die block, the hot air transport tube at the right side of the processing line, and the cold air drawn from outside the building through an open door at the left side of the processing line.

Figure 5.29 gives a typical cooling curve of melt blowing at different throughputs. The cooling profile of polymer melt at higher throughput was lower than that at low throughputs because the high throughput polymer melt needs more distance for cooling at the same airflow rate. In this analysis the shoulder or isothermal region that is assumed to be the crystallization region is located about 47mm from the die tip in the case of low throughput and about 125 mm from the die tip in the case of high throughput. The crystallization region also is very important to determine the distance from die to the collect that must be larger than the length from the die tip to this crystallization region or the nowovens will stick on the collector.

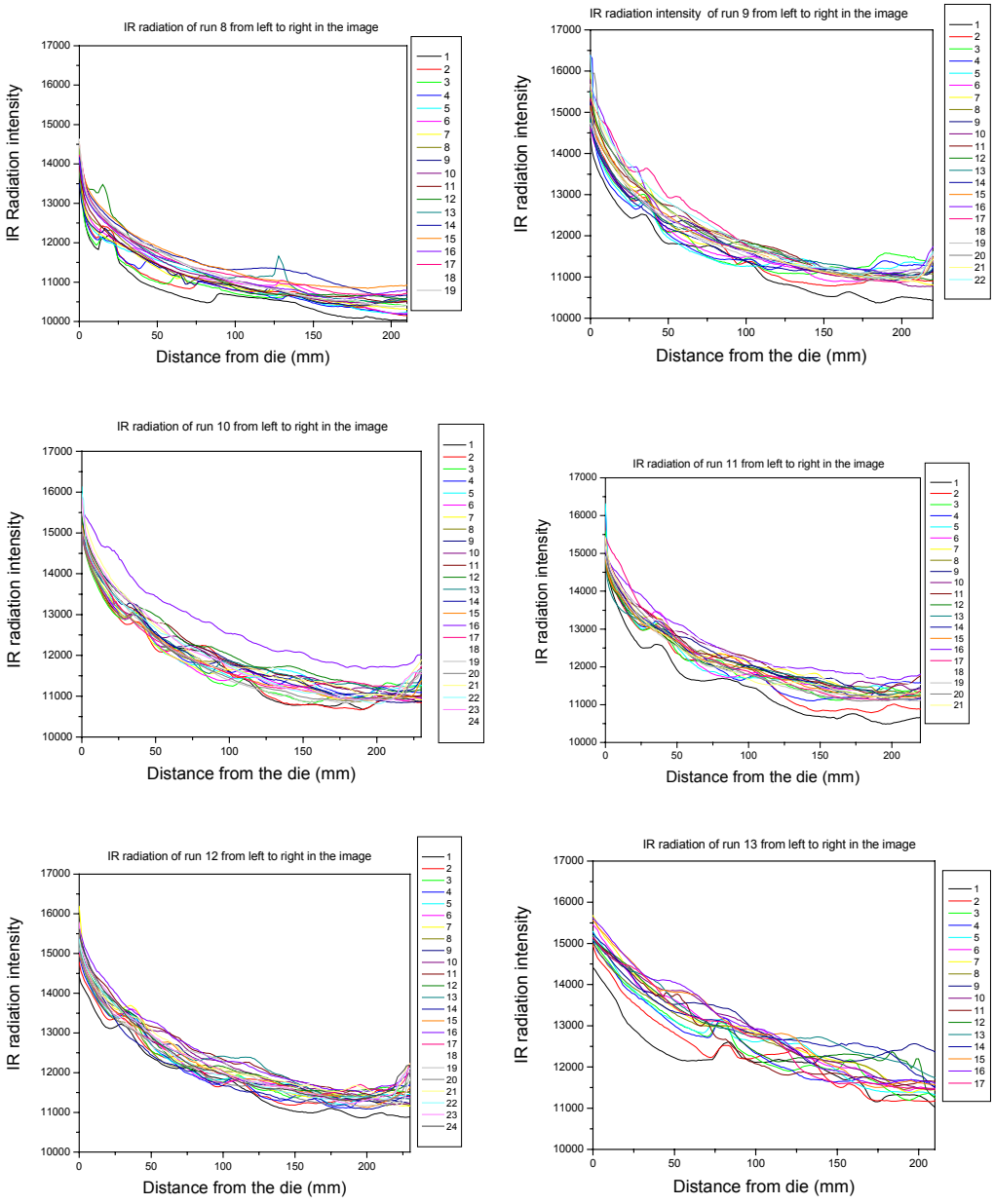

Figure 5.27 IR Radiation obtained from IR Image of Melt Blowing Process.

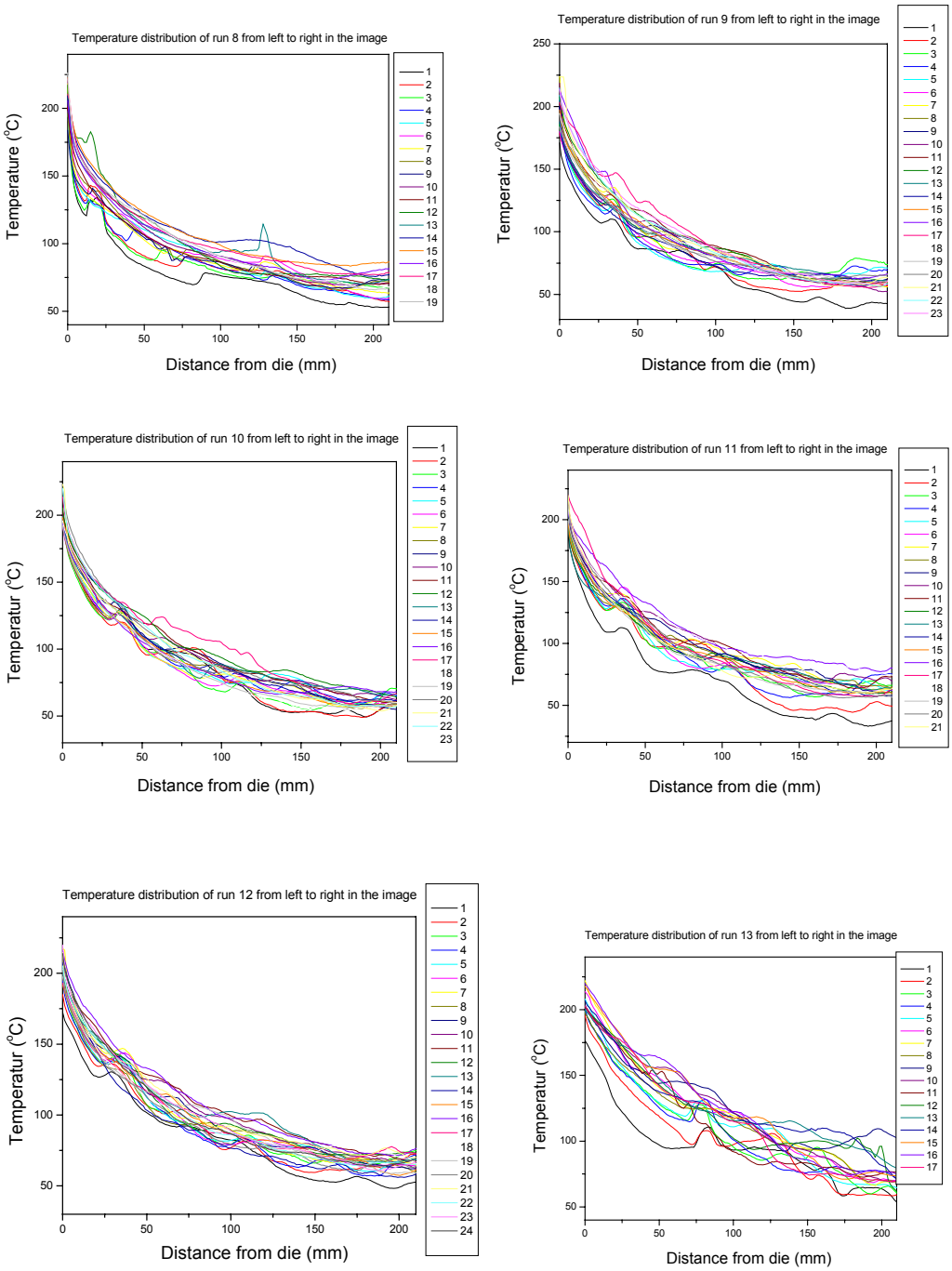

Figure 5.28 Temperature Distribution obtained from IR Image of Melt Blowing Process.

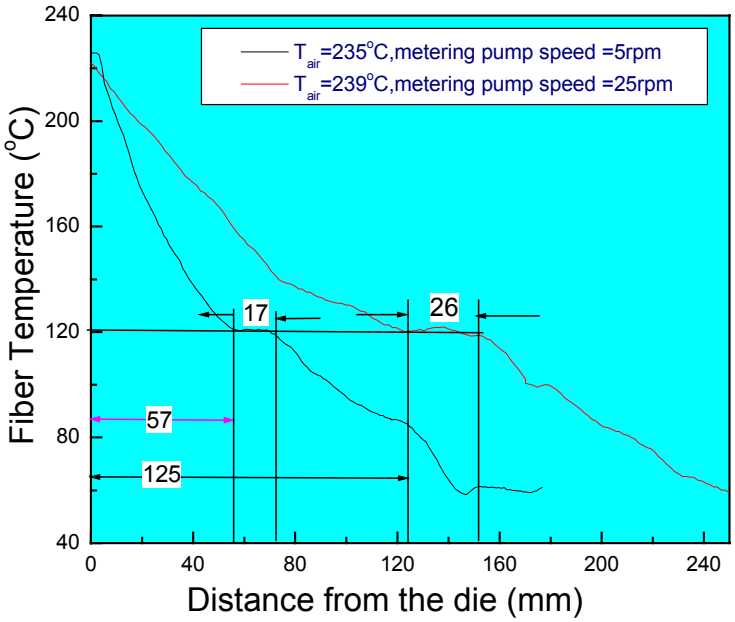

Figure 5.29 Comparison of Typical Cooling Curve of Melt Blowing Runs.

Different temperatures at different locations on the die tip lead to uneven flow of the polymer melt, which can cause variation of in weight at different positions. Figure 5.30 shows the basis weight of fabric produced in different runs. The basis weight varied only slightly in the machine direction, which means that the temperature and flow of polymer melt change very little with the time evolution; but the basis weights varied approximately 15% in the cross machine direction. The latter is produced by the uneven distribution of polymer across the machine direction due to temperature variation across the die block. The results of basis weight are consistent with different runs that have various processing conditions.

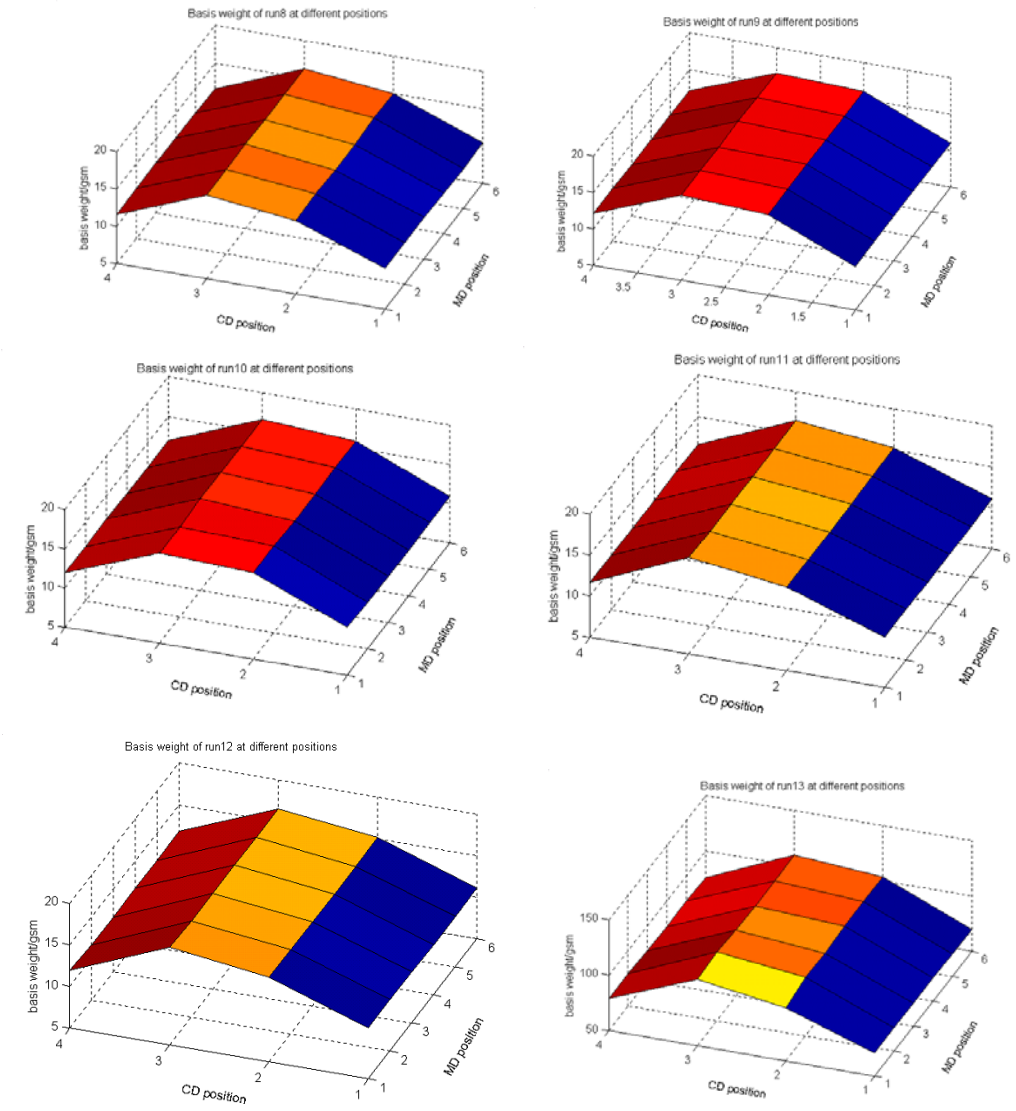

Figure 5.30 Basis Weight of Melt Blowing Fabric at Different Positions.

§5.2.4 Polymer degradation in the melt blowing process

The melt blowing of PP in air is accompanied by thermal oxidative degradation of the processed polymer. These processes take place most intensively on the fiber surface, and this may result in strengthening the adhesive interaction between polymer fiber and modifiers as well as in increased adsorbtivity of melt blown products [79]. The reduction of the degree of polymerization is often an outcome of polymer processing in the viscous flow state. Obviously, degradation will affect the polymer rheological properties, which will in turn affect the flow behavior and control of the process. In this section, the effect of processing conditions on polymer properties, especially rheological properties, was studied. The results may give some information for controlling the process and product quality.

From the plots presented in Figure 5.31 and 5.32, it can be observed that the viscosity of tested PPs decreased with time, which means that the polymer underwent a thermal oxidative degradation process. This degradation process, as measured by the decrease of the viscosity or loss modulus, was faster at higher temperatures. Also, the viscosity and loss modulus curves suggested that the process takes place by different mechanisms, due to the change in the slope at a temperature between 220 and 240^{o}C. Apparently, the degradation process may be at least partly controlled by controlling the processing temperature. DSC is a very convenient method to determine whether or not there is a chemical reaction during the material is under heat treatment.

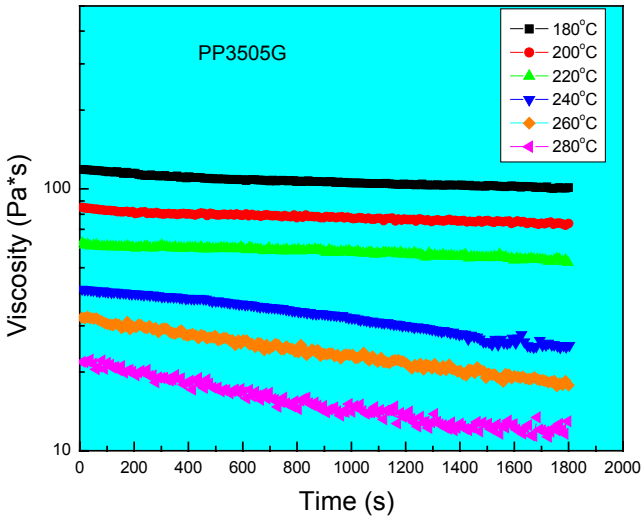

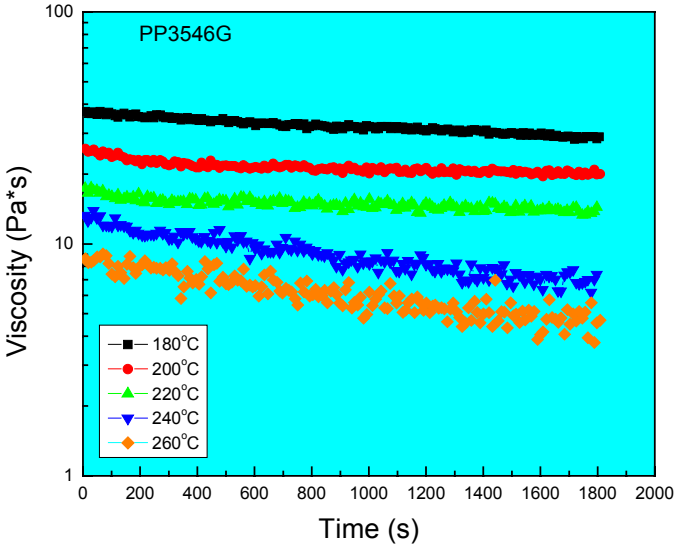

Figure 5.31 Viscosity Changing in ARES with Time Increasing.

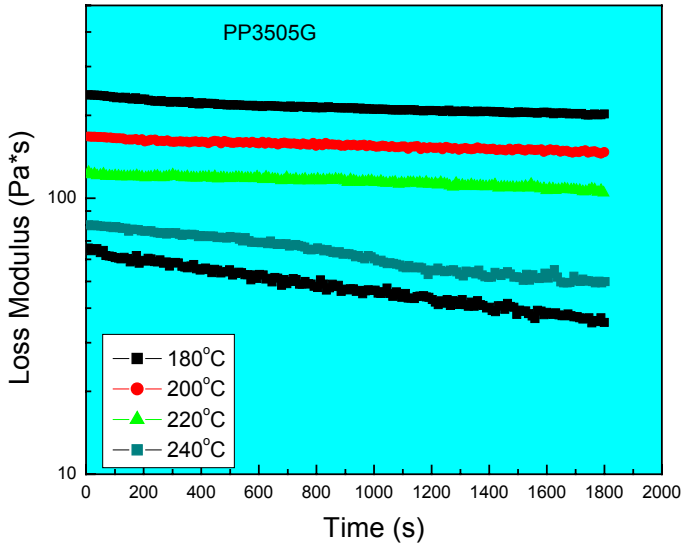

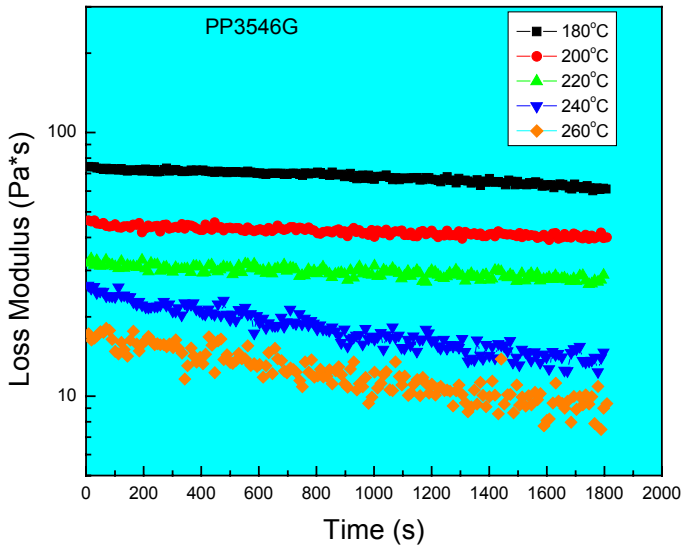

Figure 5.32 Loss Modulus Changing in ARES with Time Increasing.

In this research, DSC is used to determine the thermal stability of PP under oxidative atmosphere. Figure 5.33 is the DSC graph of PP3546G and PP3505G polymer samples. The black curve represents the sample that was put in the sample holder without a hole on the lid trapping a very small amount of air was trapped in the sample holder. The red curve (displaced upwards for comparison) represents the samples that were placed in the sample holder with a hole on the lid and purged with nitrogen for half an hour. Comparing these two curves, we can see that there is only a small difference between them, the small peak at a temperature close to 200^{o}C on the black curve (heating in the presence of air) being an indication of a possible oxidative degradation, but to a very little extent. There are several mechanisms for PP degradation, including heat, reactants such as oxygen, and mechanical action that will produce free radicals leading to scission of the molecular chains. During melt blowing process, the high temperature, high shear rate and air blowing will concurrently contribute to the polymer degradation. Figures 5.34-5.39 show the effect of processing conditions, such as polymer melt temperature, airflow rate, and gear pump speed, on polymer viscosity, storage modulus, and loss modulus of the two polymers. These data indicate that polymer viscosity decreased with polymer melt temperature due to thermal degradation. Polymer viscosity also decreased with increase of airflow rate, and this may be due to the enhancement in thermo-oxidative degradation rate. But higher airflow rates cool down the polymer melt more quickly, so there may be a competition between thermal degradation and cooling effects.

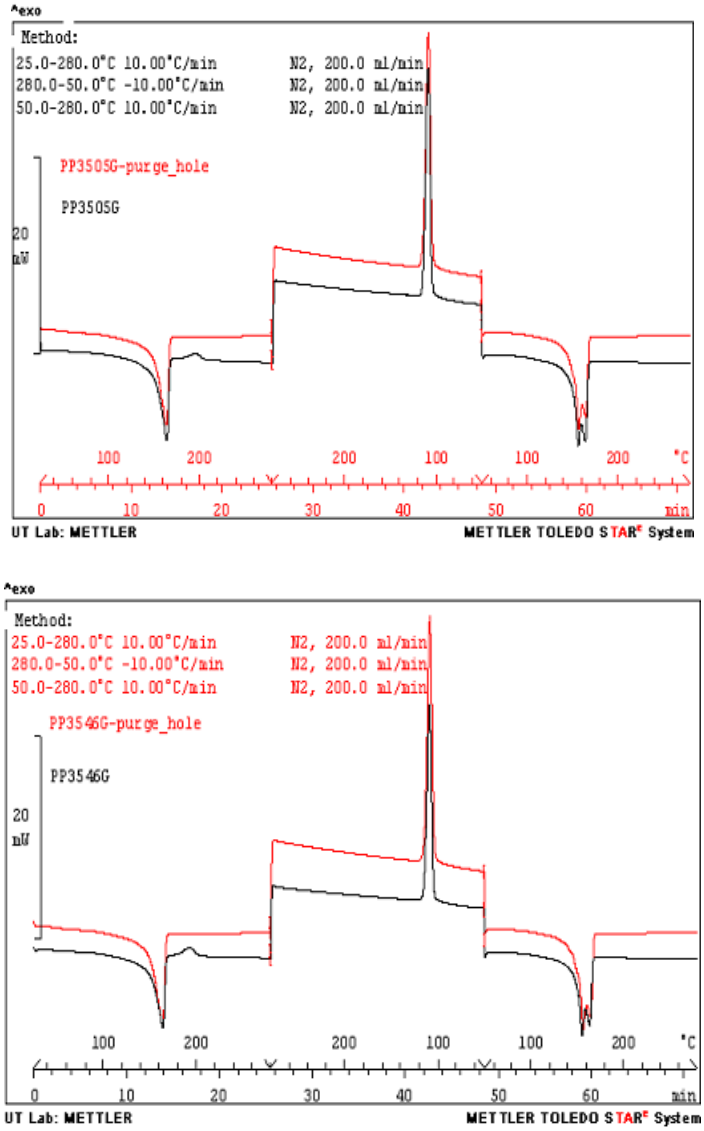

Figure 5.33 DSC Trace of PP during Heating and Cooling Cycle.

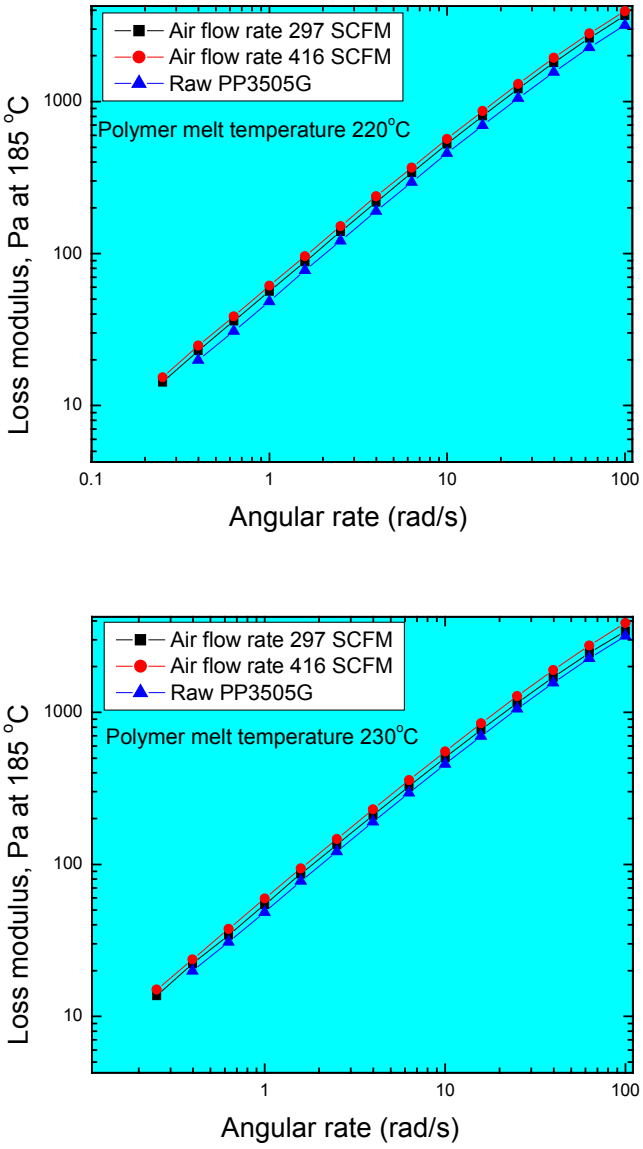

Figure 5.34 Changing of Loss Modulus of PP 3505G during Melt Blowing Process.

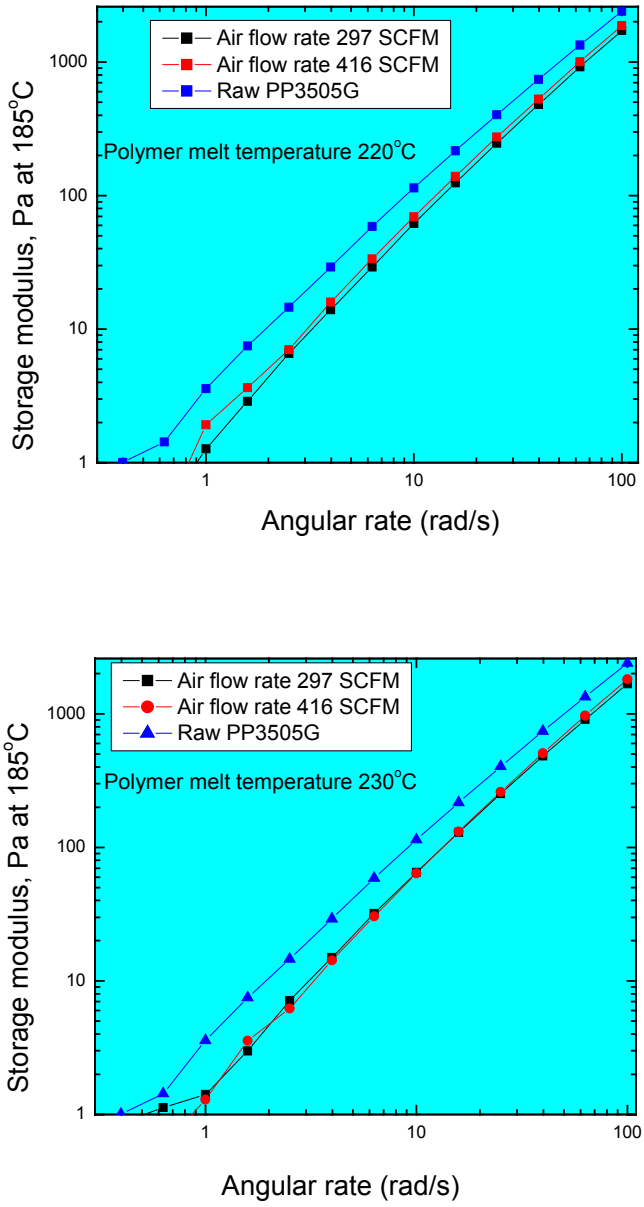

Figure 5.35 Changing of Storage Modulus of PP 3505G during Melt Blowing Process.

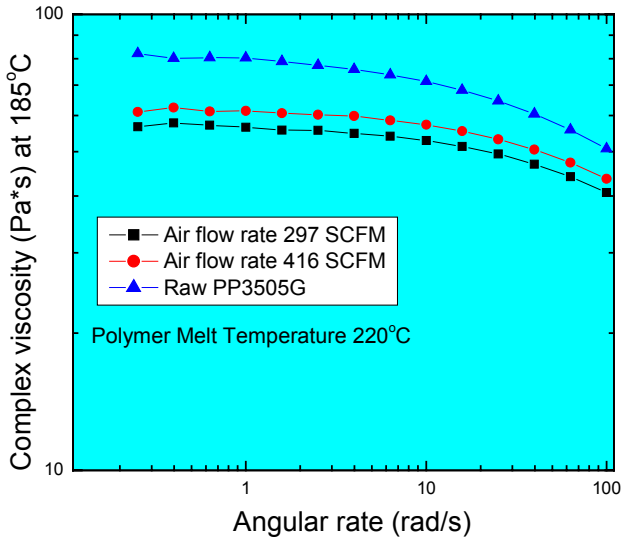

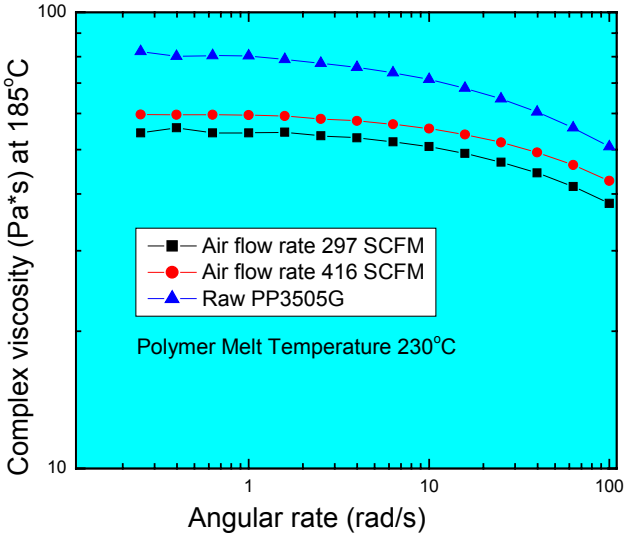

Figure 5.36 Changing of Complex Viscosity of PP 3505G during Melt Blowing Process.

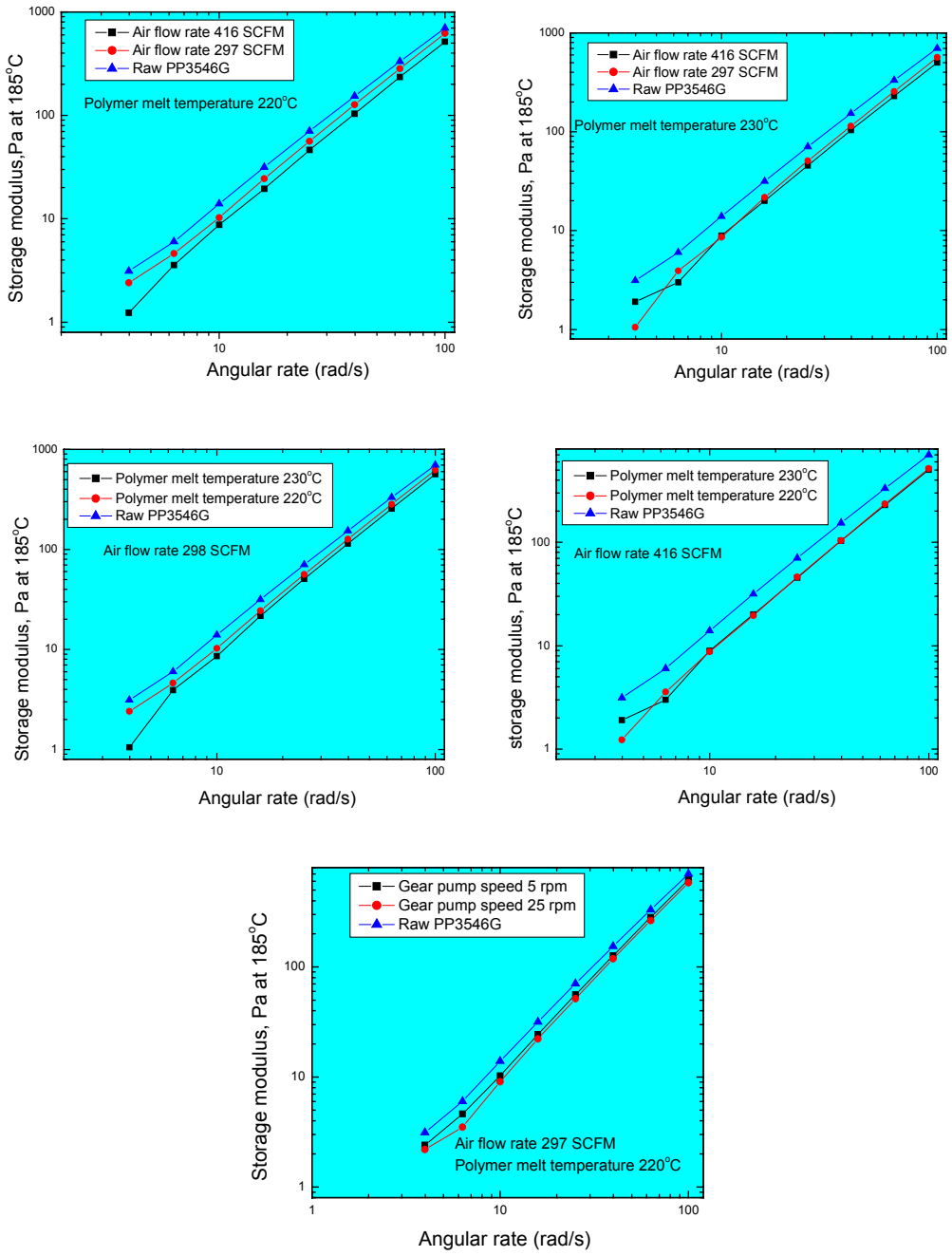

Figure 5.37 Changing of Storage Modulus of PP 3546G during Melt Blowing Process.

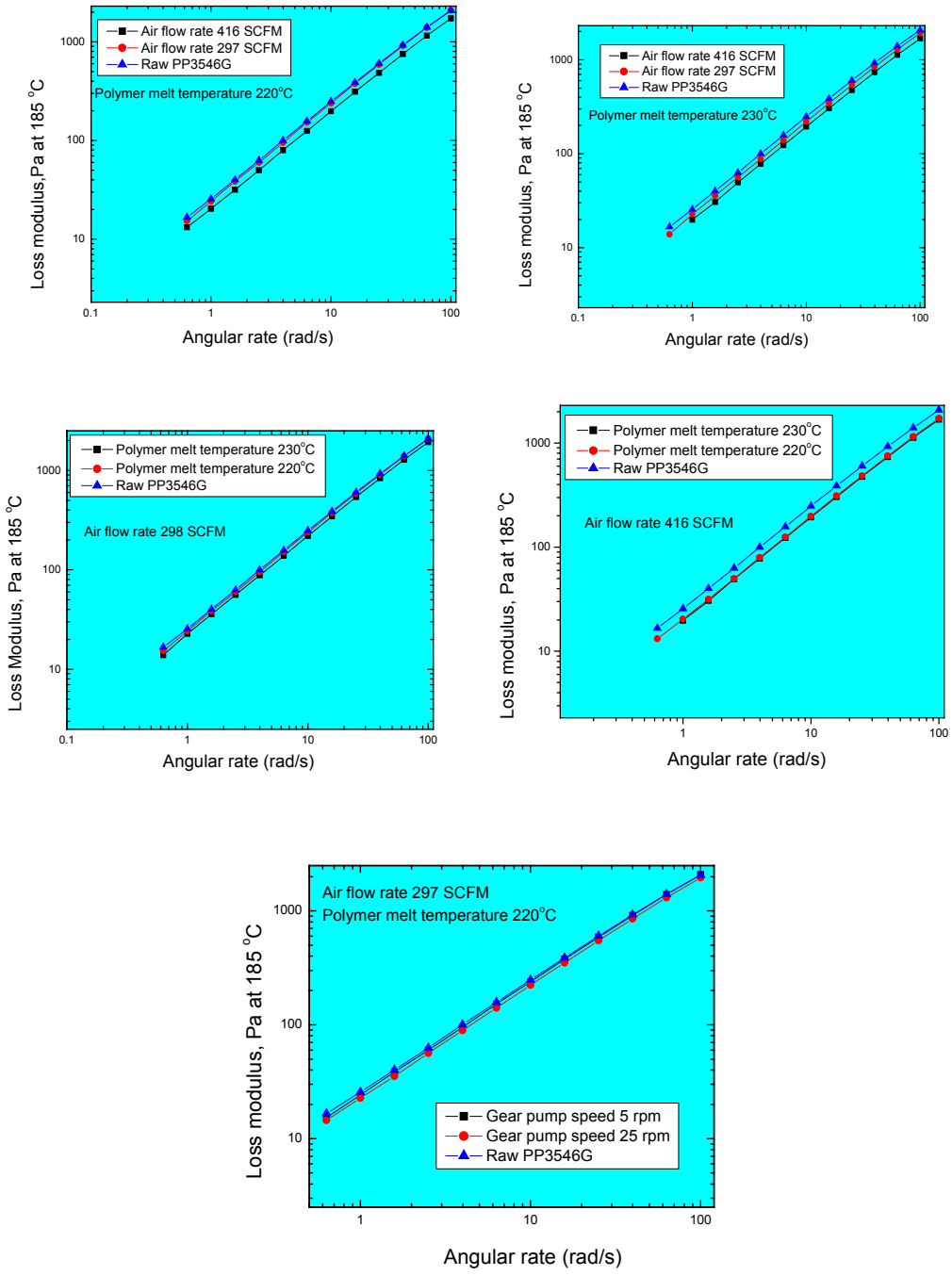

Figure 5.38 Changing of Loss Modulus of PP 3546G during Melt Blowing Process.

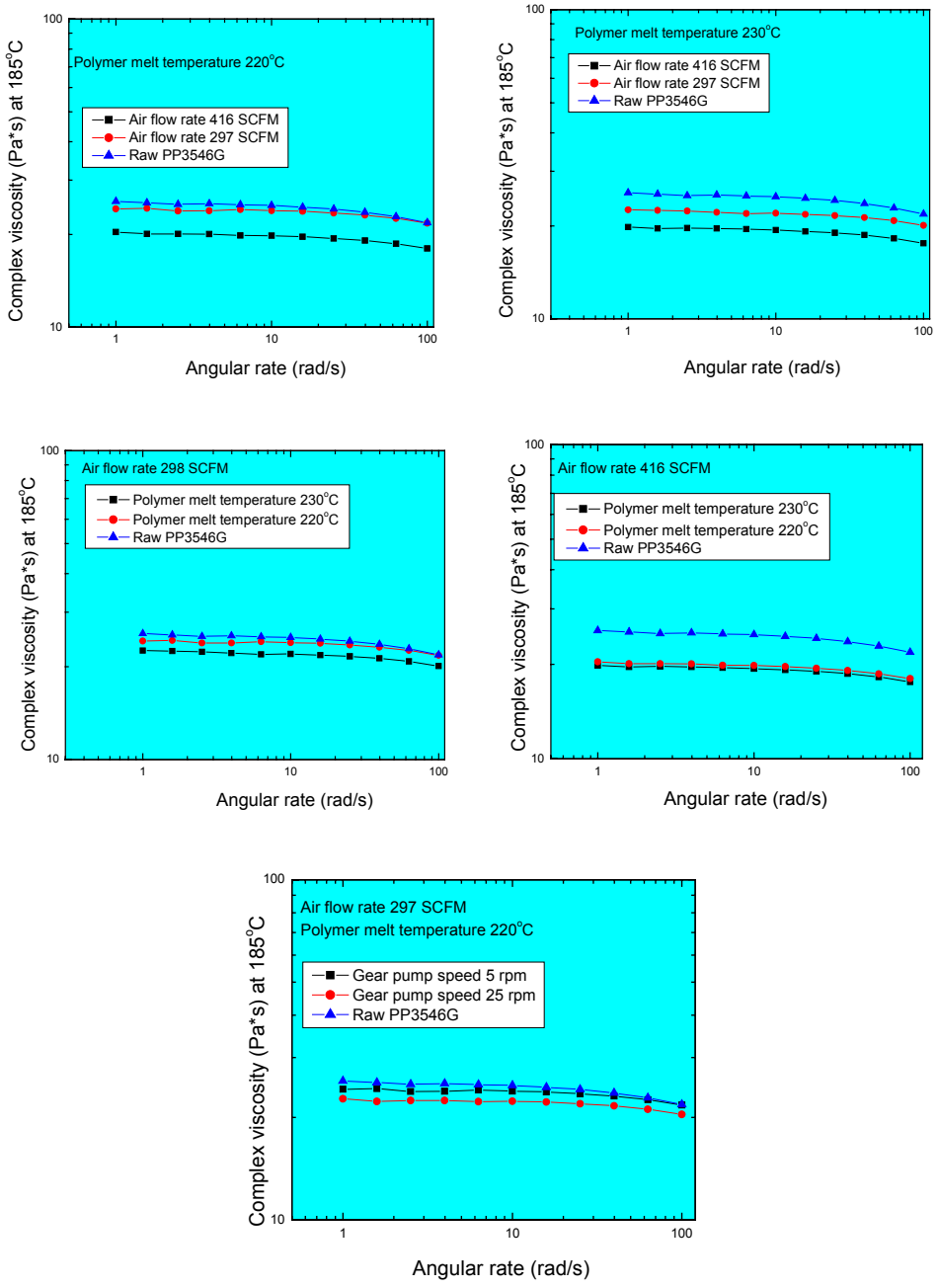

Figure 5.39 Changing of Complex Viscosity of PP 3546G during Melt Blowing Process.

Gear pumps were used to transport the polymer melt and provide a constant flow rate to the die. The gears in the pump generate high shear rates during operation, which may lead to polymer mechanical degradation. In this study, different gear pump speeds were used to control the flow rate. The data show that gear pump speed affected the degradation; high pump speed produced more degradation of PP3546G. But the extent of degradation, as occurring during the industrial processing is under a tolerant level for product quality. It can be concluded that there are several factors to control polymer degradation and that will affect viscosity, such as temperature, pump speed and air flow rate. These dynamic rheological properties can be used to determine polymer molecular weight and molecular weight distribution.

§5.2.5 Molecular weight and molecular weight distribution

Molecular weight (MW) and molecular weight distribution (MWD) are very important characteristics related to selection of polymers for a specific application and process. There are several methods to determine the MW and MWD, such as boiling point elevation, freezing point depression, vapor pressure osmometry, light scattering, and ultracentrifugation et al. The most widely applied method to determine the MW and MWD is size exclusion chromatography (SEC) [71,72]. However, it is a time consuming and labor-intensive method and the accuracy of the results depend strongly on the skills and experience of the operator. Furthermore a

high temperature SEC and special solvents are required to determine the MW and MWD of semi-crystalline polymers.

It has long been realized that the viscoelastic rheological properties of polymer melts are related to molecular motions and are very sensitive to the MW and MWD [71-73]. Also it has been noted that the linear viscoelastic rheological properties of polymer melts are strong functions of MW and MWD. It is possible that the MW and MWD can be determined by measuring the linear viscoelastic rheological properties of polymers [74-76]. Compared with other methods, rheological measurements are quick, easy, and inexpensive, thus providing an opportunity to develop real time, online process and quality control analysis of polymer properties in industrial applications.

A double-reptation mixing rule with a single exponential relaxation function that relates the relaxation modulus to the MW and MWD was introduced by Mead [77]. Mead's approach is applied in the ^{RSI}Orchestrator^{TM} software installed on the computer connected with ARES [78], which is used to determine the MW and MWD of PP in this research.

The double-reptation mixing rule, used in the calculations is given as

$$G(t) = G_N[\int_0^\infty W(M)\sqrt{F(M,t)}dM]^2 \tag{5.18}$$

where $G(t)$ is the relaxation modulus and can be determined from the linear viscoelastic experiments, G_N is the plateau modulus, $W(M)$ is the weight based MWD, and $W(M)dM$ represents the weight fraction of material with molecular

weights between M and $M+dM$. The function $F(M,t)$ is the monodisperse relaxation function, which represents the time dependent fractional stress relaxation of monodisperse polymer following a small step strain. A single exponential form of this function is

$$\sqrt{F(M,t)} = \exp(\frac{-t}{2\lambda(M)}) \tag{5.19}$$

where,

$$\lambda(M) = K_\lambda M^\alpha \tag{5.20}$$

and where $\lambda(M)$is the characteristic relaxation time for the monodisperse system and K_λ is a coefficient that depends on the precise chemical structure of the polymer and temperature. The relaxation time exponent α indicates how strongly the relaxation time of a polymer is related to its molecular weight.

The relaxation spectrum $H(\lambda)$ can be obtained from linear viscoelastic rheological data $G'(\omega)$ and $G''(\omega)$, using the following equations,

$$\frac{G'}{\omega^2} = \int_0^\infty \frac{\lambda(H(\lambda))d\lambda}{1+(\lambda\omega)^2} \tag{5.21}$$

$$\frac{G''}{\omega} = \int_0^\infty \frac{H(\lambda)d\lambda}{1+(\lambda\omega)^2} \tag{5.22}$$

The relaxation modulus $G(t)$ can be calculated from the following equation

$$G(t) = \int_{-\infty}^{+\infty} H(\lambda)e^{-t/\lambda} d\ln\lambda \tag{5.23}$$

Figure 5.40 gives the algorithm to calculate the molecular weight and molecular weight distribution from rheological properties. The "Synthesize Molecular Weight" function in ^{RSI}Orchestrator^{TM} software is designed to calculate the molecular weight and molecular weight distribution with $G'(\omega)$ and $G''(\omega)$ by synthesizing a distribution based on material properties and an initial guess for molecular weight and molecular weight distribution [78]. Dynamic rheological data are calculated from the initial conditions and then compared with the experimental data to determine how close the two sets of data are. The calculation procedure is repeated until a predetermined acceptable error is reached. In the case of PP, the software gives the three parameters, K_λ , α , G_N , for the calculation. Figure 5.41 gives the calculation of the molecular weight and molecular weight distribution. The error for the calculation of molecular weight and molecular weight distribution for PP3546G was relatively large due to the low instrument sensitivity for low viscosity polymers.

Figure 5.42 and 5.43 give the molecular weight and molecular weight distribution of PP after the melt blowing processing. Apparently the polymer degraded during the process, but its molecular weight distribution changed very little. During the polymer degradation, the possibility is greater for long chains to be broken than short chains, and one long chain will form two short chains, so the molecular weight distribution will be narrowed. Since the original polymer has a very narrow molecular weight distribution, the change of molecular weight distribution is small.

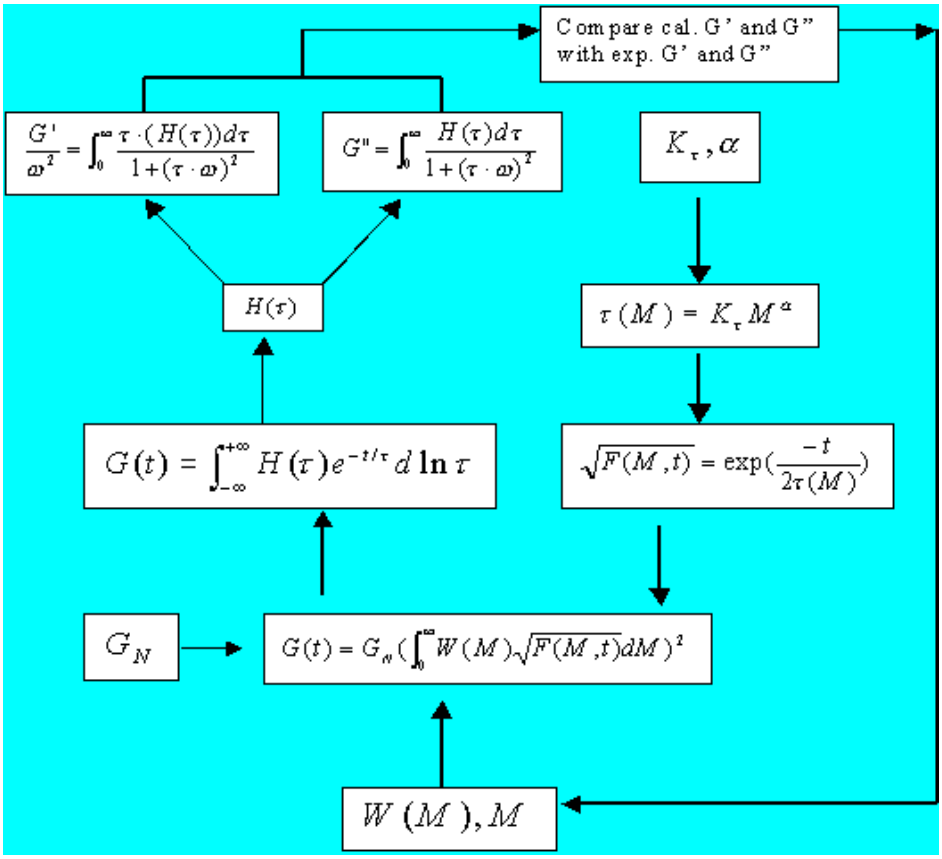

Figure 5.40 Algorithm for Calculation of the Molecular Weight and Molecular Weight Distribution.

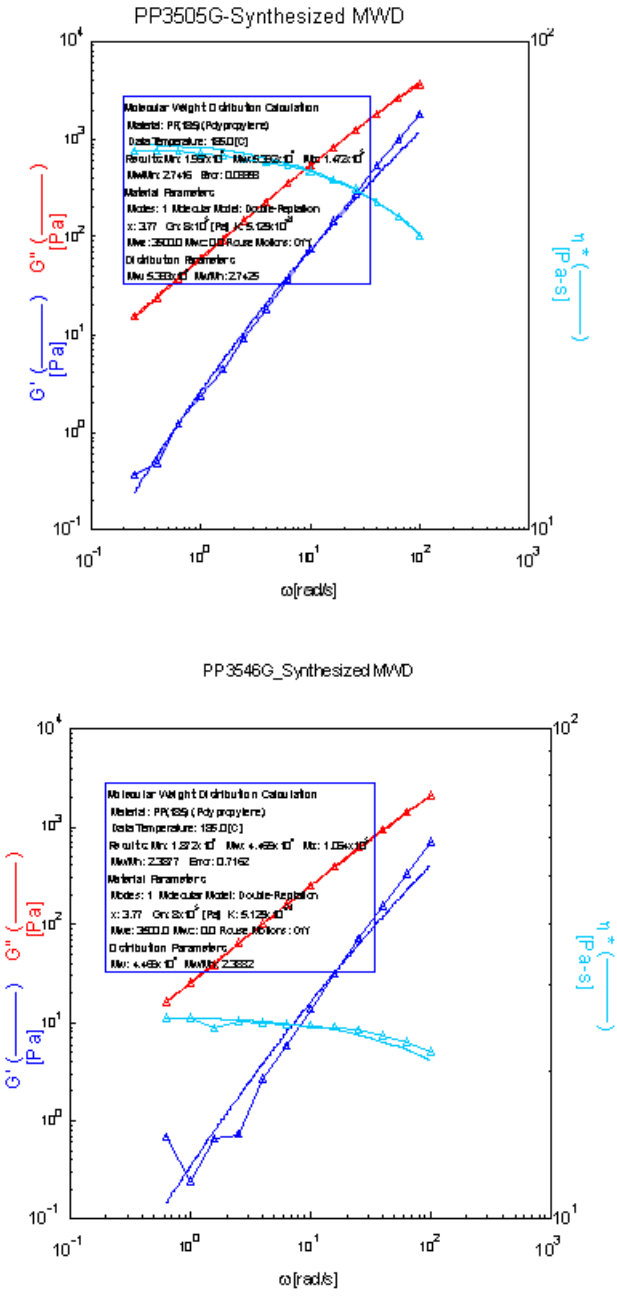

Figure 5.41 Calculation of Molecular Weight and Molecular Weight Distribution.

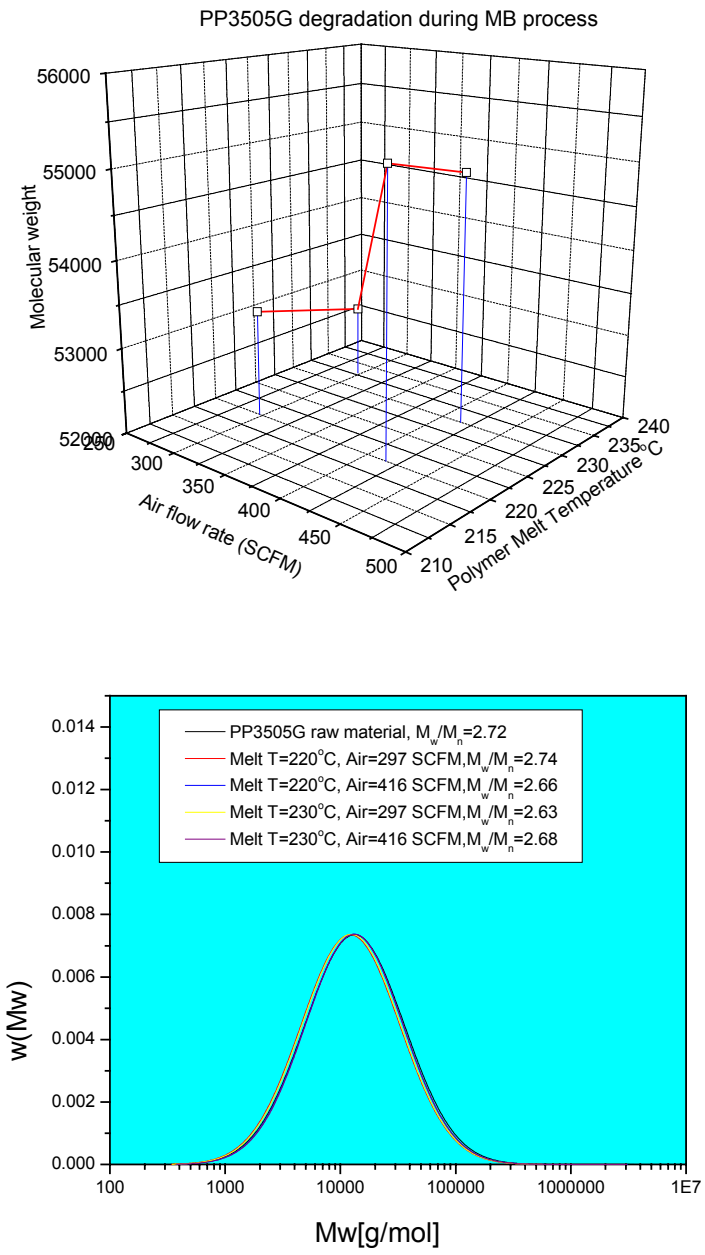

Figure 5.42 Changing of Molecular Weight and Molecular Weight Distribution of PP 3505G.

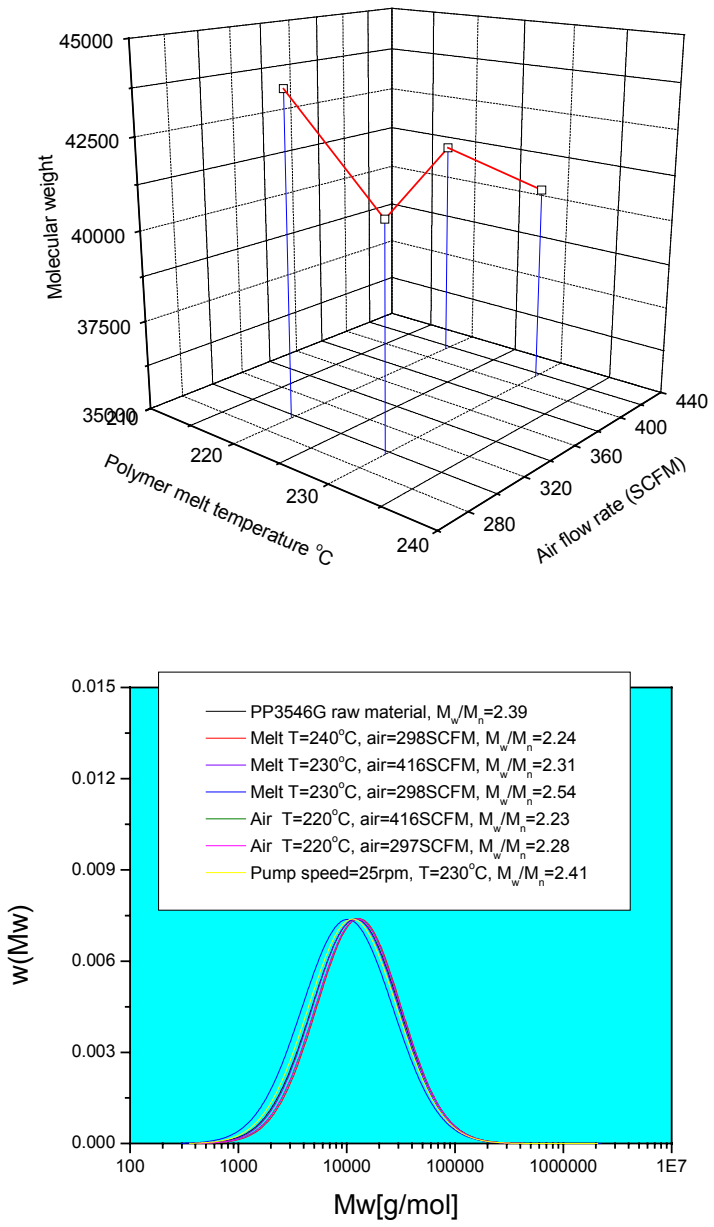

Figure 5.43 Changing of Molecular Weight and Molecular Weight Distribution of PP 3546G.

§5.3 DEVELOPMENT OF ONLINE RHEOLOGICAL SENSOR

§5.3.1 Design of the online rheological sensor

The theoretical background discussed in the Chapter 3 was the foundation for the design of the online rheological sensor. Those equations were used to calculate the gear pump specification based on certain shear or elongational rates. Figure 5.44 shows the general scheme for designing the online sensor. The online rheometer system can be divided into three sub-systems: mechanical system, measurement and control system, and interface and computer system. Figure 5.45 shows the schematic of the online rheological sensor and photos. The mechanical system includes the sensor block, adaptor for the connection between twin-screw extruder and sensor block, dies and die holder. Capillary dies and semi-hyperbolic dies can be inserted at the bottom of the sensor block and can be sealed by two die holders respectively, which are hollow screws and can be easy dismantled to change or clean dies. The measure and control system includes pressure transducer, thermocouple, heating elements, and gear pumps, which are installed on the sensor block, and gear-pump motor controller, temperature controller, and pressure readout instruments, which are installed in the control box. The interface and computer system includes an RS485 serial interface for the communication between the computer and control box, a laptop computer that is a laptop with software such as Labview, OPC server, and Excel. The sensor has been installed on the twin-screw extruder to do the further testing and will be used to do the online measurements.

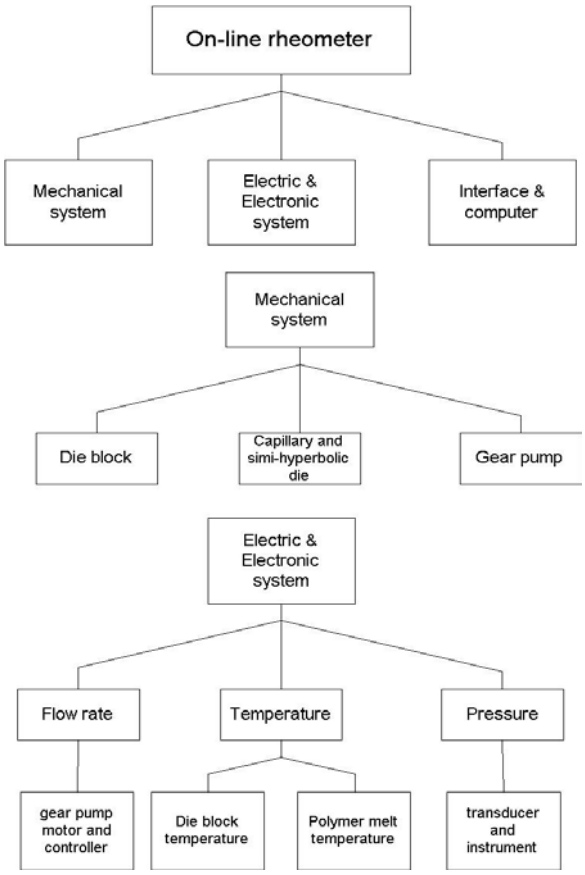

Figure 5.44 General Design of Online rheometer.

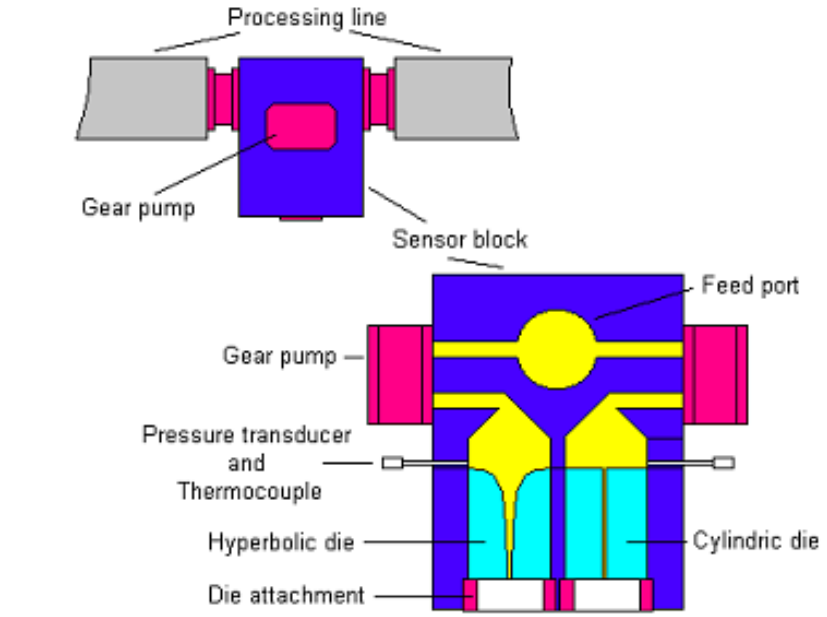

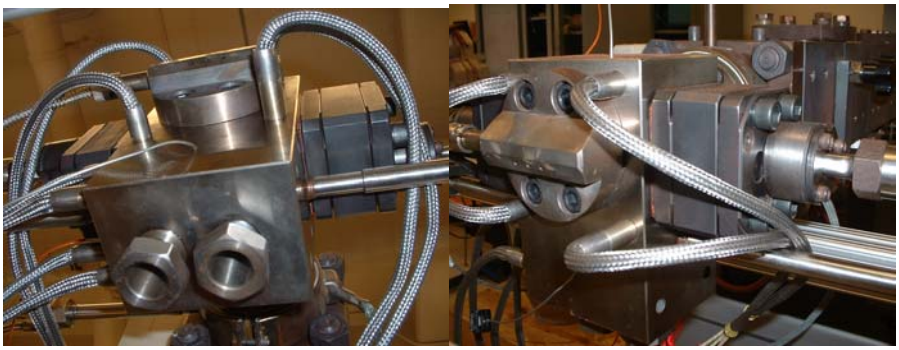

Figure 5.45 Schematic of Rheological Sensor and photos.

Two gear pumps whose speeds are controlled by digital motor speed controllers are used to control the shear rate and elongational rate by drawing polymer melts from the main processing stream from a twin-screw extruder. The gear pumps drive the melt through two dies, e.g. capillary and semi- hyperbolic die, so the shear and elongational viscosities of a polymer with the same thermal history can be measured simultaneously. Two hyperbolic or two capillary dies may be inserted in the die holders to measure the elongational viscosity at two Hencky strains, or the shear viscosity at two conditions simultaneously. Pressure transducers combined with thermocouples measure the pressure drop and temperature of polymer flow. Two groups of heating elements are used to control the temperature of sensor block that is divided into two zones in order to control the temperature more uniformly. Two thermocouples are connected with the two temperature controllers that can communicate with the laptop. The temperature of sensor block can be controlled to be the same temperature as the polymer melts from the main processing stream or at another temperature.

All the data and operation commands can be sent or received by the instruments independently; the communication between instruments and laptop is set through a serial interface and special software, such as OPC server. Labview is used for the process control and data acquisition, which will be discussed in the following sections. Since the capillary and semi-hyperbolic dies were built for the ACER, their dimensions were used to determine the gear pump displacement based on the theoretical analysis described in Chapter 3, which is 2CC/revolution. The speed of

the gear pump can be calculated by the code written in Labview based on the setting shear and elongational rate and gear pump displacement following the volumetrical flow rate equations described in Chapter 3.

§5.3.2 Hardware communication

5.3.2.1 RS485 serial communication Interface

As specified in the EIA-485 Standard, *Standard for Electrical Characteristics of Generators and Receivers for Use in Balanced Digital Multipoint Systems*, RS-485 expands on the RS-422 standard by increasing the number of devices from 10 to 32 and by working with half-duplex bus architectures [80]. RS-485 addresses the issue of using multiple transmitters on the same line. RS-485 defines the electrical characteristics necessary to ensure adequate signal voltages under maximum load and short-circuit protection, also it can withstand multiple drivers sending conflicting signals at the same time. For RS485 the cable can be up to 1200 meters long, and commonly available circuits work at 2.5 MB/s transfer rate, which are very important for the application in industrial processing automation and control. RS 485 is used for multipoint communications, where more devices may be connected to a single signal line. Typical half-duplex multidrop bus architecture involves a master-slave protocol, where each slave unit has its unique address and responds only to packets addressed to this unit. These packets are generated by Master (e.g. PC), which periodically polls all connected slave units. However, in a

half-duplex system, all transmitters and receivers are connected to the same transmission line. A half-duplex system is often referred to as a two-wire system. The connection of RS485 serial interface with the instruments is based on this principle. Figure 5.46 shows a typical half-duplex system, which includes the master and several slave devices. Due to some unknown reason, there was interference between instruments installed on the same RS485 serial bus, which included the data flowing malfunctions. The data can be read from the temperature controller and commands can be sent to the pressure indictors to do the calibration, but at the same time the pressure cannot be read from the pressure indictors and the temperature set points cannot be written to the temperature controller by the laptop. The problem was solved by introduced another RS485 serial bus, which makes the temperature controllers and pressure indicators to work independently. A RS485 serial interface with two communication ports from National instruments was used for the online rheological sensor, and the interface can be connected to the laptop through the universal serial bus port (USB). Experience indicated that using this design instruments from the same manufacturer could be installed on the same serial bus and instruments from different manufacturer may not be installed on the same serial bus due to different design of the commands and signal levels. If more serial communication buses are needed for further research, 8 and 16 serial buses boards are available from National Instruments. A desktop computer is recommended for the future process control since more measure and control boards from different companies can be installed in the desktop computer.

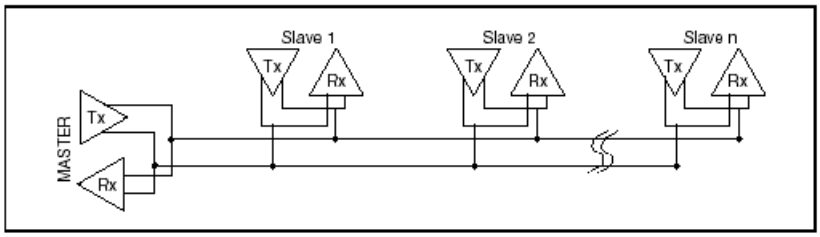

Figure 5.46 Schematic of a Typical Half-duplex System [80].

Before starting communication between the laptop and instruments through RS485 serial interface, the serial ports must be configured correctly. The serial configuration utility is fully integrated into the Windows 2000/XP Device Manager, which can be used to view or change the configuration of serial ports on the computer.

To configure a serial port, complete the following steps:

1. Select **Start»Settings»Control Panel** and double-click the **System** icon.

2. Click the **Hardware** tab and then click the **Device Manager** button.

3. Double-click the **Ports (COM & LPT)** icon.

4. Double-click the port you want to configure and refer to the following instructions:

• To view the hardware resources assigned to the serial port, click the **Resources** tab.

• To view or change the port settings, click the **Port Settings** tab.

For the Port Settings Tab:

• To change the RS-485 transceiver mode, or to enable or disable the FIFOs on the serial hardware, in the **Port Settings** tab, click the **Advanced** button.

5. To save your changes, click the **OK** button. To exit without saving the changes, click the **Cancel** button.

In the **Port Settings** tab, you can change any of the settings by clicking the arrow button to the right of a field. When you click the arrow button, a list of valid values for that field appears and you can select the desired setting from the list. Figure 5.47 shows the **Port Settings** tab. Most RS 485 systems use Master/Slave architecture; Single twisted pair cable is used in this application for the signal connection. In this version, all devices are connected to a single twisted pair cable for a certain communication port. Thus, all of them must have drivers with tri-state outputs (including the Master). Communication goes over the single line in both directions. It is important to prevent more devices from transmitting at once. The standard DB-9 connector on most serial cables was used to connect the interface with the instruments. Figure 5.48 shows the connection and function of pins.

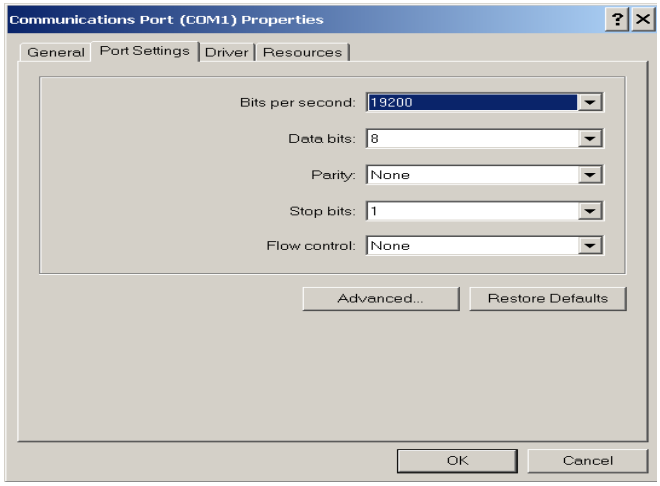

Figure 5.47 The Port Settings Tab.

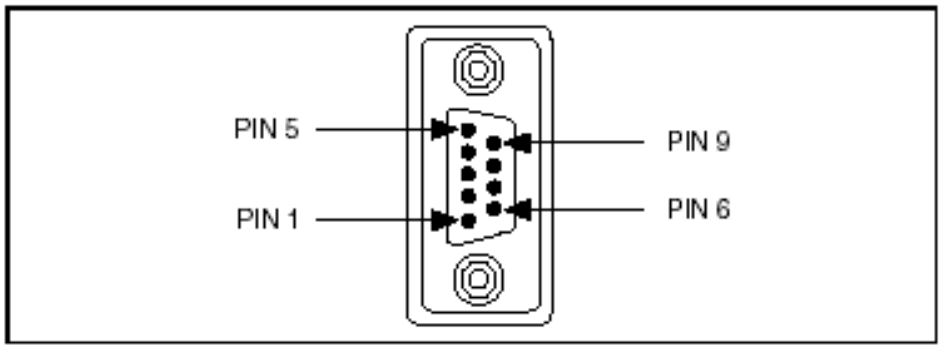

DB-9 Pin	232 Signal	485 Signal
1	DCD*	GND
2	$\overline{\text{RXD}}$	CTS+ (HSI+)
3	$\overline{\text{TXD}}$	RTS+ (HSO+)
4	DTR*	RXD+
5	GND	RXD–
6	DSR*	CTS– (HSI–)
7	RTS	RTS– (HSO–)
8	CTS	TXD+
9	RI*	TXD–

Figure 5.48 The Positions and Functions of Pins of DB9 Connection.

5.3.2.2 MODBUS and OPC server

The MODBUS Serial Line protocol is a Master-Slaves protocol [81, 82]. Only one master (at the same time) is connected to the bus, and one or several (247 maximum number) slaves' nodes are also connected to the same bus, which can be a serial communication. At the physical level, MODBUS over Serial Line systems may use different physical interfaces (RS485, RS232) [82]. The RS485 two-wire interface is the most common since it has the capability of connecting multiple nodes. In this application, an RS485 interface has been used for the communication between the laptop and instruments, which include temperature controllers and pressure indicators. A MODBUS communication is always initiated by the master, a computer. The slave nodes will never transmit data without receiving a request from the master node and they will never communicate with each other. The master node initiates only one MODBUS transaction at the same time. The master node issues a MODBUS request to the slave nodes in two modes: in unicast mode, the master addresses an individual slave. After receiving and processing the request, the slave returns a message (a 'reply') to the master. In that mode, a MODBUS transaction consists of 2 messages: a request from the master, and a reply from the slave. Each slave must have a unique address (from 1 to 247) so that it can be addressed independently from other nodes; in broadcast mode, the master can send a request to all slaves [82]. No response is returned to broadcast requests sent by the master. The broadcast requests are necessarily writing commands. All devices must accept the broadcast for writing function. The address 0 is reserved to identify a broadcast

exchange. In the application of this online sensor, the unicast mode is adopted to do the communication between the computer and instruments.

Two different serial transmission modes are defined: the RTU (Remote Terminal Unit) mode and the ASCII mode. It defines the bit contents of message fields transmitted serially on the line. It determines how information is packed into the message fields and decoded. The transmission mode (and serial port parameters) must be the same for all devices on a MODBUS serial line. Although the ASCII mode is required in some specific applications, interoperability between MODBUS devices can be reached only if each device has the same transmission mode: all devices must implement the RTU Mode. The ASCII transmission mode is an option. Devices should be set up by the users to the desired transmission mode, RTU or ASCII. Default setup must be the RTU mode. All the instruments in this online sensor application use the RTU transmission mode.

When devices communicate on a MODBUS serial line using the RTU mode, each 8–bit byte in a message contains two 4–bit hexadecimal characters. The main advantage of this mode is that its greater character density allows better data throughput than ASCII mode for the same baud rate. Each message must be transmitted in a continuous stream of characters. The format for each byte as defined by MODBUS to be 11 bits in RTU mode is: Coding System: 8–bit binary; bits per byte: 1 start bit; 8 data bits, least significant bit sent first 1 bit for parity completion; 1 stop bit. Even parity is required; other modes (odd parity, no parity) may also be used [81]. In order to ensure a maximum compatibility with other products, it is

recommended to support also no parity mode. The default parity mode must be even parity. In this application, no parity is used to set up all the communication between the laptop and instruments, so the parameters in the port and instruments setting should be same with the parameters setting in MODBUS. Figure 5.49 shows the communication protocol selection and connection setup, which has the same parameters that are defined by the instruments manufacturer.

Objective Linking and Embedding (OLE) for Process Control (OPC) was designed to bridge Windows based applications and process control hardware and software applications [81]. It is an open standard that permits a consistent method of accessing field data from plant floor devices. This method remains the same regardless of the type and source of data. OPC servers provide a method for many different software packages to access data from a process control device, such as a PLC or DCS. The purpose of OPC is to define a common interface that is written once and then reused by any business. Once an OPC server is written for a particular device, it can be reused by any application that is able to act as an OPC client.

OPC servers use Microsoft's OLE technology (also known as the Component Object Model, or COM) to communicate with clients. COM technology permits a standard for real-time information exchange between software applications and process hardware to be defined. Figure 5.50 shows the concept that how the data is exchanged between the devices and clients through OPC server. The clients can be Labview, Excel, Word etc software.

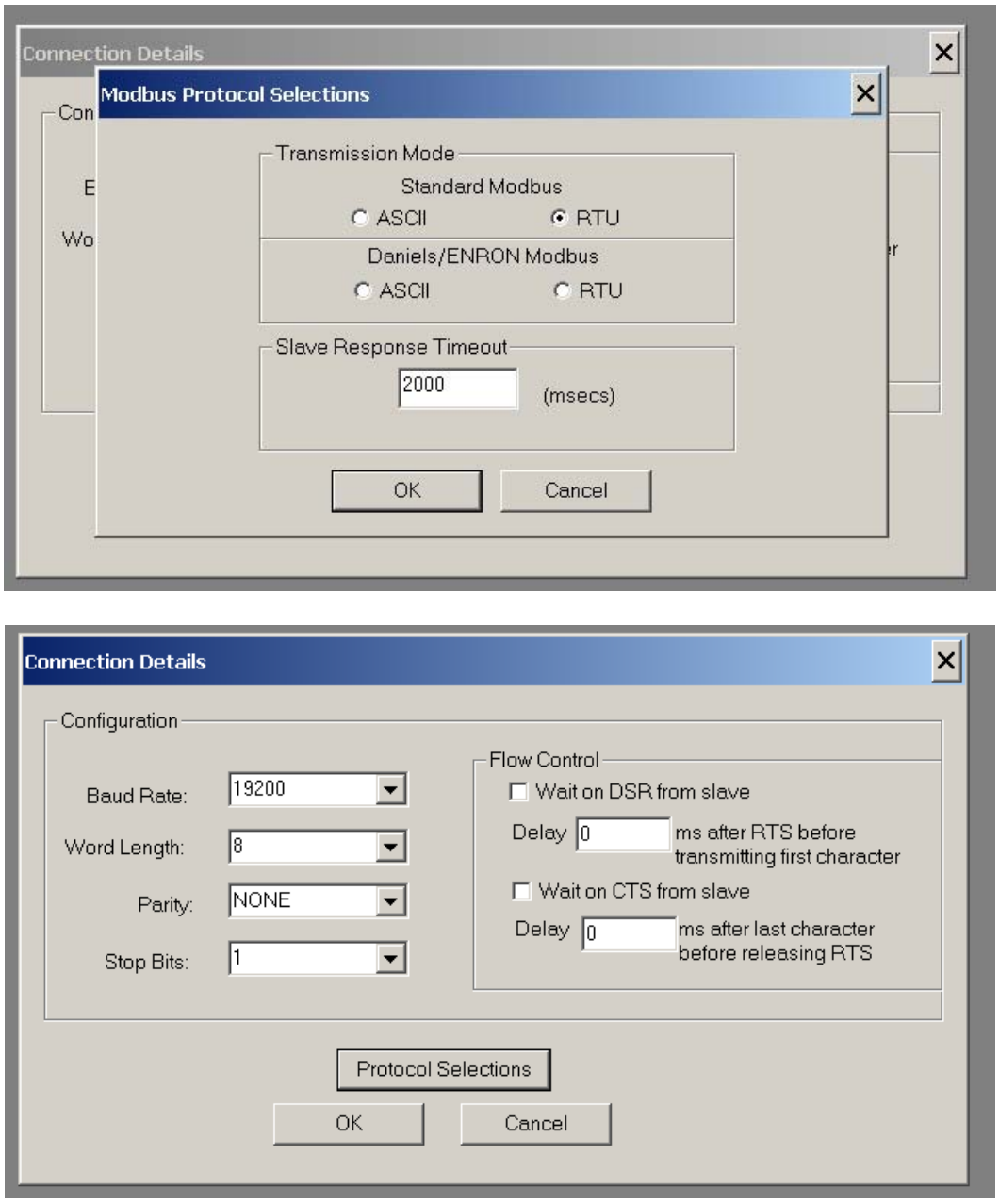

Figure 5.49 Connection of MODBUS with Instruments through RS485 Interface.

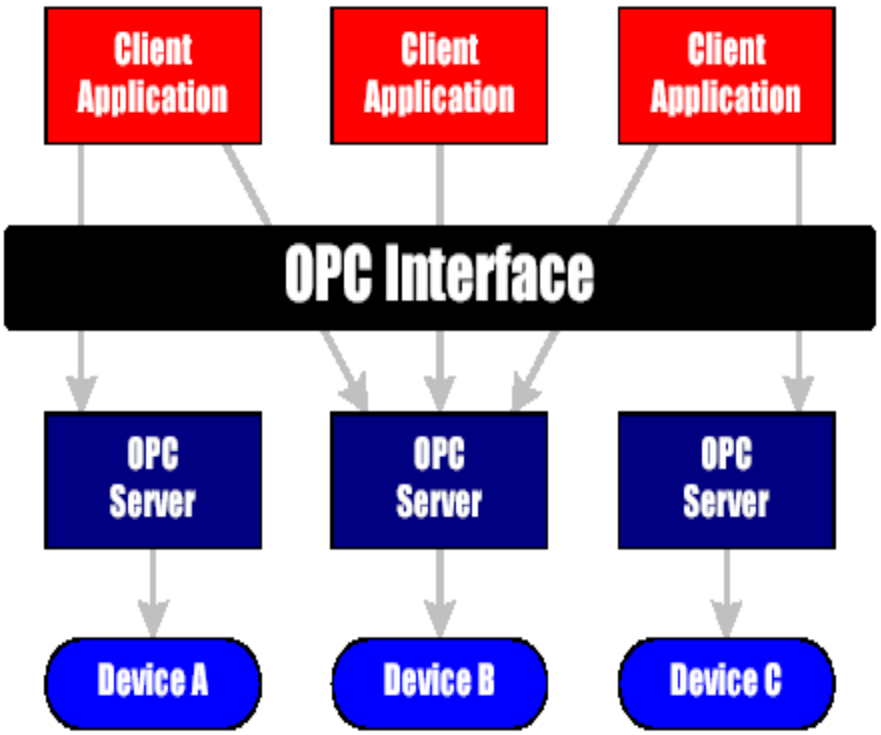

Figure 5.50 Data Exchanged between Devices and Clients through OPC Server.

An OPC server for Modbus software from Win-Tech Technology was used for this application. Before an OPC server can be used for the communication, it has to be configured properly. The configuration included the scan definition and file settings. The former included communication port, poll rate, data point address, slave node, and scan length, which were critically important to get access to the data. The later included files set for different data and commands used for the data acquisitions and control for the online rheological sensor, such as pressure, temperature of polymer melt and sensor block, temperature set point, calibration, etc. Figure 5.51 gives the information on how the configuration of OPC server was set; some parameters for data scanning were defined for a particular data point of an individual instrument. Figure 5.52 shows some files for the data points that the OPC server collected and can be exchanged with other application software. After the OPC server is configured successfully, it can show all the data read form the instrument, which is independent of Labview and can exchange data with Labview. A certain OPC sever file named, as "mbOPCsvr.tst" for Win-tech MODBUS OPC server needs to be saved in order to be started when the OPC server is called by other applications, such as Labview. When Labview calls the OPC server, a window of OPC server will pop out and try to communicate with instruments, but the connection of OPC server between the software and instrument through RS485 serial bus still needs to be turned on manually by selecting the communication ports that are communication port 4 and port 5 in the function of connection in the manual bar of OPC server.

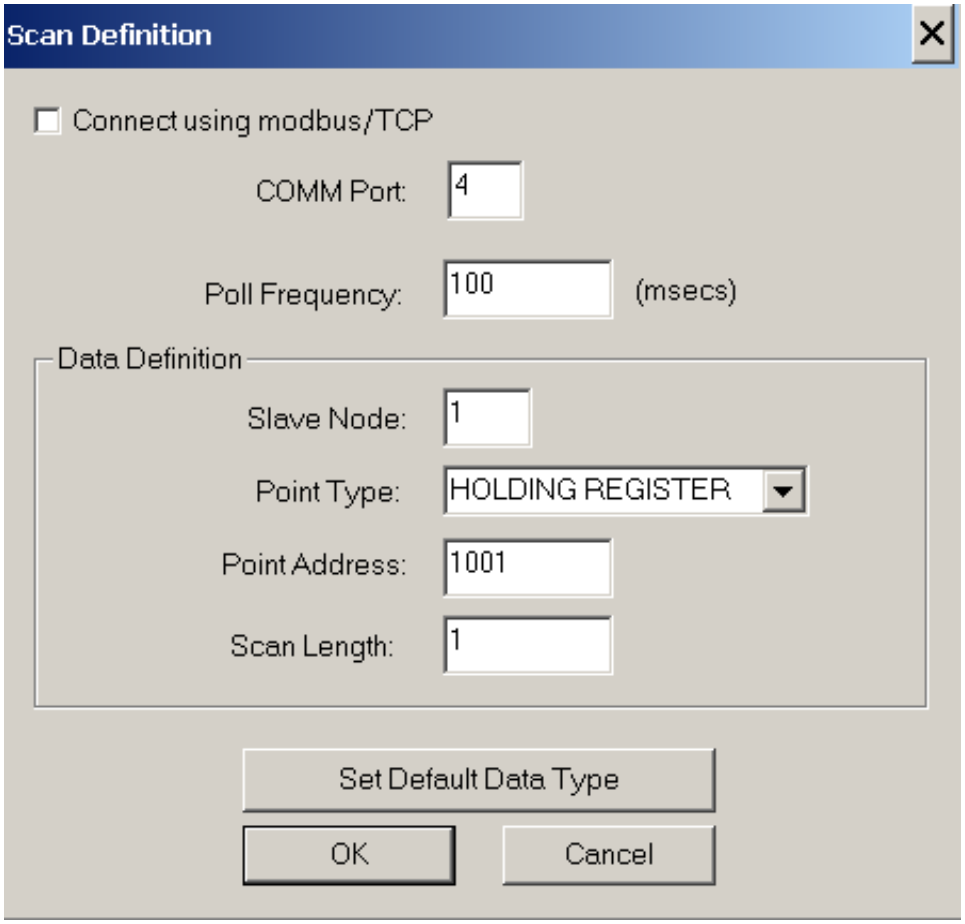

Figure 5.51 Configuration of MODBUS OPC Server with Instruments through RS485 Interface.

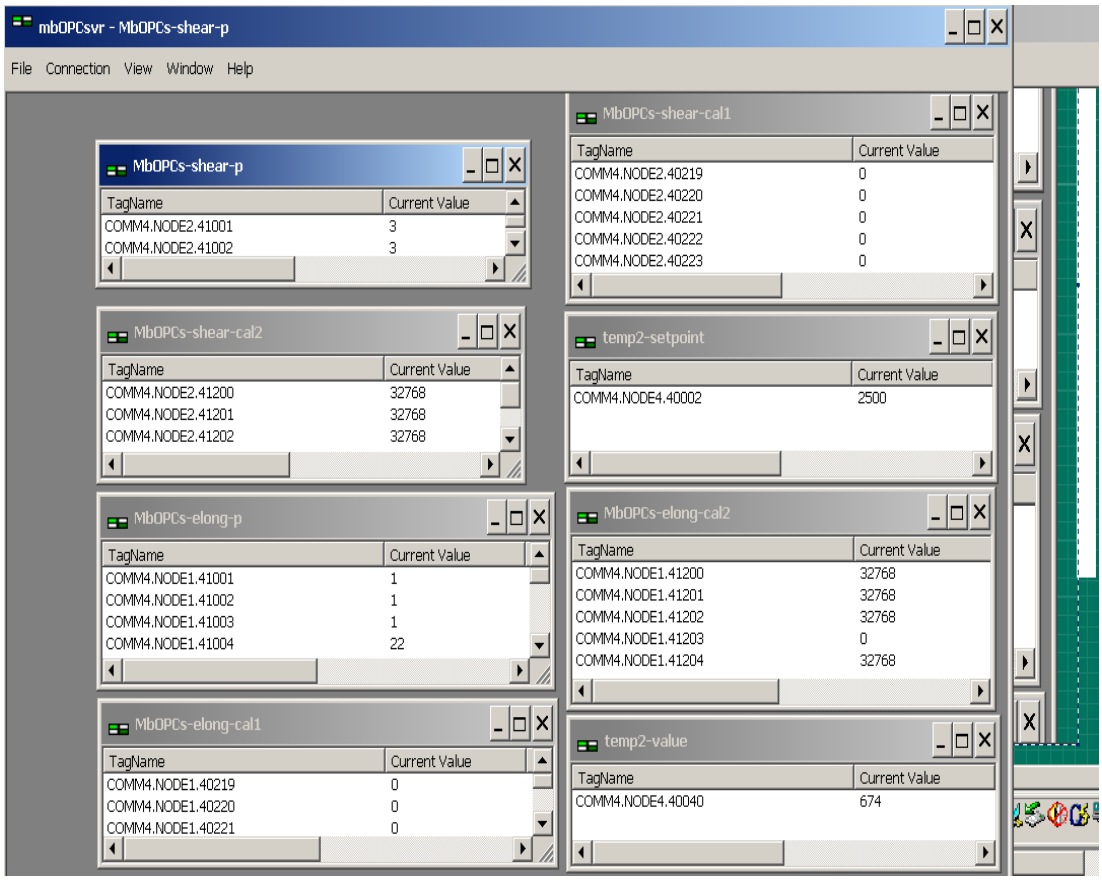

Figure 5.52 Connection to Addresses in Instruments by MODBUS OPC Server.

§5.3.3 Programming in Labview

LabVIEW is a graphical programming language, which uses icons instead of lines of text to create applications for measurement and control [83]. Comparing with text-based programming languages, such as FORTRAN, C et al, where instructions determine program execution, LabVIEW uses dataflow programming, where the flow of data determines execution. In LabVIEW, a user interface is created with a set of tools and objects. The user interface is known as the front panel. Then code is added by using graphical representations of functions to control the front panel objects. The code is built in the block diagram. The block diagram very much resembles a flowchart. LabVIEW programs including front panel and block diagram are called virtual instruments, or VIs, because their appearance and operation imitate physical instruments [83]. Every VI uses functions that manipulate input from the user interface or other sources and displays that information or moves it to other files or other computers. A VI contains the following three components:

• **Front panel**—Serves as the user interface.

• **Block diagram**—Contains the graphical source code that defines the functionality of the VI.

• **Icon and connector pane**—Identifies the VI so that you can use the VI in another VI. A VI within another VI is called a subVI. A subVI corresponds to a subroutine in text-based programming languages.

The front panel is the user interface of the VI. Figure 5.53 shows the example of a front panel in this application. The front panel includes controls and indicators, which are the interactive input and output terminals of the VI, respectively. Controls are knobs, push buttons, dials, and other input devices. Indicators are graphs, and other displays. Controls simulate instrument input devices and supply data to the block diagram of the VI. Indicators simulate instrument output devices and display data the block diagram acquires or generates. After the front panel is built, some specified codes using graphical representations of functions are added to control the front panel objects. So the block diagram contains this graphical source code. Figure 5.54 shows the example of a diagram. Front panel objects appear as terminals on the block diagram. After a VI front panel and block diagram are built, the icon and the connector pane should be built so this VI can be used as a subVI. Figure 5.55 shows the control panel, diagram and icon of a subVI. Every VI displays an icon, in the upper right corner of the front panel and block diagram windows. An icon is a graphical representation of a VI. It can contain text, images, or a combination of both. When a VI is used as a subVI, the icon identifies the subVI on the block diagram of the VI. A connector pane also need to be built, to use the VI as a subVI. The connector pane is a set of terminals that correspond to the controls and indicators of that VI, similar to the parameter list of a function call in text-based programming languages. The connector pane defines the inputs and outputs that can be wired to the VI that can be used as a subVI. Several subVI are used for the application of online sensor.

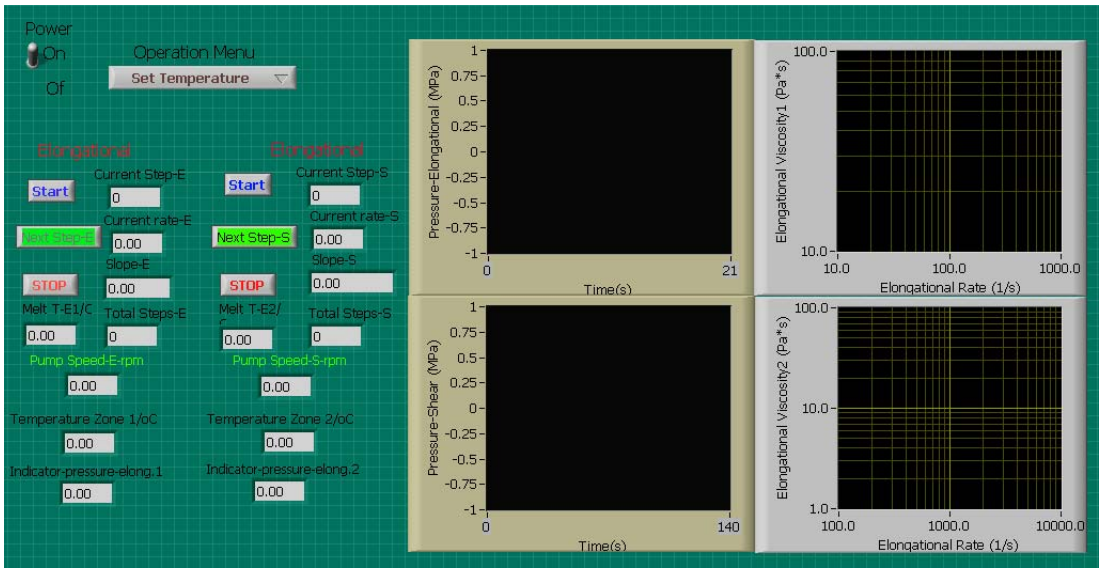

Figure 5.53 Front Panel for Online Sensor in Labview.

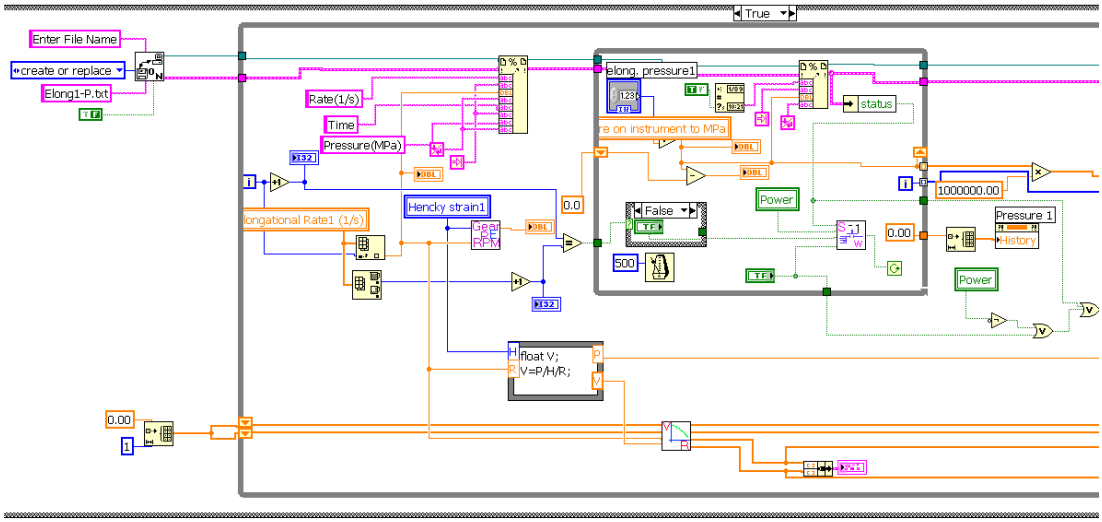

Figure 5.54 Diagram for Online Sensor in Labview.

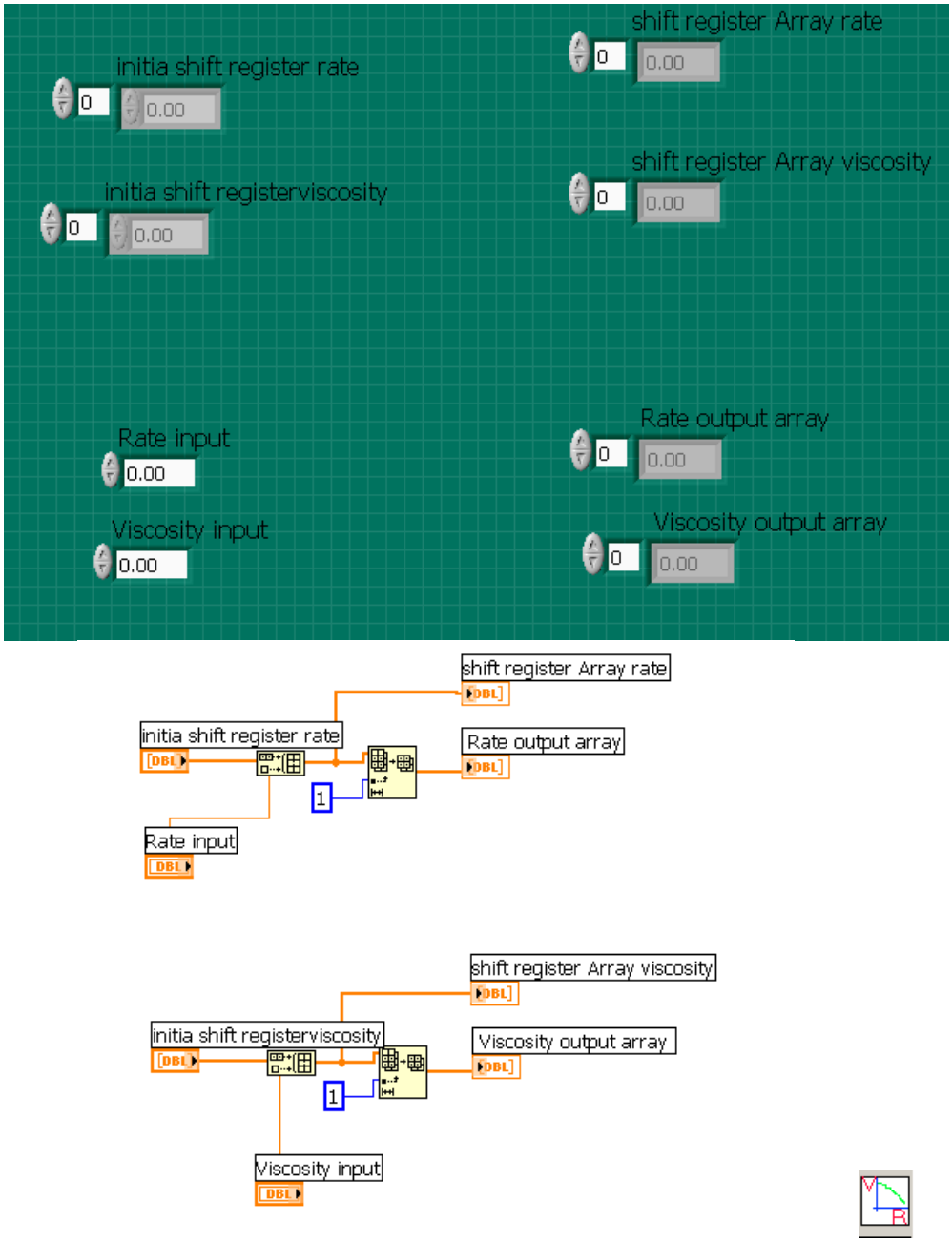

Figure 5.55 SubVI and Icon for Online Sensor in Labview.

In this section, some details of the Labview code for the online rheological sensor are discussed.

Figure 5.56 gives the code for the pressure calibration. The code is written using the sequence structure in Labview, and will execute according to their sequence after the calibration button in the operation menu is clicked that means its value is true. The pressure instruments need to be set at the remote control state before the calibration can be done. A command "1" is sent to the address in MODBUS "0219", then a command "1" is sent to the address in MODBUS "41201" to do the zero calibration, after that a command "1" is sent to the address in MODBUS " 41202" to do the span calibration. The instrument will finish the calibration in 2 seconds after it receives the command. A command "0" is sent to all addresses mentioned above to finish the calibration. The calibration is very important for the pressure transducer since it works at different temperatures, which cover from room temperature to more than 300^{o}C and the zero point will shift with temperature.

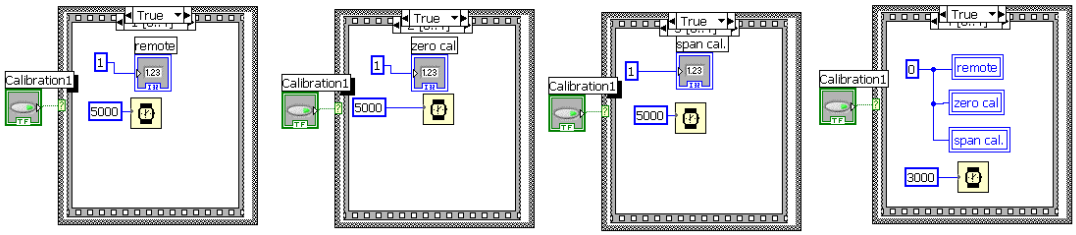

Figure 5.56 Pressure Transducer Calibration Code in Labview.

Figure 5.57 shows the data socket connection between Labview control and indicator variable with the OPC server. Labview has a powerful function that is the data socket connection, which enables Labview to subscribe or publish data with other application software, such as OPC server, Excel, and Internet explorer etc. The control variable, pressure, can subscribe data through certain configuration by selecting the right address in MODBUS through the OPC server shown in Figure 5.57. Right click the mouse button after moving the mouse arrow to the variables that the data socket connection need to be built, Labview will show some functions that include data operation, then Labview will show the data socket connection after moving the mouse to the function, data operation. After that, Labview will show how to set the data socket connection step by step in the case that the physical communication between the computer and instruments has been set up.

Another very important point for the online measurement code is how to get the steady state pressure data. When a certain shear or elongational rate is set, the gear pump will draw polymer melt from the main processing stream and push the polymer melt through the die. The pressure drop at the die will build up and will reach a steady state that is the right data for the calculation of viscosities. There will be some noise in the signal for the pressure. The signal will reach steady state after the polymer melt has been flowing for enough time that is based on the shear or elongational rate; so linear fitting is a good method to get the steady state data. This code is a subVI, so the main code will call it after one measurement is determined to calculate the viscosity.

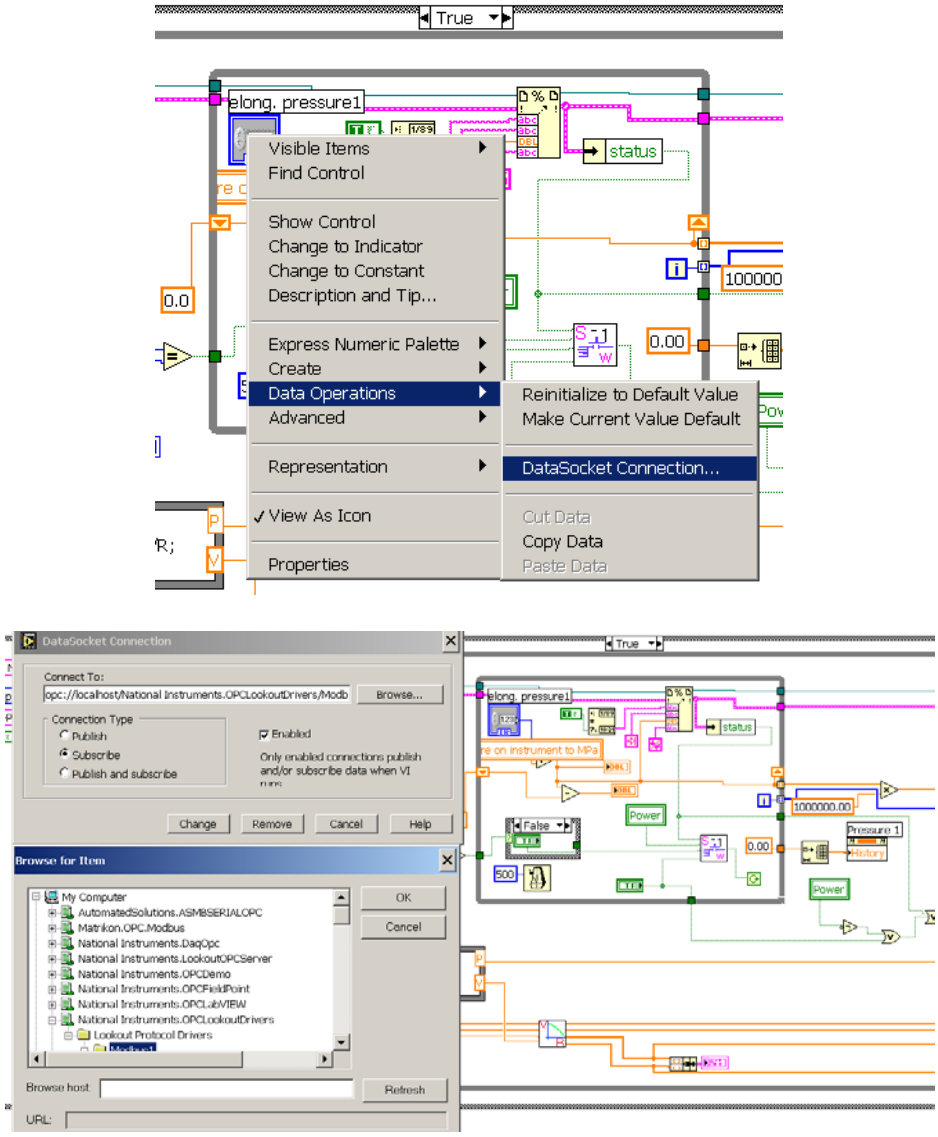

Figure 5.57 Data Socket Connection for Online Sensor in Labview.

Linear fitting will be repeated until a certain criterion set point is reached by means of rejecting the data collected during the early period, which represents the data collected at an unstable state. Figure 5.58 shows the Labview code and demonstration result of acquisition the steady state pressure from the pressure signal.

Figure 5.59 shows the main code for the control and indicator for the online sensor in Labview, which corresponds to the front panel. In this code, there are lots of control and measurement variables, such as setting temperature, hardware setting, pressure plots, pressure indicator, and temperature indicator, all of which can be displayed on the control panel based on the selection of function in the operation manual. The display of these variables is controlled by setting the display control function to be true that represents display or false that represents hidden. Since the MODBUS communication protocol can transmit the integer only, the temperatures data from the instruments have to be divide by 10 and the temperature setting command have to be multiplied by 10. Different pressure transducers have different pressure ranges, but the instruments will transmit the pressure data based on the signal generated by the pressure transducers when the pressure is applied on it, so the data received from the instruments may be not the exact pressure, which is multiplied or divided by a certain integer for different pressure transducers. It is necessary to do the scaling with different pressure transducers. The scaling can be done easily by inputting a number when the hardware is setting, and the number can be calculated according the comparison of the number shown on the indicator in the front panel with the number shown on the pressure instruments.

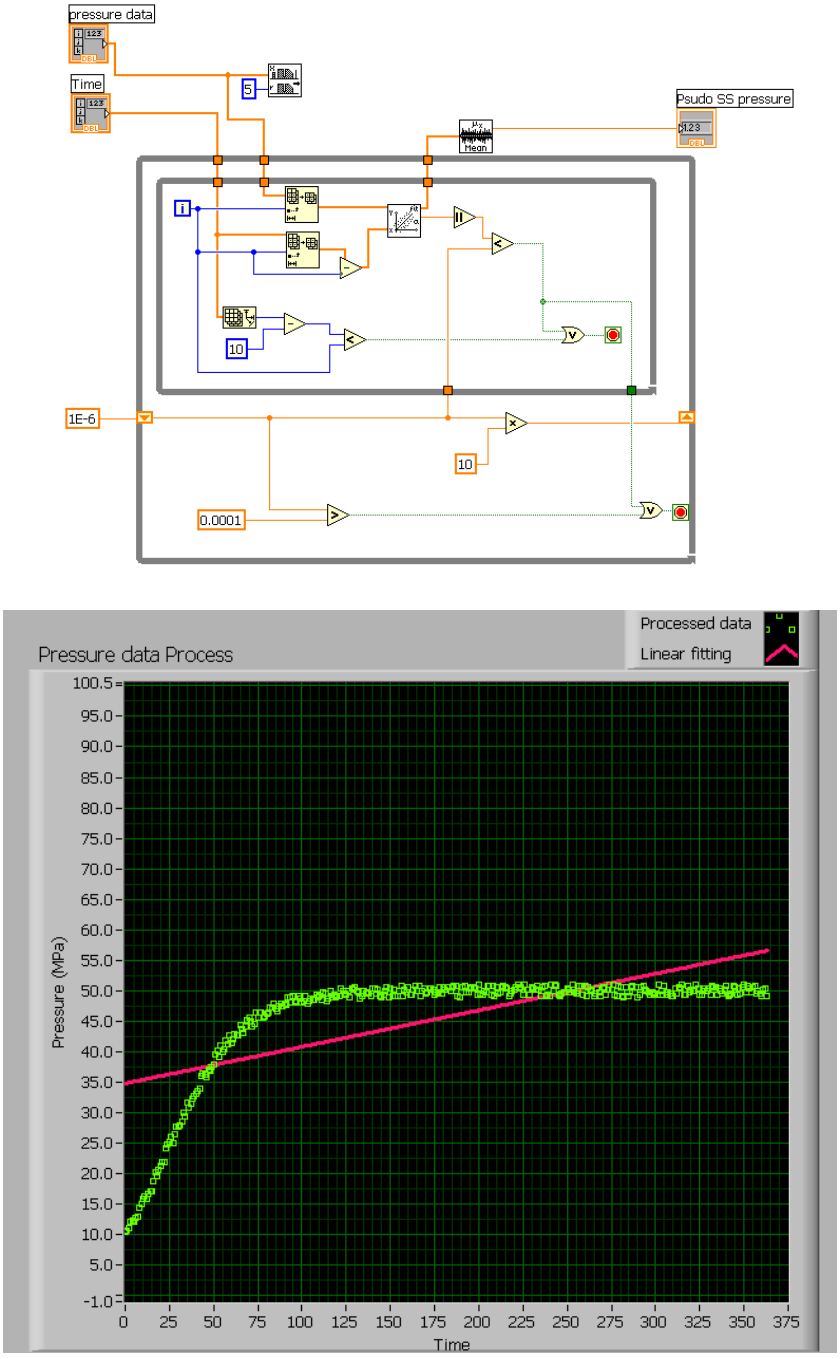

Figure 5.58 Acquisition of Steady State Pressure for Online Sensor in Labview.

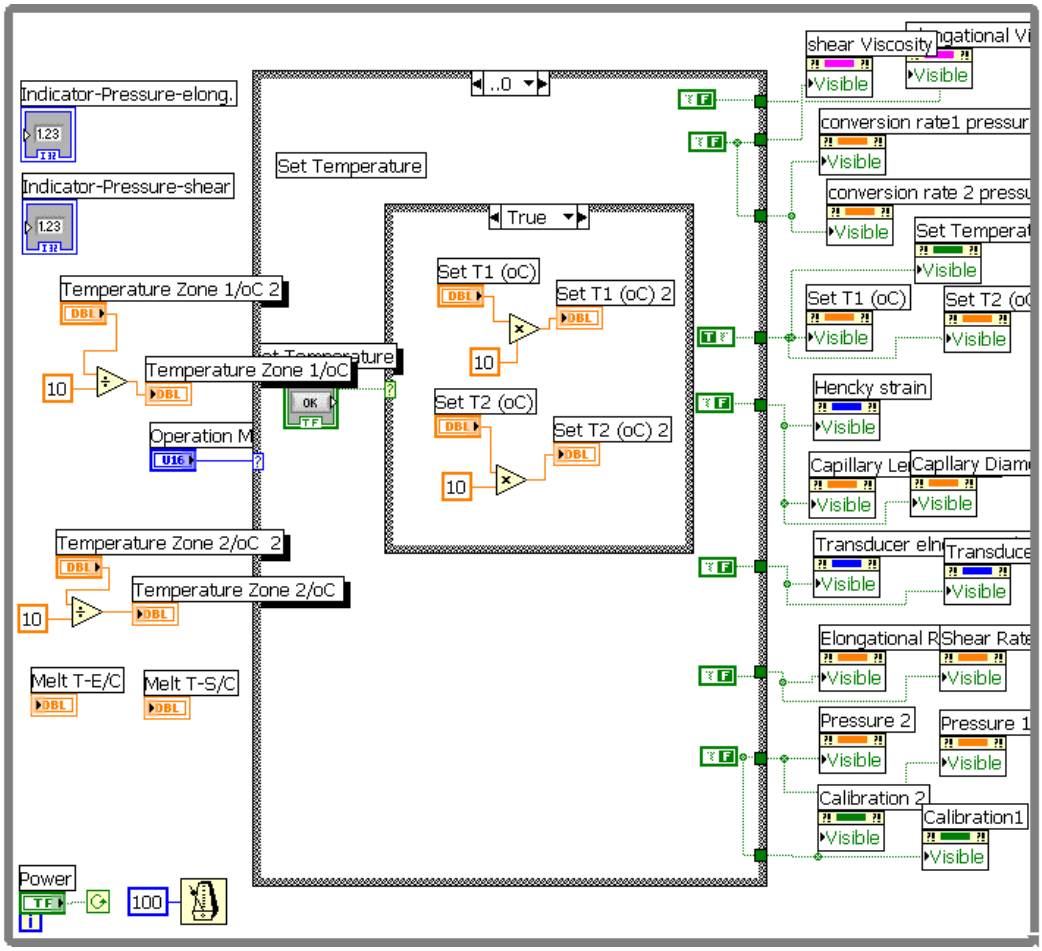

Figure 5.59 Main Code for Control and Indication for Online Sensor in Labview.

Figure 5.60 shows the main code for measuring the elongational and shear viscosities. In this code several subVIs, such as gear pump speed calculation, power switch, plot viscosity and acquisition of steady state pressure, are used. In this code, the measuring of shear viscosity and the measuring of elongational viscosity are parallel, so their operation will not interfere with each other. Any one of them can be started or stopped by the operator. Two Labview codes wre written for the online rheological sensor, one is for measurement of shear and elongational viscosities simultaneously; the other is for measurement of elongational and elongational viscosities with different Hencky dies simultaneously. The second code is very similar to the first one, in which the code for the shear viscosity is substituted by code for the elongational viscosity modified to set up the right communication with the instruments. Two methods shown in Figure 5.61 are used to save all the data on the hard disk in the laptop. One is to save all original pressure data with time evolution, which can be used to check the transition region before the pressure will reach the steady state or to do the manual calculation due to some unknown disturbance that might happen during the operation. The data is saved as text files following the format that is rate, time and pressure. The name of these files can be modified based on the experimental conditions after the start button is clicked. The other is to save the viscosity results by using Excel. The file name can be written by the operator based on the experiments conditions and polymer grades. These Excel files include the information of hardware, polymer melt temperature, shear or elongational rates and viscosities.

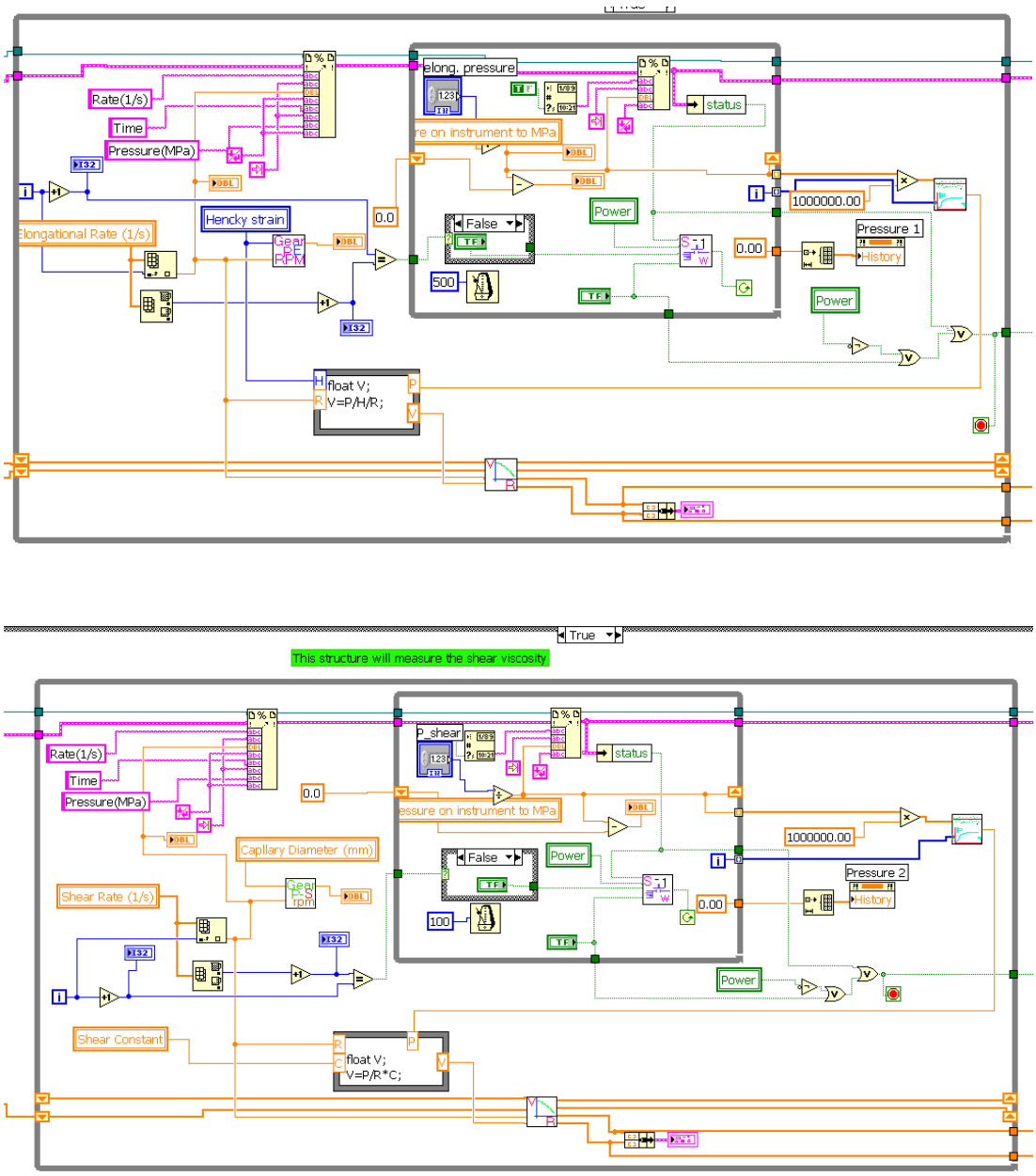

Figure 5.60 Main Code for Measuring Shear and Elongational Viscosity for Online Sensor in Labview.

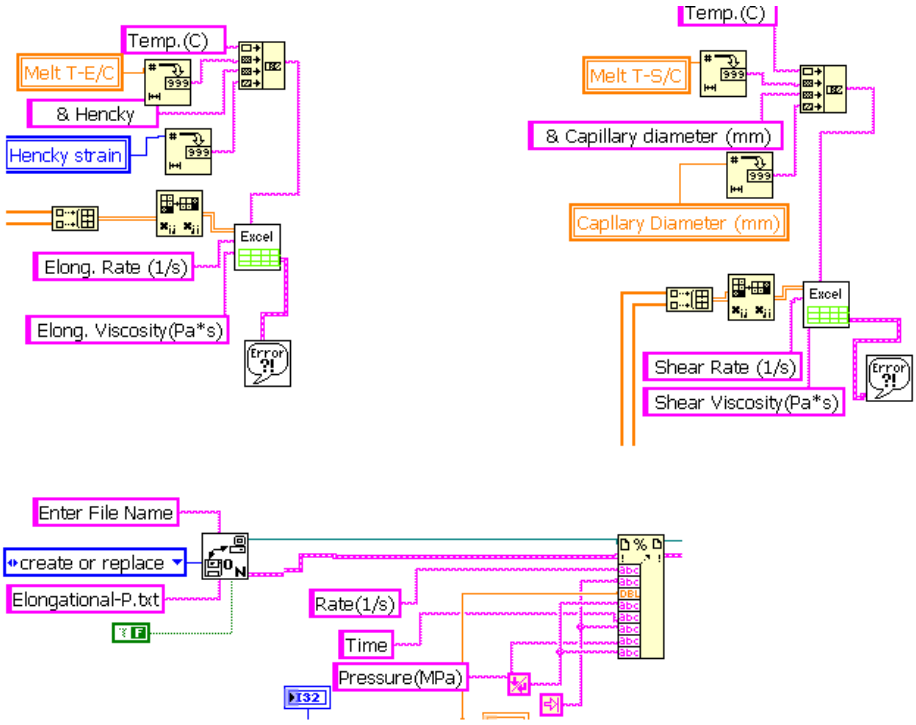

Figure 5.61 Data File Saving for Online Sensor in Labview.

§5.3.4 Verification of online rheological sensor

The principle of the design of the online rheological sensor is same with the ACER, whether a capillary or hyperbolic die is used as the geometry and pressure transducer is used to measure the pressure drop under controlled flow rate at the specified geometry. The verification of the online rheological sensor was done on ACER since it provided very accurate rheological data using PP3854 that had a relative high viscosity. The ACER was used to control the flow rate and it's pressure transducer was connected to the instrument that was designated for online measurement, and a series of pressure drop at different flow rates were recorded and the rheological properties were calculated by the online rheological sensor code in Labview. Both shear and elongational viscosity were measured by using different geometries. For the elongational viscosity, two dies, Hencky 6 and 7 die, were used to do the verification. Also the rheological properties were measured by using ACER. Figures 5.62-5.64 show the rheological properties measured by ACER and online rheological sensor code. The results show the design of online rheological sensor is good and the Labview code is bug free since the difference between the data from these two measurements is very small.

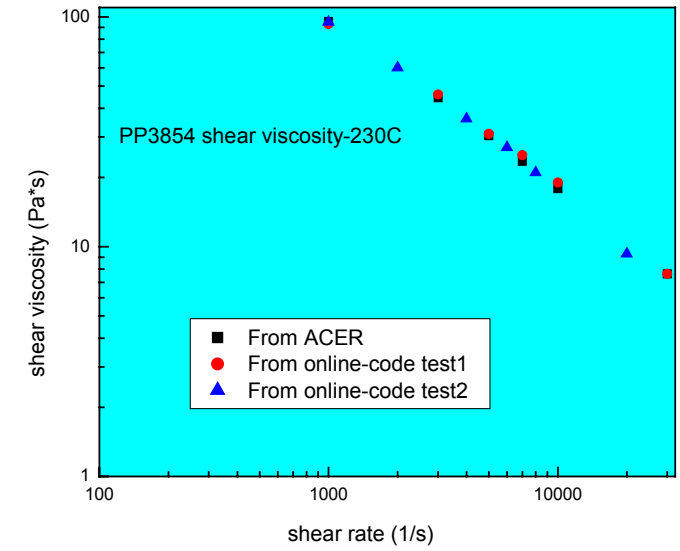

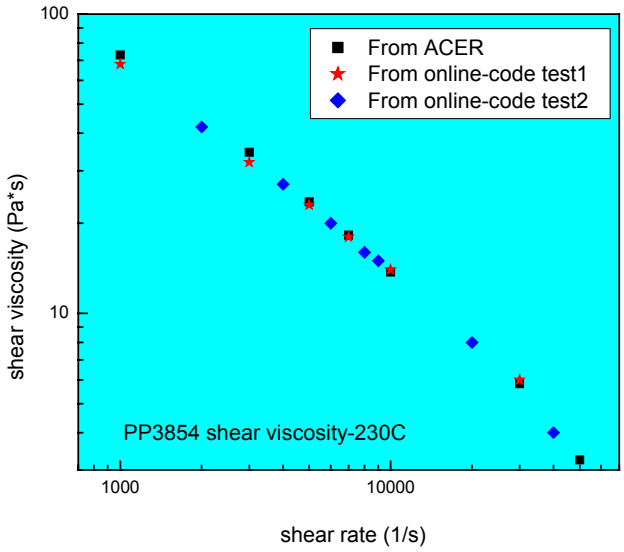

Figure 5.62 Shear Viscosity of PP 3854 from different Methods.

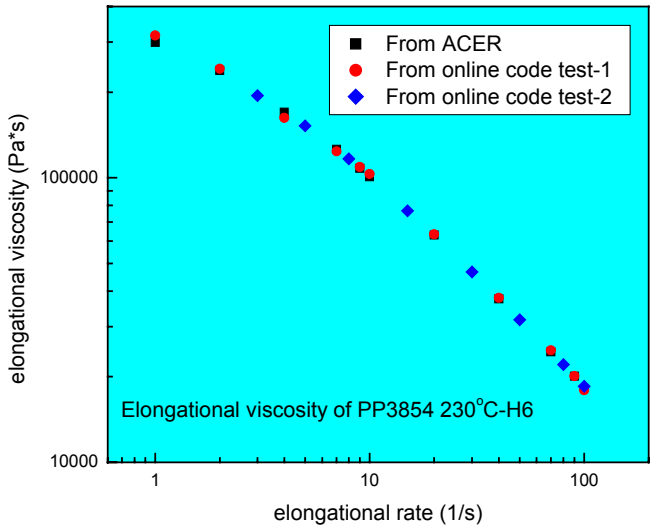

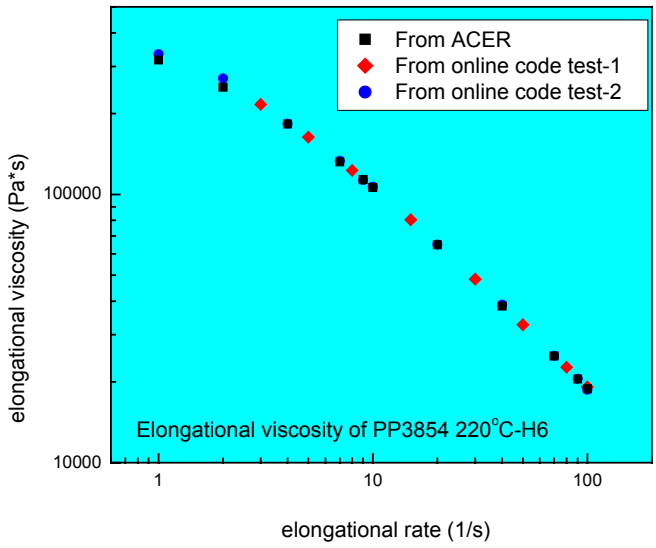

Figure 5.63 Elongational Viscosity of PP 3854 from different Methods-H6.

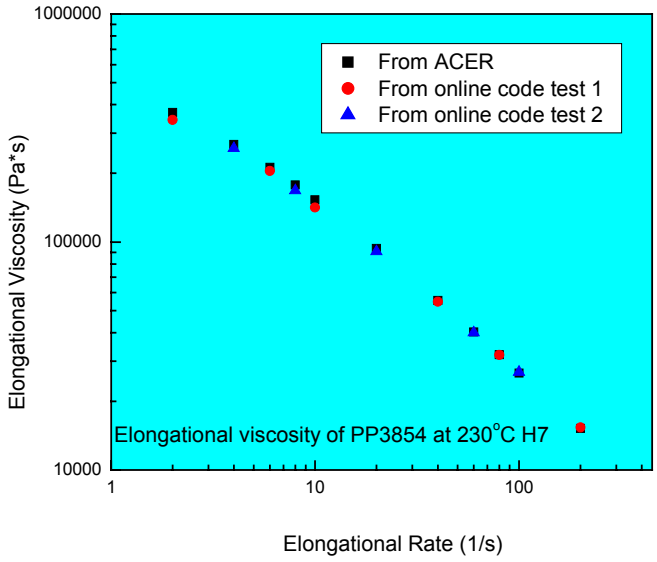

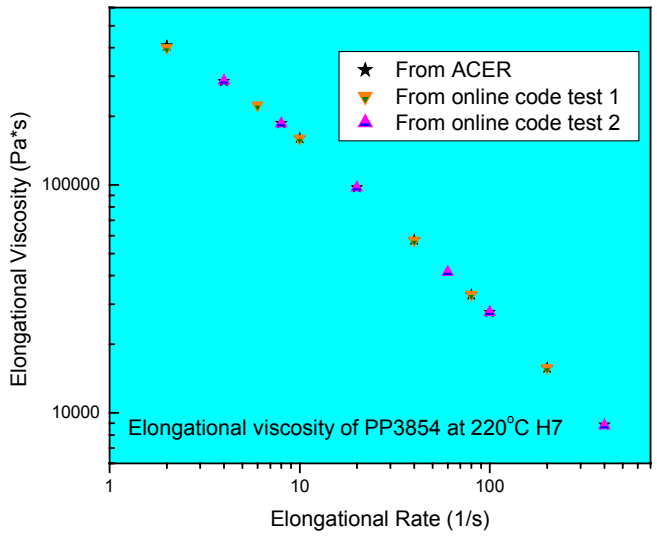

Figure 5.64 Elongational Viscosity of PP 3854 from different Methods-H7.

CHAPTER 6

CONCLUSIONS AND FUTURE WORK

§6.1 CONCLUSIONS

Rheological properties of two melt blowing PP grades, whose melt flow rates are 1200 and 400 respectively, were determined using the ARES and ACER. The polymer rheological properties include complex viscosity, loss modulus, storage modulus, normal force and stress relaxation, shear viscosity, and elongational viscosity. Elongational viscosity is measured by a technique involving converging flow through semi-hyperbolic dies that have the characteristic of Hencky 5, 6, and 7. The semi-hyperbolic shape of the die enables a constant elongational strain rate throughout the die. Besides the molecular characteristics mentioned above, the rheological properties of polymer melts are affected considerably by the processing conditions, namely temperature, Hencky strain, and strain rate. At very low strain rates, polymer melts show Newtonian fluid behavior. All polymer samples showed strain rate thinning of viscosity at relative high strain rates.

The temperature shifting of viscosities was achieved using the shift factors obtained from the zero-shear viscosity of polymer melts, which was calculated based on the Carreau rheological model, for the construction of master curves. The

temperature shift factors showed an expected Arrhenius type dependence on temperature. Following the research results accomplished in this group the Hencky strain shifting of elongational viscosities was achieved by calculating the shift factor that is defined as the ratio of relaxation times. Their ratio depends on the entropies of orientation, which in turn are functions of Trouton ratio and the Hencky strains. By combining the shift factors obtained in the temperature and Hencky strain shifting respectively, elongational viscosities were simultaneously shifted with respect to both temperature and Hencky strain to create general master curves. The Carreau and Cross models were used to fit the master curves. The former shows good curve fitting at the low strain rate and the latter shows good curve fitting at the high strain rate. Thus, equations are available to calculate the shear and elongational viscosities of each polymer at different processing conditions.

In order to fundamentally understand the melt blowing process, several melt blowing experiments were conducted. The correlations of processing conditions and properties of melt blown fabric that include air permeability, hydrohead, tensile strength and fiber diameters were determined by introduction of some dimensionless numbers, i.e. air Reynolds number, polymer Reynolds number and Hencky strain. The rheological properties of PP were calculated based on the master curve functions obtained from the Carreau and Cross rheological models.

A high resolution IR camera was used to capture thermographs that can be used to determine the temperature profile during melt blowing. From these thermographs, it appears that a plateau or shoulder in the temperature profile is

present as the fiber is drawn down by the high velocity air. This plateau or shoulder indicates the crystallization of PP during the melt blowing process. It can be assumed that the fiber attenuation will be essentially end when significant crystallization has occurred due to enhanced fiber stiffness. Also the uneven temperature field on the die block leads to uneven polymer distribution during the polymer extrusion, which results in variation of the uniformity of the nonwoven fabric across the machine direction. This is valuable information for the control of product uniformity.

Polymer degradation is inevitable under high temperature, high shear rate and the harsh environment during the processing. DSC studies showed that the two analyzed polymers were slightly oxidized in the presence of air. The thermal stability of these two polymers depended on the processing temperatures and shear rates. Under the conditions studied, the results showed that these polypropylene grades were relatively more stable below about 240^{o}C, and degrade faster above this temperature. During the melt blowing process, these polymers inevitably degraded to a small extent, dependent on the processing variables such as melt temperatures, airflow rate and throughput. The effects of processing variables on the polymer degradation were different for different polymers, and this may be caused by different degradation mechanisms.

The rheological properties of PPs were used to determine the molecular weight and molecular weight distribution by using the code and parameters for PP provided by ARES software. The molecular weight distribution changed slightly after the melt

blowing process. Using the rheological properties to determine the polymer molecular weight and molecular weight distribution is an efficient technique.

Polymer rheological properties were used to determine the correlation between the dimensionless numbers and properties of melt blown nonwovens; some error may be introduced since all the rheological properties were determined by off-line rheometers and polymer degradation inevitably happened during melt blowing that lead to the changing polymer viscosities. It will be advantageous to obtain online rheological properties for the future applications in process modeling and process control. The theory and knowledge of measuring shear and elongational viscosity in the laboratory were used to develop the online rheological sensor, which can measure the shear and elongational viscosities simultaneously online by drawing a small amount of polymer melt from the main processing stream. The control and measurement system for the online rheological sensor, which can be operated manually or by a laptop, were accomplished by fabrication of a control box and setting up the communication between the control box and a laptop. The RS485 serial interface was used to do the physical connection between the control box and laptop, and an OPC server for MODBUS communication protocol was used to bridge the communication between the laptop and control box. Software based on Labview were developed to do the control and measurement, which turned the whole system into a virtual instrument. The software was verified by comparing the shear and elongational viscosities obtained from the newly developed Labview code with the results obtained from ACER.

§6.2 FUTURE WORK

Polymer degradation will occur during the processing and it will be determined by polymer composition, polymer structure, polymer additives, and processing conditions. Polymer rheological properties are often measured in the laboratory by using off line instruments, and it takes some time to melt the polymer, so the thermal history and degradation during the measurement can affect the polymer rheological properties. There will be no doubt that some error will be introduced when these off line rheological properties are used to do the process modeling and to correlate the properties with the processing conditions. It is advantageous to measure the rheological properties online. The online rheological sensor developed in this research can be used to measure the shear and elongational viscosity simultaneously during polymer processing, such as polymer extrusion, spunbonding and melt blowing etc. Extensive research of polymer rheology can be achieved by using online rheological sensors to direct the polymer processing. The online rheological sensor should be installed on the 6'' melt blowing line to get the online rheological data with different processing conditions and polymer grades in the near future. The rheological properties and processing condition correlation should be obtained by online measurement and rheological constitutive equations can be used to do the processing modeling and processing control. Also this online rheological sensor should be a valuable tool for process monitoring and quality control.

REFERENCES

REFERENCES

1. H. A. Barnes, J. F. Hutton, and K. Walters *An Introduction to Rheology* Elsevier Science Publishers B. V., Amsterdam, (1989).
2. F. T. Trouton, *Proc. of the Royal Society* **A, 77**, 426, (1906).
3. V. A. Wente, *Industrial and Engineering Chemistry,* **48**, 1342, (1956).
4. R. D. Orwoll, *Advances in Polymer Technology*, **3(1)**, 23, (1999).
5. T. O. Broadhead, W. I. Patterson, and J. M. Dealy, *Polym. Eng. Sci*. **36**, 2840, (1996).
6. J. M. Dealy, and T.O. Broadhead, *Tech. Rheol. Meas*. 285, Chapam & Hall, London, UK,(1993)
7. J. M. Dealy, *Annu. Tech. Conf. – Soc. Plast. Eng*. **49**, 2296, (1991).
8. A.L. Kelly, M. Woodhead, P. D. Coats, D. Barnwell and K. Martin, *Int. Polym. Process,* **15(4)**, 355, (2000).
9. R .Gendron, P. Sammut, A. Correa, and C.L. Rohn, *Annu. Tech. Conf. – Soc. Plast. Eng*. **58**, 984, (2000).
10. J. Meissner, *Rheological Acta,* **8**, 78, (1969).
11. J. Meissner, *Rheological Acta,* **10**, 230, (1971) .
12. J. Meissner, T. Raible, and S. E. Stephenson, *Journal of Rheology,* **25,** 1, (1981).
13. J. Meissner, *Trans. Soc. Rheol.* **16**, 405, (1972).
14. J. Meissner, *Chem. Eng. Commun.* **33**, 159, (1985).
15. A.S. Lodge and J. Meissner, *Rheological Acta,* **11**,351, (1972).

16. F. N. Cogswell, *Trans. Soc. Rheol.* **16**, 383, (1972).

17. H. Munstedt, *Journal of Rheology,* **24,** 421, (1979).

18. F. N. Cogswell, *Polymer Engineering Science,* **12,** 64, (1972).

19. H. Münstedt, *Rheol. Acta,* **14**, 1077, (1975).

20. H. Münstedt and H. M. Laun, *Rheol. Acta,* **20**, 211, (1981).

21. H. Münstedt and S. Middleman, *J. Rheol.* **25**, 29, (1981).

22. H. Münstedt, S. Kurzbeck, and L. Egersdörfer, *Rheol. Acta,* **37**, 21, (1998).

23. H. Münstedt, M. Schwetz, M. Heindl, and M. Schmidt, *Rheol. Acta,* **40**, 384, (2001)

24. H. C. Kim, A. Pendse, and J. R. Collier, *J. of Rheology*, **38(4)**, 831, (1994).

25. J. R. Collier and S. Petrovan*, J. of Applied Polymer Science*, *69*, 2357, (1998).

26. S. Petrovan, J. R. Collier and G. H. Morton, *J. of Applied Polymer Science*, **77**, 1369, (2000).

27. J. A. Covas, J. M. Nobrega and J. M. Maia, *Polymer Testing*, **19**, 165, (2000).

28. A.L. Kelly, P.D. Coates and T. W. Dobbie, *Plastics Rubber composite Process Application,* **25**, 313, (1996).

29. J. M. Dealy, *Annu. Tech. Conf. – Soc. Plast. Eng.,* **58**, 362, (2000).

30. A.L. Kelly, P.D. Coates, D.J. Fleming and T.W. Dobbie, *Annu. Trans. Nord. Rheol. Soc.*, **3**, 61, (1995).

31. A. L. Kelly, M.Woodhead, R. M. Rose and P. D. Coats, *Annu. Tech. Conf. – Soc. Plast. Eng*., **57,**1979, (1999).

32. S.H. Chiu and S.H. Pong, *Polymer degradation and Stability*, **64(2)**, 239, (1999).

33. J.M. Dealy, *Annu. Tech. Conf. – Soc. Plast. Eng.* **58,** 1054, (2000).

34. A. M. Jones and L. D. Wadworth, *TAPPI Nonwovens Conference* Atlanta, GA, April, (1986).

35. S.R. Malkan, Ph. D Dissertation, the University of Tennessee at Knoxville, (1990).

36. G. Staeffer and B.C. Goswami, *Book of Papers, INDA-TEC'90*, 385, (1990).

37. A.Y. A. Khan, Ph. D Dissertation, The University of Tennessee at Knoxville, (1998).

38. L.D. Wadsworth and A.O. Muschelewicz, *Fourth International Conference on Polypropylene Fibers and Textiles,* **47**,1, Nottingham, England, September 23-25, (1987).

39. K.M. Narasimhan and R.L. Shambough, *INDA-TEC*, Hilton Head, S.C., May 18-21, (1987).

40. M.W. Milligan and B. D. Haynes, *Journal of Applied Polymer Science*, **58**, 159, (1995).

41. B.D. Haynes and M.W. Milligan, *INDA Journal of Nonwoven research*, **3(4)**, 20, (1991).

42. H. Yin, Z. Yan and R.R. Bresee, *International Nonwoven Journal*, **8(1)**, 60, (1999).

43. H. Yin, Z. Yan, W.C. Ko and R.R. Bresee, *International Nonwoven journal*, **9(4)**,25, (2000).

44. R.R. Bresse and U. A. Qureshi, *International Nonwoven Journal*, **11(2)**, 27, (2002).

45. V. Bansal and R.L. Shambaugh, *Industrial Engineering Chemistry Research*, **37**, 1799, (1998).

46. A. S. Harpham and R.L. Shambaugh, *Industrial Engineering Chemistry Research*, **36**, 3937, (1997).

47. R.L. Shambaugh and R. Chhabra, *TAPPI journal*, **81(3)**, 199, (1998).

48. R. Shambaugh, *TAPPI journal,* **80 (9)**, 163, (1998).

49. R.L. Shambaugh, *Industrial Engineering Chemistry Research*, **27**, 2363, (1989).

50. M.A.J. Uyttendaele and R.L. Shambaugh, *AICHE Journal*, **36 (2)**, 175, (1990).

51. R.L. Shambaugh, *TAPPI, Journal*, **80 (9)**,163-166, (1997).

52. B.D. Haynes, Ph. D, Dissertation, the University of Tennessee at Knoxville, 1991.

53. R. B. Bird, W.E. Stewart, and E.N. Lightfoot, *Transport Phenomena,* John Wiley & sons, Inc, (2001).

54. P. K. Liaw, H. Wang, L. Jiang, B. Yang, J. Y. Huang, R. C. Kuo, and J. G. Huang, *Scripta Materialia*, **42**, 389, (2000).

55. H. Wang, L. Jiang, P. K. Liaw, C. R. Brooks, and D.L. Klarstrom, *Metallurgical and Materials Transactions A,* **31**, 1307, (2000).

56. L. Jiang, H. Wang, P. K. Liaw, C. R. Brooks, and D.L. Klarstrom, *Metallurgical and Materials Transactions A,* **32**, 2279, (2001).

57. B. Yang, P. K. Liaw, H. Wang, L. Jiang, J. Y. Huang, R. C. Kuo, and J. G. Huang, *Materials Science and Engineering,* **314** , 131, (2001).

58. L. Jiang, H. Wang, P. K. Liaw, C.R. Brooks, and D. L. Klarstrom, *Transactions of Nonferrous Metals Society of China*, **12**, 734, (2002).

59. H. Wang, L. Jiang, Y.H. He, L. J. Chen, P. K. Liaw, R.R. Seeley, and D.L. Klarstrom, *Metallurgical and Materials Transactions,* A, **33**, 1287, (2002).

60. P. Micic, S. N. Bhattacharya, and G. Field, *Polym. Eng. Sci.* **38**, 1685 (1998).

61. P. Micic, S. N. Bhattacharya, and G. Field, *Int. Polym. Proc.* **XIII**, 50 (1998).

62. M. Yamaguchi and M. Takahashi, *Polymer,* **42**, 8663 (2001).

63. J.R.Collier, S.Petrovan, and P.Patil. *Journal of Applied Polymer Science* **87**, 1387 (2003)

64. J.R.Collier, S.Petrovan, and Y.Wang, *Annual TANDEC Conference*, **11,** (2001).

65. P.Patil, Ph. D, Dissertation, the University of Tennessee at Knoxville, 2002.

66. J.R.Collier, S.Petrovan, and Y.Wang, *Annual TANDEC Conference*, **13,** (2003).

67. X. Wei, Ph. D, Dissertation, the University of Tennessee at Knoxville, 2002.

68. R.B.Bird, C.F.Curtiss, R.C.Armstrong, and O.Hassager. *Dynamics of Polymeric liquids Volume I Fluid Mechanics*. John Wiley & Sons, New York.,(1987).

69. P.J.Carreau, D.C.R.De Kee, and R.P.Chhabra. *Rheology of Polymeric Systems Principles and Applications*. Hanser Publishers**,** New York, (1997).

70. J.R.Collier, S.Petrovan, and P.Patil. *Journal of Applied Polymer Science* **87**, 1397 (2003)

71. J.D.Ferry. *Viscoelastic Properties of Polymers*. Wiley, New York, (1980).

72. W.W.Graessley. *Advanced Polymer Science* **16**, 1 (1974).

73. C.Tsenoglou. *Macromolecules* **24**, 1762 (1991).

74. S.Wu. *Polymer Engineering and Science* **25**, 122 (1985).

75. W.J.McGrory and W.H.Tuminello. *Journal of Rheology* **34**, 867 (1990).

76. H.Braun, A.Eckstein, K.Fuchs, and C.Friedrich. *Applied Rheology,* 116 (1996).

77. D.W.Mead. *Journal of Rheology* **38**, 1797 (1994).

78. ^{RSI}Orchestrator^{TM}, [V.6.4.4], Rheometric Scientific, (1998).

79. L. S. Pinchuk, V. A. Goldade, A. V. Makarevich, V. N. Kestelman, *Melt blowing*, Springer, 2002.

80. National Intruments, *serial communication manual,* 2002

81. WINPASO INC., win-tech software design, OPC server for MODBUS manual, 2003.

82. http://modbus.org, *MODBUS over Serial LineSpecification & Implementation guide,* 2002

83. National Instruments, *Labview 7.0 express manual*, 2003

84. John R. Collier, Simioan Petrovan, Yizhong Wang, Hollie Bernard, Noah McMillan, Melissa Folk, Chrissy Rayner, Chris Reneau, Chris Eash, Nick Allred, and Nick Johnson, *Annual TANDEC Conference*, **12,** (2002).

85. John R. Collier, Peter Liaw, Bing Yang, Yizhong Wang, Hollie Bernard, Noah McMillan 1, Melissa Folks, and Chrissy Rayner, *Annual TANDEC Conference*, **12,** (2002).

86. K. Feigl, F.X. Tanner, B.J. Edwards , and J.R. Collier, *J. Non-Newtonian Fluid Mech.* **115**, 191(2003).

VITA

Yizhong Wang was born in Zhejiang, P. R. China in 1970. He joined the Department of Polymer Science and Engineering at Beijing University of Chemical Technology, China in 1988. Four years later, he received a Bachelor of Science degree in Polymer Science and Engineering. In September 1992, he joined the Department of Polymer Science and Engineering at the same Institute and earned a Master of Science degree in Polymer Material Science and Engineering in 1995. In August of that year, he worked as an assistant professor at that Institute. In December 1999, he earned his Ph. D degree in Material Science and Engineering and became an associate professor at that Institute. He joined the Department of Chemical Engineering at the University of Tennessee, Knoxville, as a graduate student in June 2001. He will receive his Ph. D degree in Chemical Engineering in May 2004.